Chemical Vapor Etching of GaAs by CH_3I

by

Charles Winslow Krueger

BS, Chemical Engineering
University of Pennsylvania, 1986

MS, Chemical Engineering Practice
Massachusetts Institute of Technology, 1987

Submitted to the Department of Chemical Engineering in Partial Fulfillment of the Requirements for the Degree of Doctor of Philosophy in Chemical Engineering

at the
Massachusetts Institute of Technology

February, 1994

Signature of Author _____
Department of Chemical Engineering
February 15, 1994

Certified by _____
Dr. Maria Flytzani-Stephanopoulos
Thesis Supervisor

Certified by _____
Professor Robert A. Brown
Thesis Supervisor

Accepted by _____
Professor Robert A. Cohen
Chairman, Committee for Graduate Students

Chemical Vapor Etching of GaAs by CH_3I

by

Charles Winslow Krueger

Submitted to the Department of Chemical Engineering on December 13, 1993 in Partial Fulfillment of the Requirements for the Degree of Doctor of Philosophy in Chemical Engineering

Abstract

The etching reaction of CH_3I vapor with gallium arsenide (GaAs) single crystals has been experimentally investigated in a cold wall, horizontal, atmospheric pressure gas flow reactor. This etching process was studied for application as a complementary *in situ* etch in organometallic vapor phase epitaxy (OMVPE) reactors. The requirements for applying this etch process are that the surfaces be etched smoothly and free of any chemical contamination. A series of parametric experiments was performed in order to determine the optimum etch conditions.

Etching was also studied on substrates patterned with inert masks and on substrates with different crystallographic orientations. The effects of adding an arsenic source, trimethylarsenic, to the etch mixture was also investigated. Finally an etch mechanism was postulated based on the results of etch rate studies and the identification of etch products. This mechanism was tested by comparing simulated etch rates to experimentally observed etch rates. The etch is seen to occur under a condition of gas phase kinetic control with the decomposition of CH_3I in the gas phase being the rate limiting step.

Thesis Supervisor: Maria Flytzani-Stephanopoulos
Title: Principal Research Associate
Thesis Supervisor: Robert A. Brown
Title: Professor

Acknowledgements

I would like to thank my advisors Miretta Stephanopoulos and Bob Brown for their guidnance and support over the years of this project. Chris Wang, who tolerated my presence in her lab for so many years, deserves something beyond normal gratitude. My other two committee members, Karen Gleason and Leslie Kolodzieski have also been most helpful over the years.

The folks at Lincoln Laboratory and Group 83 - so many of whom contributed in small and large ways - receive a collective thankyou. I would like to further acknowledge the help I received in the early going from Dave Tracy and Don Kolesar who taught me many things about working with my hands and about life in general. Dave Hovey and Jon McMillan from the glass shop were invaluable over the years. Mary Finn, for her reliable Auger analysis and Paul Nitishin for his SEM work deserve special recognition. Additionally special thanks go to Gerry Iseler, George Turner, and Hong Choi who allowed me into their labs at various times without always knowing exactly what I was doing. Mike Connors for doing the nitride depositions and Bill McGilvary for his help in the photolithography lab and for many enjoyable conversations. Additionally I want to thank Dorothy Hsieh for an enjoyable and productive summer during her tenure as a UROP student.

I want to thank Beth for her friendship, companionship and support over the years. My roommates, John, Dave, Bob, and Chris for keeping life outside of school entertaining. And all the rest of my friends from MIT. And last, but not least, my parents and family.

Contents

Chapter 1

Introduction

1.1 MOTIVATION

Epitaxial growth of crystalline semiconducting materials is an important process for fabricating thin layers of high quality material. Chemical vapor deposition (CVD) epitaxial growth processes are an important technology which includes organometallic vapor phase epitaxy (OMVPE), a growing technology which involves the use of one or more organometallic precursor species. The continued importance of these technologies provides a major motivation for the subject of this thesis, the chemical vapor etching of gallium arsenide (GaAs). Chemical vapor etching is the reverse analog to CVD and is easily implemented into existing CVD/OMVPE reactor systems *in situ*, allowing for increased process flexibility by combining growth and etching into one reactor system.

For a vapor etching process to be applied to semiconductor processing, the etched crystal surface should be mirror smooth. This is typically accomplished if material is etched in a layer by layer fashion. In addition, the etch process should introduce no chemical impurities or residues on the surface. Temperature is an important process parameter due to undesirable effects of dopant and/or alloy interdiffusion (Kuech, et al, 1988). These solid state diffusion

processes are generally highly activated motivating the need to develop a vapor etching process at low temperatures. Other issues include the ability to etch at uniform rates over wide areas and to controllably reproduce etch rates.

The etchant source compound that has been chosen for this study is methyliodide (CH_3I). This chemical has been chosen for several reasons. It is known to decompose into methyl radicals and iodine atoms at temperatures above 400°C (Saito, et al, 1980), both of these free radical species are expected to be potential etchants. The compound is a liquid at room temperature (bp = 43°C) making it easy to handle and easy to implement into existing CVD/OMVPE reactor systems with a conventional bubbler/carrier gas arrangement. It is non-flammable but has toxic properties and should be handled accordingly. The undecomposed compound is non-corrosive so upstream contamination problems are avoided, although some iodine compounds produced from its decomposition (I_2, HI) are expected to be corrosive to downstream components of a reactor system.

The semiconductor material which is the main object of this study is gallium arsenide (GaAs). GaAs is a III-V crystalline compound and is probably the most technologically important semiconductor material after silicon. For example, a subject search on the Applied Science Index for 1992 revealed over 900 references to silicon, over 500 references to GaAs with other materials such as indium phosphide, indium arsenide and aluminum gallium arsenide each having on the order of 100 or fewer references. It is thereby seen that gallium

arsenide is an important semiconductor material. GaAs exhibits several desirable material and electrical properties. The theoretical electron mobility is nearly 30 times higher than for silicon, meaning that circuits fabricated using GaAs in place of silicon should be 30 times faster. GaAs, unlike silicon, has a direct band gap, a property that allows the material to be used as a light waveguide and permits fabrication of semiconductor lasers based on this property. These devices would be employed in the future development of an optical computer. At this time the major limitations to using GaAs in place of silicon have to do with processing the material into micron and submicron scale devices.

Studying vapor etching can also provide fundamental information into the general class of gas-solid reactions such as CVD and OMVPE. Reactions of free radicals with the semiconductor material can occur as side reactions in the industrially important processes of reactive ion etching (RIE) and other plasma-activated, isotropic etch processes, which can lead to polymer deposition and undercutting of masked features which are generally undesirable. (Sidewall polymer deposition is often desired for suppressing sidewall etching reactions. Nevertheless, this deposition inevitably leaves chemical impurities on the sidewalls). Recently, RIE of GaAs with iodine and methane containing gasses has been succesfully demonstrated (Pearton, et al, 1992, Bharadwaj, et al, 1991).

1.2 OBJECTIVES

There are two main objectives of this thesis which are concerned with applying the CH_3I vapor etch *in situ* of OMVPE reactor systems.

The first objective was to demonstrate the chemical vapor etching of GaAs by CH_3I and determine operating conditions under which etched surfaces are free of morphological imperfections and chemical impurities. These characteristics are necessary if the etch is to be employed as an *in situ* substrate cleaning process. A test of the etch process is to determine the quality of OMVPE GaAs deposited on etched surfaces.

The second objective is to examine CH_3I vapor etching on patterned GaAs substrates. *In situ* etching of patterned substrates is another potentially useful application for vapor etching. When etching microscopic features, effects such as surface diffusion and adsorption/desorption with gas phase diffusion can lead to non-uniform etching near masks and an amplification of surface reactivity differences on non-planar structures.

In light of these two objectives it is desired to develop an understanding of the etch mechanism. Determination of rate controlling steps through parametric experiments and identification of etch products will aid in deducing details of the etch chemistry.

1.3 METHOD OF APPROACH

The approach taken to meet these objectives was primarily experimental. It was first necessary to demonstrate viability and determine conditions under which specular etched surfaces could be produced. Parametric etch studies in a cold wall horizontal gas flow reactor were performed and etch rate and etched surface morphology was studied as a function of susceptor temperature, CH_3I concentration, and total gas flow rate. Growth of OMVPE GaAs on some of the etched samples was performed and the etched-surface/grown-layer interface was probed for chemical impurities by both C-V and SIMS depth profiles. Most of these experiments were performed on GaAs crystals of (100) orientation, misoriented 2° to the (110) direction, the standard substrate orientation for OMVPE growth of GaAs. In addition, CH_3I vapor etching of (100)$Al_xGa_{1-x}As$ epitaxial layers and (111)Ga and (111)As GaAs bulk substrates was examined.as well as microfacets of (111)Ga and (111)As exposed on the (100)GaAs substrates.

Etching of GaAs substrates patterned with inert masks of silicon nitride (Si_xN_y) was studied as a function of mask size. Mask undercutting and etch uniformity near the masks were the primary concerns in these investigations. Finally, the addition of an arsenic source, trimethylarsenic (TMAs) on the etch rates of (100) substrates was also examined to see if any effects on etch rate, uniformity, or surface morphology could be found.

Based on the parametric experimental results combined with etch product analysis, etch mechanisms can be hypothesized. These hypotheses are tested by incorporating proposed mechanisms into a previously developed computer model of the gas dynamics in a vertical rotating disk reactor and comparing the model predictions to etch data gathered in that reactor system.

Finally, addition of trimethylarsenic (TMAs) to the CH_3I etch mixture is investigated. Previous investigations of vapor etching of GaAs by HCl showed favorable effects on etched surface morphology from adding arsine (AsH_3) to the etch mixture (Bhat, et al, 1975). In this work it is of interest to see the effect that TMAs addition has on the etch rate as well as on the etched surface morphology.

Chapter 2

Background: Chemical Vapor Etching Techniques

Etching of semiconductor materials is an important process for constructing integrated circuits and other electronic and optoelectronic devices. There are a wide variety of techniques currently employed for etching materials, the choice of one of these will depend on several factors. There are several methods by which GaAs can been etched using chemically reactive vapors. In general, the etching reaction must be activated and there are several means to achieve activation. Heating the reaction zone is the simplest (thermochemical) but the chemistry can also be initiated by photons (photochemical), or a plasma. In this chapter, the work to date on purely thermochemical induced etching will be reviewed as is relevent to this thesis.

2.1 THERMOCHEMICAL VAPOR ETCHING OF GaAs

The majority of the work to date on thermochemical vapor etching of GaAs involves the use of chlorine containing compounds as the etching vapor, including Cl_2, HCl, and $AsCl_3$ (references follow). In addition, chemical vapor etching of GaAs has been reported using

brominated compounds ($AsBr_3$, PBr_3, HBr) (references follow), hydrogen (H_2) (Okubora, et al, 1986), and water vapor (H_2O) (Lin, et al, 1970). There has also been some work on pure thermal evaporation of GaAs in a vacuum (Saito, et al, 1988, Haynes, et al, 1986). A few of these studies have identified etch products, allowing for clearer speculation about the etch mechanism.

2.1.1 Chlorine (Cl_2) Vapor Etching of GaAs

There have been several studies of the reactions of molecular chlorine and atomic chlorine with GaAs surfaces. Most of these studies were performed under moderate to high vacuum conditions, sometimes utilizing a molecular beam. Several details about the etch mechanism and kinetics have been determined and of all the chemical vapor etching reactions, the mechanism of the Cl_2+GaAs reaction is probably the deeply studied and hence the most well understood.

The reaction of Cl_2 with GaAs(100) was studied under vacuum conditions under moderate heating and high flow rates of Cl_2 (Ha, et al, 1988). Total Cl_2 pressures from 0.09-20 torr and surface temperatures from 25-150°C were investigated. Cl_2 flow rates were chosen so as to exceed the etch rates by a factor of 50, assuring little depletion of Cl_2. Below 75°C, the reaction was characterized by the formation of a liquid layer on the GaAs surface which interfered with the etching reaction. At higher temperatures, the etch rate depended linearly on Cl_2 pressure for low pressures but at higher Cl_2 pressures

the rate was observed to saturate. This saturation behavior is argued to be consistent with a two step surface reaction model where the first step is the reaction of an active surface site with Cl_2 and the second step is the regeneration of the active sites through the formation of volatile etch products. Etched surface morphologies were rough for all etch conditions.

Another study of the Cl_2+GaAs focussed mainly on determining the etch products by *in situ* mass spectroscopy (Hou, et al, 1989). Surface temperatures were varied between 300-600K but the flux of Cl_2 was not varied and was introduced as a supersonic molecular beam using an expansion nozzle and skimmer arrangement. The major result of this study was the observation that the arsenic product changed from $AsCl_3$ below 450K (177°C) to As_4 at higher temperatures. The gallium product remained $GaCl_3$ at all temperatures up to 600K (327°C).

An extensive study of the Cl_2+GaAs reaction compared different surface crystallographic orientation as well as varying surface temperature and Cl_2 pressure (Furuhata, et al, 1990). Etching was performed in vacuum chamber with Cl_2 pressures between $8x10^{-5}$ and $1x10^{-3}$ torr and surface temperatures from 100-700°C. Substrate orientations examined were (100), (110), (111)As, and (111)Ga. The kinetics of the reaction on (100), (110), and (111)As were very similar and three temperature regimes were identified. The low temperature regime (<150°C) was characterized by saturation of the etch rate with increasing Cl_2 pressure and a 10 kcal/mol activation

energy; evidently the rate is limited by surface kinetics. In the middle temperature regime (150-450°C) the etch rate was independent of temperature and a linear dependence of the etch rate on Cl_2 pressure was observed, indicating that the supply of Cl_2 to the surface was rate limiting. The high temperature regime (>450°C) was characterized by an activation energy of 16 kcal/mol. The kinetics of the reaction on (111)Ga surface were the same in the high temperature regime but at lower temperatures, the 16 kcal/mol activation energy persisted and the rate dropped off rapidly. Based on this evidence, it is concluded that the etch rate in the high temperature regime is controlled by the formation/desorption of GaCl. For the (111)Ga surface this is the only mechanism available for Ga removal whereas the other orientations allow for formation of the more volatile $GaCl_3$. This is probably due to steric effects as gallium is bonded to the (111)Ga surface with three bonds. No direct evidence for the etch product identities was provided. The etch surface morphologies were smooth on the (100) surface in the intermediate temperature regime (Cl_2 flux limited) but were degraded in the high and low temperature (kinetic) regimes.

Balooch and Olander (1986) studied the Cl_2+GaAs reaction under high vacuum conditions using modulated molecular beam of Cl_2 and mass spectrometric detection of etch reaction products. The beam intensity was $1x10^{17}$ molecules Cl_2/cm^2-s and surface temperatures from 300-800K were examined. Volatile reaction products were identified to be $GaCl_3$ and $AsCl_3$ at low temperatures and GaCl and AsCl at higher temperatures (>550K). Incedent Cl_2 reaction probability increased

from 0.002 at 300K to a maximum of 0.3 at 450K corresponding to the maximum $GaCl_3$ and $AsCl_3$ production rates. From the phase lag between detected product mass signals and the Cl_2 mass signal, it was determined that the $GaCl_3$ production was the slow reaction on the surface at low temperatures. Indeed, at these temperatures, the surface developed a Ga-rich, chlorine containing "scale" which apparently inhibited etching. It was found that ion bombardment (Ar^+) at 300K increased the etch rate by a factor of 6 by facilitating the removal of the Ga-rich scale from the surface. It was concluded that ion-bombardment has the main effect of exciting gallium-chloride compounds on the surface to a state with a high desorption constant.

Sugata, et al (1987) looked at the reaction of Cl radicals with GaAs and AlGaAs in a high vacuum system. An electron cyclotron resonance (ECR) plasma was used to generate Cl radicals from Cl_2. Etching of microfaceted structures on bulk (100)GaAs wafers revealed that (100) > (111)Ga by a factor of 35 (300°C), consistent with the findings of Furuhata, et al (1990) for Cl_2. Etched surfaces of GaAs(100) were generally rough, even under conditions where the gas supply of Cl was apparently rate limiting, this result is attributed to initial surface irregularity from the native oxide layer or possibly an unidentified contaminant. Analysis of etch profile shapes from circle and square shaped masks revealed a temperature effect on the isotropic etching. Below 400°C, faceted sidewalls with sharp corners were formed. Above this temperature, the features were isotropically etched (retaining the original square or circular shape).

Based on these five studies, a reasonable picture of the Cl_2+GaAs etching reaction can be drawn. Vapor Etching of GaAs by Cl_2 proceeds via the rapid adsorption and dissociation of Cl_2 on the GaAs surface. Volatile etch products are $GaCl_3$ and $AsCl_3$ at low temperatures and GaCl and either AsCl or As_4 at higher temperatures. Formation/desorption of the gallium species is the rate limiting step as long as the supply of chlorine to the surface sufficient. The fact that different arsenic products have been observed in different studies (Balooch and Olander, 1986 vs. Hou, et al, 1989) is most likely attributable to differences in the surface Cl_2 fluxes in these two studies. This would suggest that chlorine preferentially reacts with gallium over arsenic and only at conditions where excess chlorine is available at the surface will AsCl desorb as an etch product.

The structure of the (111)A or (111)Ga surface is such that formation of $GaCl_3$ is unfavorable due to primarily to steric effects. The (111)Ga facet is seen therefore to etch most slowly at low temperatures where $GaCl_3$ is the main etch product. At higher temperatures, the volatility of GaCl is high enough that it is the dominant etch product and the (111)Ga etch rates are therefore comparable to the other orientations. In all of these studies, reported surface morphologies were rough and only under conditions where the rate limiting step was the gas supply rate of Cl_2 to the surface were smooth surfaces obtainable.

2.1.2 Hydrogen Chloride (HCl) Vapor Etching of GaAs

Vapor etching of GaAs with HCl stands out as one process which has been applied to device fabrication as well as having been studied from a fundamental perspective. HCl vapor etching has been successfully employed as an intermediate processing step *in situ* of an OMVPE reactor during the fabrication of AlGaAs/GaAs laser diodes (Nido, et al, 1987 and Shimoyama, et al, 1988). Earlier work on the subject had demonstrated viability of the process and determined optimal processing conditions. A key finding from these studies is that good etched surface morphologies could be obtained only under a condition where the etch rate was controlled by the gas phase mass transport of etchant species to the surface, a condition which typically requires surface temperatures in excess of 800°C.

The polishing etching of Te-doped (100)GaAs by H_2/HCl/AsH_3 vapor mixtures was examined in a horizontal, cold wall flow reactor operated at atmospheric pressure (Bhat, et al, 1975). A typical etch gas mixture consisted of 900 ml/min H_2, 3 ml/min AsH_3, and 2 ml/min HCl. In addition, Cr- and Zn-doped (100)GaAs and Te-, Zn-, Cr-, and Si-doped (111)B GaAs substrates were examined. In investigating the etch rate as a function of surface temperature, two temperature regimes were identified, a low temperature ($T < 850°C$), kinetically controlled regime and a high temperature ($T > 850°C$) mass transport limited regime. Smooth etched surfaces could only be obtained in the mass transport limited (high T) regime whereas in

the low temperature regime faceting, pitting, and hillock formation occured. Etch rates were identical for all substrate orientations and dopant types above 870°C. The low temperature, kinetic regime was characterized by an activation energy of 1.25 eV/molecule (29 kcal/mol) for the (100) substrates and 1.85 eV/molecule (43 kcal/mol) for the (111)As substrates. Raising the arsine flow had no effect on the etch rates in the high temperature regime but lowered etch rates in the low temperature regime. Varying the HCl flow rate in the high temperature regime revealed a superlinear dependence of etch rate on HCl concentration, consistent with the mass transfer limitation hypothesis. Later work (Bhat and Ghandi, 1978) successfully demonstrated the use of HCl etching as an *in situ* cleaning step prior to OMVPE growth of GaAs from trimethylgallium and arsine.

The H_2/HCl vapor etch system was also investigated in a hot wall reactor without AsH_3 (Dorshchand, et al, 1983). As in the previous study, substrate orientation and dopant type were varied and, in addition, the effect of changing the total gas flow rate to the reactor was examined. Overall, the results of this study were in agreement with those of Bhat et al (1975) discussed above. In contrast to the results from the previously discussed study, three temperature regimes were identified and a dependence of etch rate on substrate orientation and dopant type was observed in all three regimes. The key result from this work is the effect of the total gas flow on the etch rate. For the two low-temperature regimes, the etch rate was observed to remain constant with an increase in the total flow rate

above a critical value (> 25 l/hour H_2), suggesting that surface reactions are rate controlling. In the high temperature regime, increasing the flow rate caused the etch rates to increase, as is expected with a mass transfer controlled process. Etched surface morphology was best under mass transport limited etch conditions.

One further study of HCl/H_2 etching of GaAs was also in general agreement with the previous two (Pelosi, et al, 1983). At 720°C, the dependence of (100)GaAs etch rate on HCl concentration was seen to be somewhat sublinear, consistent with the previously hypothesized surface kinetic limitation at temperatures below 870°C. Surface morphologies at under these conditions were rough.

Saito and Kondo (1990) used *in situ* mass spectroscopy to examine the etch products from the reaction of HCl and HCl/H_2 vapors. The total pressure was $1.8x10^{-4}$ torr for HCl alone and $2.8x10^{-4}$ torr for the H_2/HCl mixture and the surface temperature was 500°C. The etch rates for both mixtures were equal but the etch product mass spectra were different. For pure HCl, the products were primarily arsenic and gallium chlorides, the largest ion fragments peaks corresponding to $AsCl_2^+$ and $GaCl_2^+$. For the H_2/HCl mixture (H_2:HCl = 4:1), the main arsenic products were arsenic hydrides and As_2. The gallium product mass peaks were considerably lower than for HCl etching alone, the largest ion fragment corresponding to $GaCl^+$. The sharp drop of the gallium product signals in the mass spectrum was not explained.

2.1.3 $AsCl_3$ Vapor Etching of GaAs

The vapor etching of GaAs with $AsCl_3$ was examined on (100)GaAs misoriented 2° to (110) and (111)As substrates (Bhat and Ghandi, 1977). The results of this study were in many ways similar to their previous results for HCl vapor etching discussed above. Two rate controlling regimes were identified, a high temperature (T>850°C), mass transport limited regime and a kinetic regime (700-850°C). The etch was argued to proceed via the complete decomposition of $AsCl_3$ in the H_2 ambient to form three HCl's based on the fact that etch rates were a factor of 3 higher for equal amounts of $AsCl_3$ and HCl. As with HCl etching, it was necessary to add a small flow of AsH_3 to prevent decomposition of the substrate at 900°C and a superlinear dependence of the etch rate on the $AsCl_3$ concentration was observed. Specular surfaces could be obtained for both substrate orientations studied at 900°C. Growth of high quality epitaxial layers on these etched substrates was also achieved (Bhat and Ghandi, 1978)

Jani et al (1982A) also investigated the etching of (100)GaAs by $AsCl_3$. Their results were in general agreement with Bhat and Ghandi's discussed above. Again mass transport limited etch rates were encountered at high temperatures (>850°C). The kinetic regime was characterized by a first order dependence of the etch rate on $AsCl_3$ concentration and the etched depth was linear with time.

Growth of high quality epitaxial layers by OMVPE on etched substrates was also demonstrated (Jani, et al, 1982B).

Manipulation of the $AsCl_3/H_2$ chemistry by adding GaCl to the etch mixture was done in two studies. In the first study (Bakin, et al, 1972) It was shown to be possible to obtain smooth etched surfaces on (100) and (111)As GaAs substrates at temperatures of 750°C with the $GaCl/AsCl_3/H_2$ system operated near the "zero growth" point. The addition of GaCl resulted in a lowering of the etch rate and it was argued that a diffusion hindrance arose in the gas phase causing the etched surfaces to be smooth. The second study (Heyen and Balk, 1981) was somewhat more detailed and examined the $GaCl/HCl/AsCl_3/H_2$ system. Again smooth etching could be achieved at 750°C but by independently varying the HCl concentration higher etch rates could be obtained.

2.1.4 Bromine Vapor Etching of GaAs

The chemical vapor etching of GaAs and GaP by HBr and PBr_3 was studied in a vertical reactor at atmospheric pressure (Givargizov, et al, 1980). GaAs substrates orientations of (111)Ga, (111)As, (110), and (100) were examined. For HBr/H_2 etching of GaAs, three temperature etching regimes were observed, two kinetic regimes at the lower temperatures and a high temperature mass transfer limited regime. The transition temperature between the low temperature (I) and high temperature (II) kinetic regimes was between 625 and 650°C for all orientations but the transition

transfer limited (III) regime depended on orientation; 780°C for both (111) orientations and 875°C for (100) and (110). The activation energies for the kinetic regimes are as follows; (100) E^*_I = 41 kcal/mol, E^*_{II}= 11 kcal/mol, (110) E^*_I= 39 kcal/mol, E^*_{II}= 12 kcal/mol, (111)Ga E^*_I= 47 kcal/mol, E^*_{II}= 16 kcal/mol, (111)As E^*_I= 47 kcal/mol, E^*_{II}= 20 kcal/mol. Saturation in the rate with temperature in regime III ($E^* \sim 0$), characteristic of a mass transport limitation for all orientations. No specific chemical mechanisms are postulated for any of these regimes. Etched surface morphology was observed to improve from faceted to smooth with increasing temperature for all surface morphologies, the smoothest surfaces corresponding to the mass tranfer limited regimes.

The etching of GaAs with $AsBr_3$ was studied as an *in situ* wafer preparation prior to OMVPE deposition of GaAs (Keuch, et al, 1986). The etch was determined to be mass transfer limited for temperatures between 750°C-850°C and morphologies were generally smooth for etch times below 30 minutes. Growth of GaAs on *in situ* etched GaAs(100) revealed a lowering of the electrical activity of impurities at the interface but did not significantly lower the amount of chemical impurities as measured by secondary ion mass spectroscopy (SIMS). It was postulated that the etch neutralizes the normally electrically active impurities by an unknown mechanism.

Chapter 3

Chemical Vapor Etching of (100) GaAs and $Al_xGa_{1-x}As$ by CH_3I and OMVPE Regrowth of GaAs

3.1 INTRODUCTION

Chemical vapor etching of GaAs and other related semiconductor compounds can potentially be used as a complementary *in situ* process with organometallic vapor phase epitaxy (OMVPE) and other vapor phase deposition techniques. *In situ* process integration minimizes contamination problems normally encountered during the multi-step fabrication of microelectronic devices, and can ultimately lead to increased yields and improved device performance. In recent years, OMVPE has become an increasingly popular technique for depositing thin films of many III/V and II/VI semiconductor compounds. This fact combined with the general versatility of OMVPE reactor systems for incorporating a wide variety of vapor sources makes OMVPE an ideal candidate for development of an *in situ* vapor etching process.

In this chapter, etching of GaAs and $Al_xGa_{1-x}As$ wafers by the thermochemical reaction of methyl-iodide (CH_3I) vapors will be

discussed. Parametric experimental results are presented for etch experiments performed in an atmospheric pressure horizontal flow reactor. From these experiments, a window of etch conditions is found where etched surface morphology is smooth. In addition, etch rate controlling steps are postulated based on the data and some insight into the mechanism is gained. It is finally shown that GaAs surfaces which are smoothly etched provide excellent substrates for subsequent OMVPE of GaAs.

3.1.1 Background

A number of researchers have examined vapor etching of GaAs and other III/V semiconductor materials. The results of these studies are discussed in detail in Chapter 2. Several compounds have been demonstrated to etch these materials including hydrogen chloride (HCl), arsenic trichloride ($AsCl_3$), chlorine (Cl_2), hydrogen bromide (HBr), arsenic tribromide ($AsBr_3$). In all of the studies it was found that the etched surface morphology was smoothest under a condition where the etch rate is limited by the supply of etchant molecules to the surface from the vapor phase or molecular beam. Under other conditions the etch rate is apparently limited by surface kinetics, possibly etch product desorption, leading to surface degradation and faceting. No comprehensive theory exists at this time to explain these observations.

Several of these researchers have incorporated the vapor etch as an *in situ* wafer preparation step prior to OMVPE growth. Detailed

investigations have looked into the quality of material subsequently deposited on vapor etched substrates by OMVPE. In this case, the electrical and chemical properties of the substrate/epilayer interface are of issue. Interface electrical properties are easily probed by capacitance-voltage (C-V) measurements which provides information on electrical carrier concentration as a function of depth into the epilayer and/or substrate. Additionally, interface chemical composition can be probed by secondary ion mass spectroscopy (SIMS) which provides elemental composition as a function of depth.

Bhat and Ghandhi (1978) examined the OMVPE growth of GaAs from $(CH_3)_3Ga$ and AsH_3 on (100) GaAs substrates vapor etched *in situ* by HCl and $AsCl_3$. Moderate improvements in deposited epilayer electrical properties and surface morphologies were reported as determined by room temperature mobility measurements and optical microscopy. Similar results were presented by Jani, et al (1982) for *in situ* etching of GaAs by $AsCl_3$ and subsequent OMVPE growth of GaAs. More recently, Nido, et al (1987) successfully employed *in situ* HCl etching of GaAs and $Al_xGa_{1-x}As$ as one step in the fabrication of self aligned laser diodes. Shimoyama, et al (1988) also used *in situ* HCl etching in the OMVPE fabrication of transverse junction buried heterostructure lasers.

Keuch, et al (1986) showed that employing *in situ* $AsBr_3$ vapor etching on GaAs prior to OMVPE growth of GaAs led to improved electrical properties at the etch/growth interface but this was due to

an unknown mechanism as chemical impurities at the interface were still present as determined by SIMS analysis.

Aside from chloride and bromide compounds, few other chemicals have been used to vapor etch GaAs. However, recent investigations into plasma and ion beam assisted etching have successfully demonstrated etching of GaAs from several organic and some iodine containing compounds, including CH_4 (Henry et al, 1987, Cheung et al, 1987, Carter et al, 1989, Arnot et al, 1989), C_2H_6 (Matsui et al, 1988, Pearton et al, 1989), I_2 (Flanders et al, 1990, Bharadwaj et al, 1991), and HI (Pearton, et al, 1992). Further, photochemical iodine etching of InP by laser induced decomposition of CH_3I has also been demonstrated (Durose, et al 1988).

3.1.2 Objective

The objective of this work is to investigate the chemical vapor etching of GaAs and $Al_xGa_{1-x}As$ by CH_3I and evaluate the suitability of this etch for *in situ*, substrate-cleaning prior to OMVPE growth. Detailed parametric studies were performed to determine conditions favorable to obtaining smooth etched surfaces on (100) GaAs substrates and $Al_xGa_{1-x}As$ epitaxial layers. The parameters of interest were etch temperature, CH_3I concentration, carrier gas type, total gas flow rate, and aluminum content (x) in the epilayers. The effect of varying these parameters on etch rate is also studied in order to gain insight into possible rate controlling mechanisms. Finally, OMVPE growth of GaAs on CH_3I vapor etched epilayers was

performed. The quality of these grown layers and of the substrate/epilayer interface was investigated by C-V depth profiling to determine the presence of electrically active impurities and SIMS analysis to determine the chemical identity of any chemical impurities.

3.2 EXPERIMENTAL PROCEDURE

3.2.1 Horizontal Reactor System

All etching experiments were performed in a horizontal reactor operated at atmospheric pressure with H_2 or He as the carrier gas. A schematic of this reactor system is shown in Figure 3.1. At the susceptor location, the reactor height is 15 mm and the width is 22 mm. The susceptor length is 25 mm and the susceptor is heated from below by a platinum resistance heater. Susceptor temperature is monitored by a thermocouple, enclosed in a quartz sheath and inserted directly into the susceptor center. Gaseous H_2 from a liquid H_2 supply was used without further purification, while He was purified in a titanium furnace for gettering O_2. All gas flows are controlled by electronic mass flow controllers (Tylan).

Methyl iodide was obtained at 99% purity (Aldrich) and in some cases was further purified by fractional distillation on a vacuum line or under a high purity helium ambient at atmospheric pressure. The purity of the CH_3I source, however, was not observed to have any influence on observed etch rates or etched surface morphologies

even when no purification was used. CH_3I is a liquid at room temperature (bp. = 43°C) and is therefore introduced into the reactor by passing part of the carrier gas into a temperature controlled bubbler containing the CH_3I. The concentration of CH_3I is calculated from the bubbler temperature (T_B) and the known vapor pressure of CH_3I as a function of temperature (CH_3I vapor pressure data obtained from CRC Handbook of Chemistry and Physics, 60th ed., 1979). This data was fit well by the following equation

$$\log P_{CH_3I} \text{ (torr)} = -3521.13/T_B(K) + 17.81 \qquad (3.1)$$

This formula is valid for bubbler temperatures between 0 and 25°C. CH_3I mole fractions (y_{CH_3I}) between 0.0012 and 0.03 could be obtained by suitably choosing bubbler temperature and carrier gas flow rate.

3.2.2. Substrate Preparation

The GaAs samples were Si-doped n+ (100) wafers misoriented 2° toward the (110) direction. This substrate orientation was chosen because it is commonly used for OMVPE growth of GaAs and $Al_xGa_{1-x}As$. The GaAs samples were supplied by American Xtal Technology and had a reported etch pit density (EPD) of < 500 /cm^2. For studies of $Al_xGa_{1-x}As$ etching, 2-micron thick $Al_xGa_{1-x}As$ epilayers were grown by OMVPE on the GaAs substrates and capped with a layer 500Å GaAs to prevent $Al_xGa_{1-x}As$ oxidation from ambient exposure. For etch rate studies, substrates were first half-masked with a thin

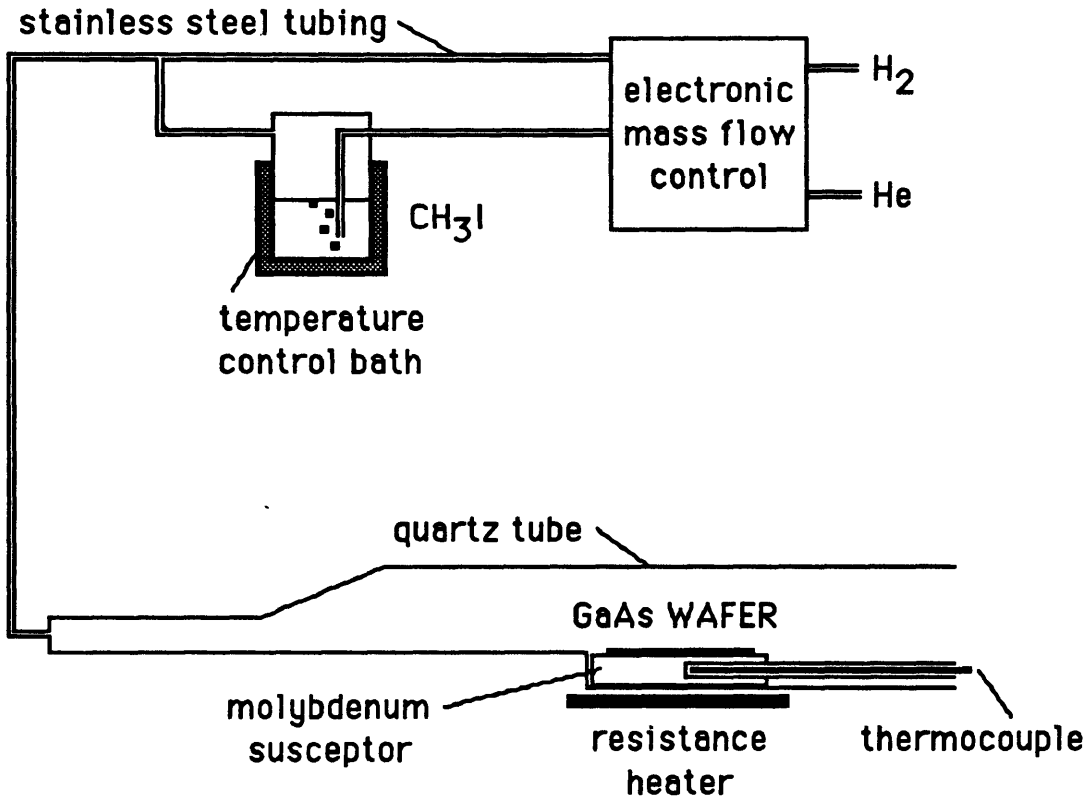

Figure 3.1: Schematic of horizontal gas flow reactor system used for CH_3I vapor etch experiments.

film (thickness = 1000Å) of PECVD silicon nitride (Si_3N_4), a ceramic material which is not affected by the vapor etch. Prior to loading into the reactor, each sample wafer was first degreased by successive rinses in trichloroethylene, acetone, methanol, and deionized water, then place in concentrated H_2SO_4 for 1 minute under moderate agitation, rinsed in deionized water, lace in concentrated HCl for 1 minute under moderate agitation, rinsed again in deionized water, and finally dried with N_2 gas.

3.2.3 Experimental Procedure: Etch Rate Studies

The wafer to be etched was cleaned by the above procedure and then placed on the molybdenum susceptor and immediately loaded into the etching reactor. Wafers were placed on the susceptor as is shown in Figure 3.2. The mask substrate boundary is oriented parallel to the flow direction and the front of the wafer is positioned 7 mm back from the front edge of the susceptor.

A single etch experiment consists of the following steps. Following a 30 minute purge with 5 slpm of hydrogen, the platinum resistance heater is switched on and the susceptor temperature begins to rise. After reaching the desired etch temperature in 10 - 15 minutes, the temperature is allowed to stabilize for 5 more minutes and the methyl iodide flow is switched on. The CH_3I is maintained at a constant value for the desired etch time and the temperature is controlled at a constant value. At the end of the experiment, the CH_3I flow is turned off, the heater power is turned off, and the flow of

carrier gas to the reactor is raised to its maximum (5000 sccm H_2). The susceptor cools rapidly, generally reaching room temperature after 25 minutes. The gas flow is switched to 1 slpm of helium, the reactor is opened, and the sample unloaded.

After etching, the silicon nitride mask was removed either by hydrofluouric acid exposure or, in the case of $Al_xGa_{1-x}As$ etched layers (which are attacked by HF solutions), by CF_4 plasma etching. The step height was then measured with a Dektac mechanical stylus, and the etch rate was found by dividing the step height by the exposure time. Figure 3.3 shows a typical etch profile obtained with the mechanical stylus. As can be seen from this figure, the etch profile is not uniform close to the step. This non-uniformity is ignored when reporting etch depths by taking etch depth measurements far from the step (between 300 and 500 microns from the step). This non-uniformity is apparently due to diffusion of etchant species from the inert mask region to the reactive GaAs surface. This effect will be discussed in more detail in chapter 4. The morphology of the etched surfaces was examined using Nomarski interference microscopy. In addition, some etched surfaces were subsequently examined with auger electron spectroscopy (AES) for determining atomic composition.

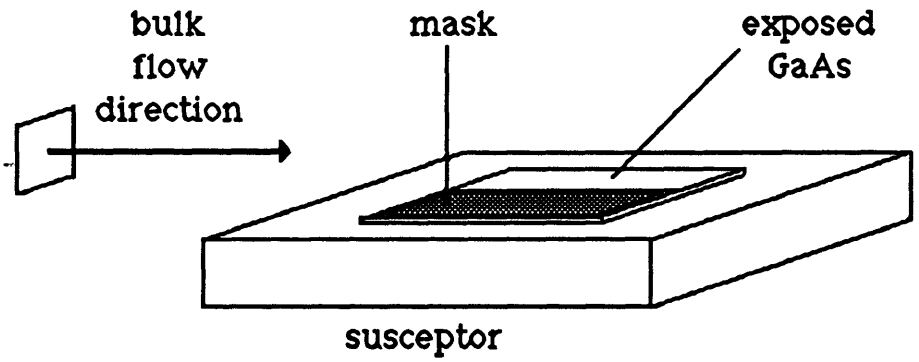

Figure 3.2: Schematic of standard test wafer and susceptor showing orientation relative to gas flow field within the horizontal reactor.

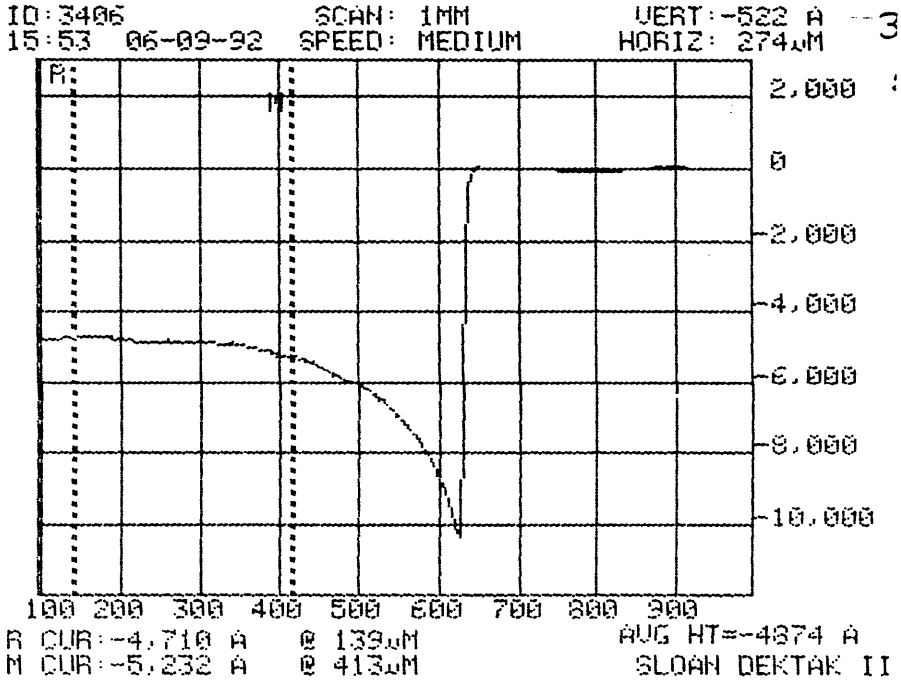

Figure 3.3: Typical Dectak etch depth profile.

3.2.4 Experimental Procedure: Regrowth Studies

For the OMVPE regrowth experiments, a modified experimental procedure was followed. First, a GaAs epilayer was grown by conventional OMVPE from trimethylgallium and arsine on a two inch diameter GaAs substrate oriented (100) + 2° to the <110> in a vertical rotating disk OMVPE reactor. This "first epilayer" sample was then removed from the vertical reactor and cleaved into several pieces, one of which was immediately loaded into the horizontal etching reactor, vapor etched by CH_3I/H_2, removed, and reloaded into the vertical reactor. Other pieces of the "first epilayer" were either loaded back into the vertical OMVPE reactor immediately, or after first being exposed to one or more standard cleaning solutions such as degreasers, organic solvents or sulfuric acid. Growth of a second epilayer of GaAs was now simultaneously performed on several different samples. Second epilayer thickness was 1 micron and both first and second epilayers were undoped. Differences between samples are expected to be observed at the interfaces between the first and second epilayers due to different impurities introduced by the various chemical treatments. These interfaces were evaluated by capacitance-voltage (C-V) measurements which provide electrical carrier concentrations as a function of depth, identifying electrically active impurities at the interface and secondary ion mass spectroscopy (SIMS) which provided quantitative elemental composition as a function of depth from the surface and allowed for detection and identification of impurities at the interface. The second

epilayer morphology was also evaluated using Nomarski interference microscopy.

3.2.5 Analysis of Reactor Operation

The horizontal reactor used for these vapor etching experiments was originally designed for use as an OMVPE reactor and is operated in a similar manner. The bulk of the flowing gas is hydrogen and the flow rates and temperatures are similar to those used in OMVPE reactors. There has been considerable work on the theory of these types of flow reactors with a particular emphasis on the structure of the flow field under typical (OMVPE) growth conditions. It is usually desired that the flow be laminar for reasons of reproducibility and grown layer uniformity. An understanding of how operating conditions influence the formation of complex, recirculating flows has been achieved and can be understood in terms of the values the Rayleigh (Ra) and Reynolds (Re) numbers (Jensen, et al, 1991). Additional information about the reactor dynamics is found from the values of the Peclet numbers for heat and mass transfer (Pe_h and Pe_m) which will govern the structure of temperature and concentration fields respectively. Ranges of typical reactor operating conditions employed in these experiments are listed in table 3.1. Based on these quantities, ranges for several important dimensionless groups can be estimated and these are listed in table 3.2.

The values of these dimensionless groups indicate several key characteristics of this reactor system. It is expected that, due to the

operating parameter	value	units
SUSCEPTOR TEMPERATURE	400 - 650	℃
REACTOR PRESSURE	1	atm
HYDROGEN FLOW RATE	500 - 5000	cc/min (STP)
CH_3I FLOW RATE	2 - 40	cc/min (STP)
REACTOR HEIGHT AT SUSCEPTOR	1.5	cm
REACTOR WIDTH AT SUSCEPTOR	2.2	cm
SUSCEPTOR LENGTH	2.5	cm
AVERAGE GAS VELOCITY (@2000 sccm, 20°C)	10	cm/second
AVERAGE RESIDENCE TIME OVER SUSCEPTOR	0.25	seconds

Table 3.1: Reactor dimensions and typical values for operating parameters

DIMENSIONLESS NUMBER	DESCRIPTION	VALUE
Reynolds number (Re)	inertial forces /viscous forces	1 - 30
Prandtl number (Pr)	momentum diffusivity/thermal diffusivity	0.7
Peclet number (heat) (Pe_h = RePr)	convective heat transfer/conductive heat transfer	0.7 - 21
Schmidt number (Sc)	kinetic viscosity /molecular diffusivity	10
Peclet number (mass) (Pe_m = ReSc)	convective mass transfer/diffusive mass transfer	10 - 300
Grashoff number (Gr)	buoyancy forces/viscous forces	100
Rayleigh Number (Ra = GrPr)		70
Damkohler Number II (surface) (Da_{II})	surface reaction velocity/diffusion velocity	s_k x 10^4 (s_k < 1.0) (s_k = surface rxn probability)

Table 3.2: Characteristic values of dimensionless groups for horizontal reactor system. Numbers are for H_2 at 500°C.

low Reynolds (Re) numbers (<100) and the relatively low Rayleigh (Ra) number (<100), that the flow field in this reactor will be laminar. Higher values of Ra (>1000) have been shown to lead to the formation of roll cells due to Rayleigh-Benard convection. Since the susceptor surface is parallel to the direction of the flow streamlines, both heat and mass transfer at the susceptor surface will occur primarily by molecular mechanisms. An important length scale for this system is therefore the height of the reactor at the susceptor location and this is the length scale used in computing the values in table 3.2. Boundary layers are not expected to form in this reactor due to the relatively low value for the Reynolds number and the flow field is fully developed at the susceptor location. Entrance effects are expected to influence the temperature field at the leading edge of the susceptor, however (Leys and Veenvliet, 1981). The entrance length is estimated to be roughly 1/4 of the reactor height, or about 5 mm, based on analogy to heat transfer in a cylindrical tube. This developing temperature field will result in an acceleration of the gas near the hot surface due to thermal expansion and therefore the velocity field near the surface will be slightly altered in this entrance region.

3.3 EXPERIMENTAL RESULTS AND DISCUSSION

3.3.1 Vapor Etching in the Horizontal Reactor: Etch Rate Parametric Studies

As was described in the previous section, etch rates are reported here as measured etch depths divided by etching time. Etch rates reported in this fashion are valid only if the etch rate is known to be constant with time. This assumption was tested by performing a set of experiments where etched depths were measured for different etch times at otherwise identical reaction conditions. The results of these experiments are shown in Figure 3.4 which shows etched depth as a function of etch time for both GaAs (100) + 2°(011) substrates and OMVPE grown $Al_{0.7}Ga_{0.3}As$ epilayers etched at 480°C with 1.5 mol% CH_3I in 2100 sccm hydrogen (y_{CH_3I} = 0.015). This figure clearly shows that etched depth is linear with time, verifying that etch rate is a constant, independent of time. Having confirmed the validity of this method for etch rate determination, the etch rate of GaAs (100) + 2°(011) was measured as a function of susceptor temperature, CH_3I inlet mole fraction (y_{CH_3I}), total gas flow rate, and, for $Al_xGa_{1-x}As$, aluminum fraction (x).

Figure 3.5 is an Arrhenius plot showing the temperature dependence of the GaAs (100) + 2°(011) etch rate at three concentrations of CH_3I; y_{CH_3I} = 0.015, 0.0058, and 0.0012. For all of these experiments, the carrier gas was 2100 sccm hydrogen. The lines shown in this plot were calculated using least squares analysis and the calculated slopes

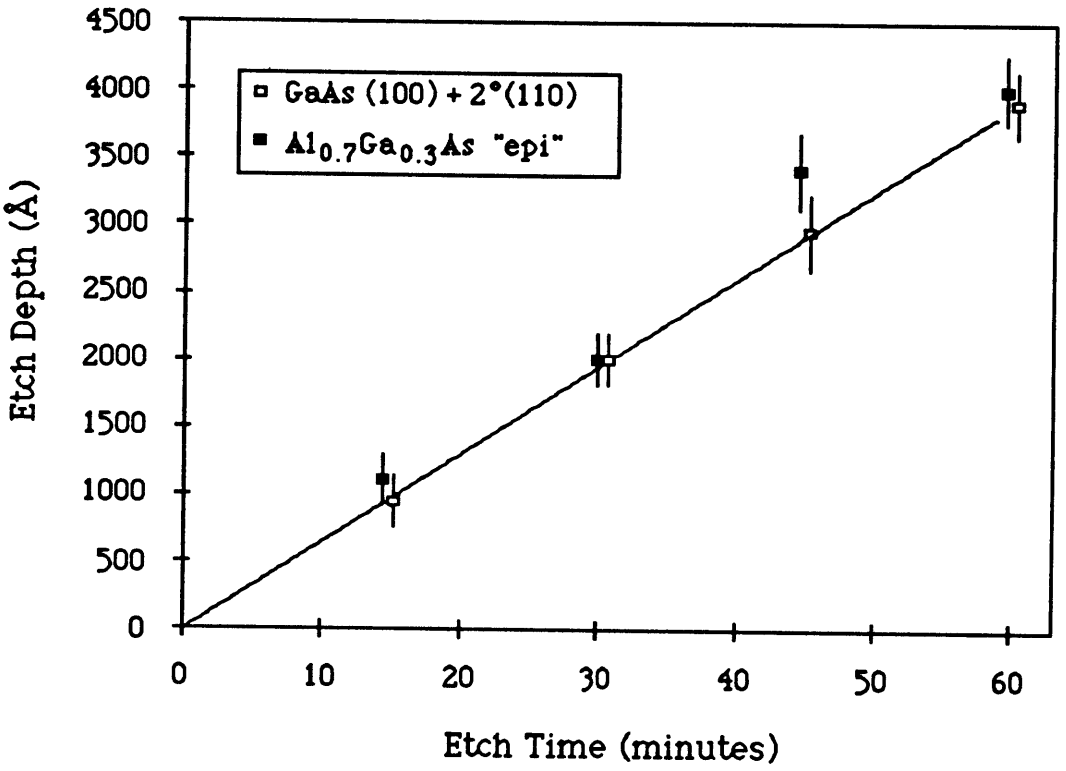

Figure 3.4: GaAs etch depth as a function of CH_3I exposure time, T = 480°C, y_{CH_3I} = 0.015,.

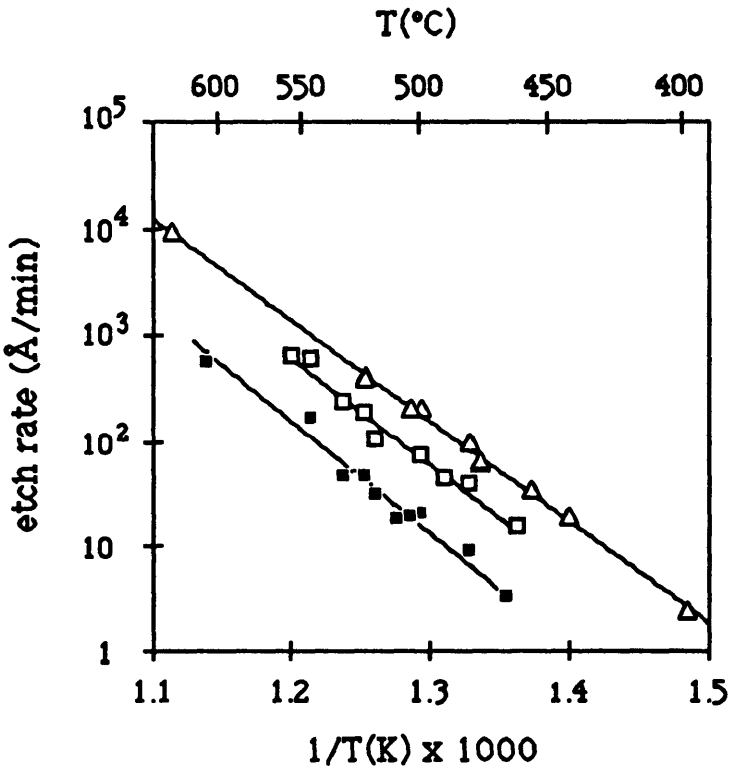

Figure 3.5: Arrhenius diagram illustrating etch rate as a function of temperature at 3 different CH_3I concentrations. y_{CH_3I} = 0.0012 (solid squares), 0.0060 (open squares), and 0.015 (open triangles).

correspond to activation energies of 43 (y_{CH_3I} = 0.015), 45 (y_{CH_3I} = 0.0060), and 47 (y_{CH_3I} = 0.0012) kcal/mol. Several experiments were also performed with y_{CH_3I} = 0.025 in 2100 sccm of helium and the activation energy was again found to be 43 kcal/mol. Although the activation energy did not depend on the carrier gas used, absolute etch rates in a helium carrier were roughly 1.5 times lower than for a hydrogen carrier gas under the same conditions of temperature, flow rate and y_{CH_3I}.

The effect of changing the inlet concentration of CH_3I (y_{CH_3I}) on the etch rate of GaAs (100) + 2°(011) substrates was studied at 4 susceptor temperatures, 480°C, 500°C, 525°C, and 550°C. The results are shown in Figure 3.6. From this data, a reaction order (n) in inlet CH_3I was determined by a least squares fit of the data to an assumed rate expression of the form:

$$\text{etch rate} = \text{constant } (y_{CH_3I})^n \qquad (3.2)$$

The reaction orders thus determined were 0.84 (480°C), 0.83 (500°C), 0.80 (525°C), and 0.68 (550°C). The computed lines corresponding to these reaction orders are also shown in Figure 3.6.

The effect of varying the total gas flow on etch rate was studied on GaAs (100) + 2°(011) substrates. In these experiments, the etch temperature was a constant 492°C, y_{CH_3I} was held constant at 0.015, and the carrier gas was hydrogen with a total flow that was varied between 500 to 5000 sccm. The results of these experiment are

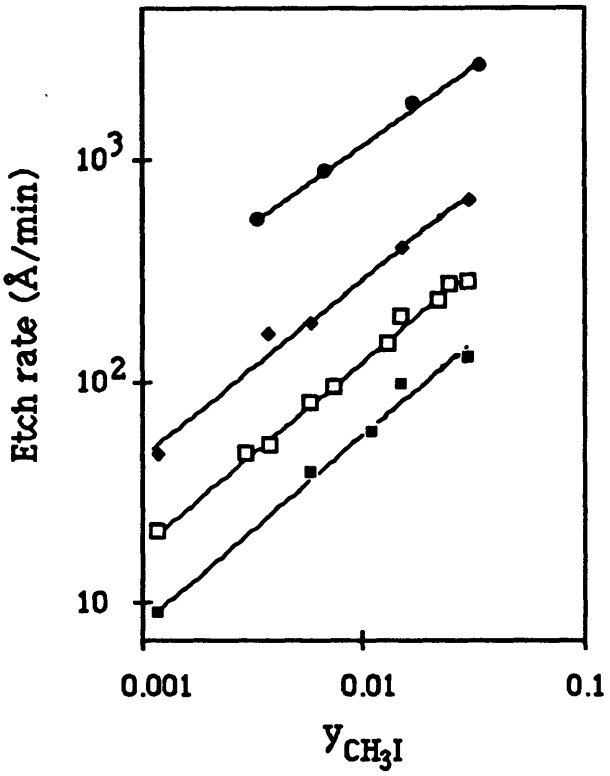

Figure 3.6: Etch rate dependence on y_{CH_3I}. Etch temperatures: 480°C (filled squares), 500°C (open squares), 525°C (diamonds), 550°C (closed circles). Lines fit to data points by least squares.

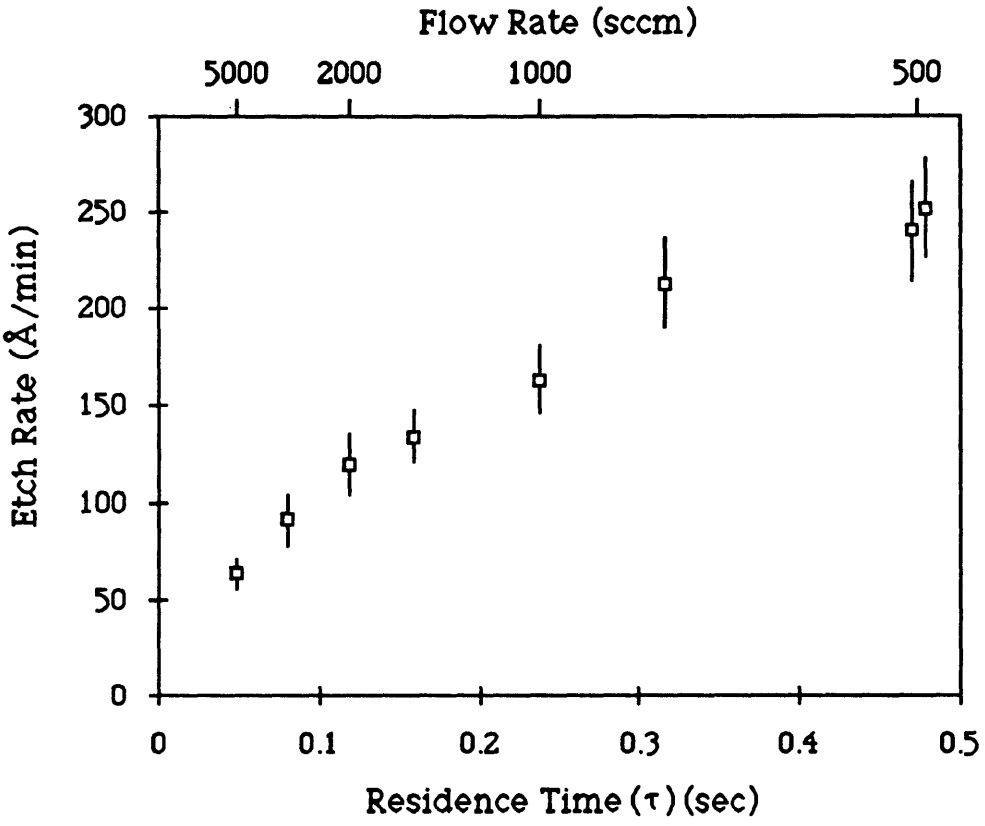

Figure 3.7: Effect of reactor gas residence time (τ) on etch rate of GaAs. Etch temperature 492°C, $y_{CH_3I} = 0.015$.

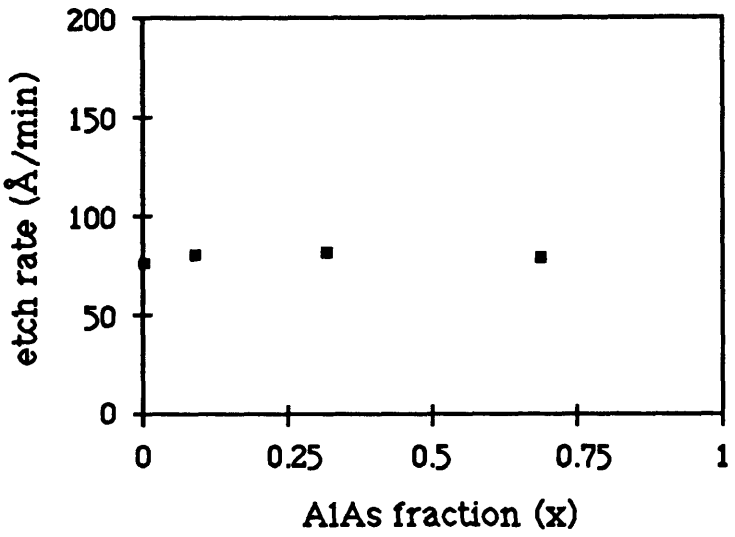

Figure 3.8: Etch rate of $Al_xGa_{1-x}As$ samples as a function of x. Etch conditions, 480°C, y_{CH_3I} = 0.015, and H_2 flow = 2100 sccm.

plotted in Figure 3.7 which shows etch rate as a function of the reactor gas residence time, τ ($\tau \sim$ 1/(flow rate)).

Finally, the effect of aluminum content (x) on the etch rate of OMVPE deposited $Al_xGa_{1-x}As$ was examined at an etch temperature of 480°C and $y_{CH_3I} = 0.015$. These results are shown in Figure 3.8 which clearly shows the etch rate to be independent of aluminum content (x) for all values studied (maximum of 0.7).

It is now of interest to properly classify the CH_3I vapor etch of GaAs based on the experimental results presented in this section. Vapor phase processes which result in a surface observable effect such as growth or etching are known to operate under a variety of rate limiting factors. These factors are generally grouped into one of two categories, vapor phase mass transport limitations and chemical kinetic limitations. Gas phase mass transport limitations will be encountered when surface reactivities are high relative to gas phase diffusion processes, this situation being characterized by the surface Dahmkohler number (Da_{II}) >>1. Experimentally, the observed temperature dependence of mass transport rate limited processes will be small, observed activation energies < 10 kcal/mol. Additionally, raising the gas flow rate in mass transport controlled processes will result in increased rates due to the associated decrease in the diffusion boundary layer thickness. This effect has been observed in OMVPE GaAs (Leys and Veenvliet, 1981)

In contrast to mass transport control, kinetic controlled processes are characterized by high activation energies (> 10 kcal/mol). From the observed activation energy (43 - 47 kcal/mol), it is clear that CH_3I vapor etching is kinetically controlled over the temperature range studied. The nature of this kinetic control becomes clearer when all of the data presented in this section are considered.

The general classification of kinetic control itself tells little about the nature of the rate limiting kinetics, ie. surface or gas phase. Such distinctions can be drawn through additional experimental analysis. One of the more revealing experiments is the effect of varying gas flow rate on the etch rate at a fixed wafer position (Figure 3.7). If surface kinetic processes are solely rate limiting, then the altering of gas phase reaction conditions would have no effect on the rate. Since an effect of flow rate is observed, the main kinetic limitation is in the gas phase. A good candidate for the rate limiting reaction is the unimolecular decomposition of CH_3I to CH_3 and I; the reported activation energy for this reaction is 42.5 kcal/mol (Saito, et al, 1980), close to our measured global activation energy of 43 - 47 kcal/mol (Figure 3.5). This contention is further supported by the observed reaction order being close to 1.0 for temperatures at or below 525°C (Figure 3.6) and by the fact that $Al_xGa_{1-x}As$ and GaAs show no differences in etch rate at 480°C (Figure 3.8).

The data in Figure 3.7 is linear in residence time for the higher flow rates (>2000 sccm, $\tau<0.12$), consistent with a plug flow reactor description of the system. Departures from plug flow behavior are

observed at higher residence times (lower gas flow velocities). At these conditions, an additional resistance appears which is likely due to an increase in the vapor phase mass transfer resistance acting in series with the gas phase decomposition resistance. The onset of an additional mixed regime may also be occuring at higher temperatures; at 550°C the reaction order in CH_3I is seen to drop to 0.63, suggesting that surface saturation kinetic resistances are acting in series with the gas phase decomposition resistance. Only a limited amount of data was gathered at higher etch temperatures, precluding further speculation on the nature of these surface kinetic effects.

3.3.2 Etching in the Horizontal Reactor - Surface Morphology

One of the most technologically important characteristics of an etch process is that the resulting surface morphology is featureless and specular. A major objective in development of CH_3I vapor etching of GaAs was, therefore, to determine conditions under which etched surfaces of GaAs remained smooth. Two factors were found to contribute to the etched surface morphology, the initial state of the surface (prior to loading into the reactor) and the etch conditions. The initial surface state was reproducibly controlled throughout these experiments in order to isolate the effects that reaction conditions have on etched surface morphology.

Control of the initial GaAs surface is achieved by employing a sequence of chemical treatments. The importance of having a clean initial GaAs surface prior to epitaxy has long been recognized in the OMVPE and MBE fields. The wafer preparation procedure developed for the CH_3I vapor etching experiments was adapted from a procedure developed for GaAs substrates prior to OMVPE growth (Wang, personal communication). The exact procedure used in this work is outlined in section 3.2.2. In general, departures from this procedure will lead to etched surfaces of inferior surface morphology. Additionally, initial surface purity is limited by the brief air exposure that the bare wafer surface undergoes just prior to loading into the reactor. At least a small degree of surface oxidation is expected to occur during this time due to both atmospheric oxygen and humidity. Nevertheless, reproducibility was quite good during these experiments as was confirmed by intermittent control experiments. Although *in situ* removal of surface oxides is presumed to occur under heating in hydrogen (Buhaenko et al, 1989), complete removal was verified by AES to a level of <1%.

An example of the time evolution of etched surface morphology is shown in Figure 3.9. This figure shows three GaAs (100) + 2°(011) surfaces etched at 500°C with $y_{CH_3I} = 0.015$ for 30, 60, and 120 minutes. Two distinct morphological features are seen to grow. Etch pits, consistently elongated in the (011) direction are observed to form and these pits increase in size linearly with time. Additionally, the bulk surface exhibits a finer, overall roughness which becomes

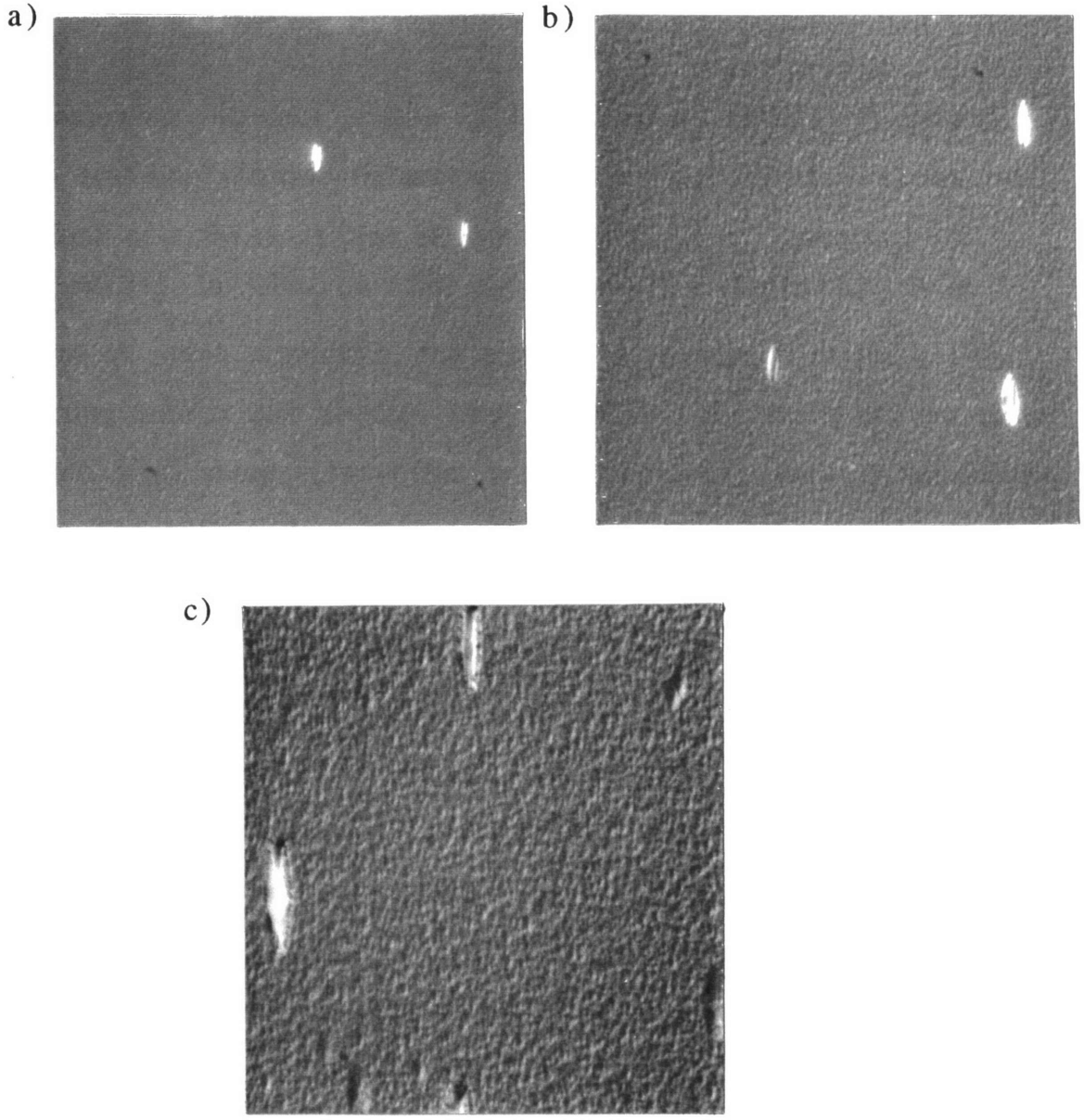

Figure 3.9: Evolution of etched surface morphology, etch conditions 500°C, y_{CH_3I} = 0.015, a) 30 minutes, b) 60 minutes, c) 120 minutes. (magnification X1060)

more apparent at longer times. The etch pit sidewalls appear to be faceted but the bulk surface roughness is more random.

A somewhat different picture of these surface features is provided from scanning electron microscopy (SEM) Figure 3.10a,b shows two portions of a GaAs surface etched at 500°C for 45 minutes with y_{CH_3I}=0.015. In 3.10a, an SEM photograph of a single etch pit is shown. A noted previously, the etch pit is elongated in the (110) direction and as can be seen from the figure, the sidewalls are quite smooth with sharp intersection angles, indicating definite crystalline habit. The bulk surface appears to have a very fine structure with length features on the order of 0.1 micrometer (1000Å). This is most likely due to the bulk surface roughness as seen in Figure 3.9a The fact that the SEM and optical images are qualitatively different is due to the fact that SEM is in general less sensitive to fine scale surface structures than Nomarski interference. It is apparent from Figure 3.10b that these etch pits exhibit variability, possibly due to different defects resulting in qualitatively similar etch pit structures.

The length of the observed etch pits can easily be measured directly from either the NIM or SEM photographs. It was therefore possible to quantitatively analyze the kinetics of etch pit growth. The evolution of etch pits was studied as a function of etch temperature and y_{CH_3I}. The length of these etch pits was observed to grow linearly with time. Figure 3.11 shows the temperature dependence of the etch pit length growth rate at constant y_{CH_3I} = 0.015 in an Arrhenius plot. The activation energy determined by least squares fit to the data is 60

a)

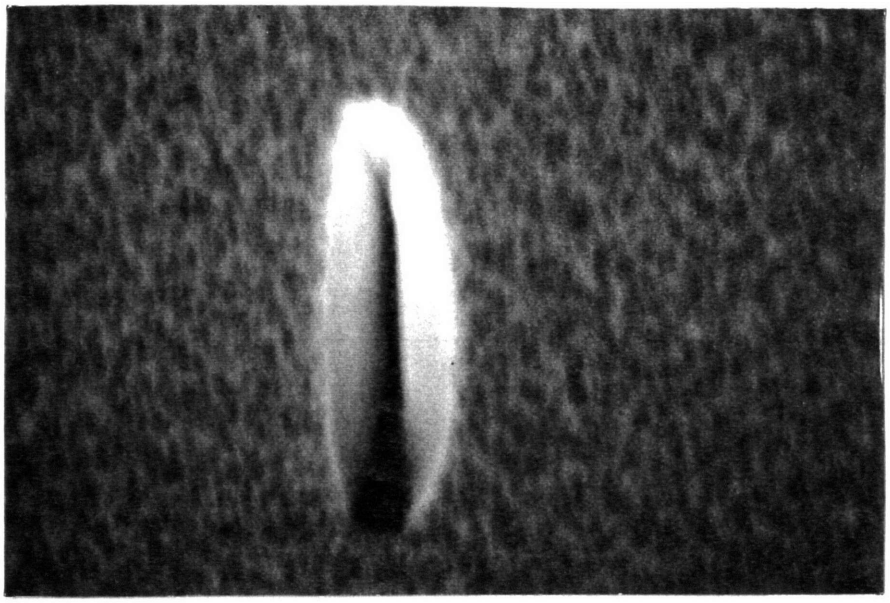

b)

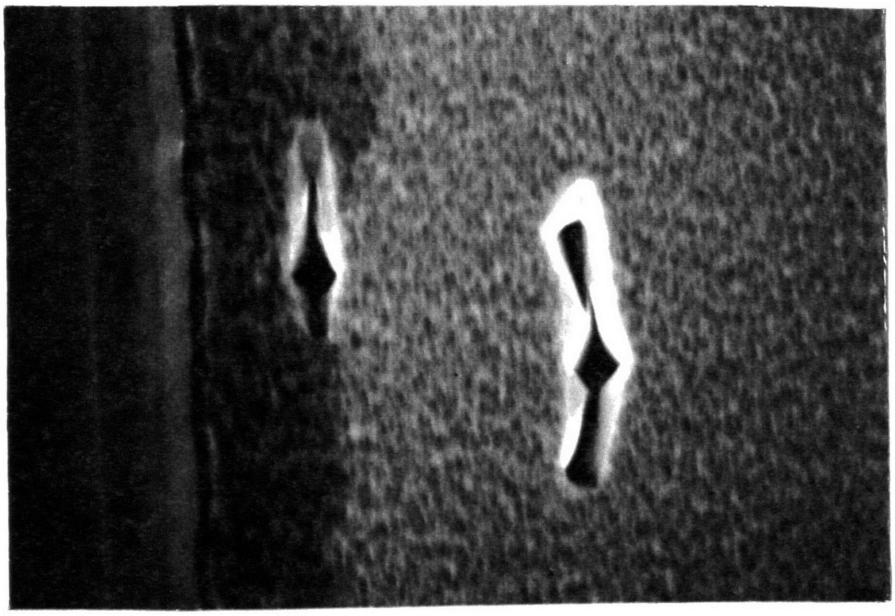

Figure 3.10: Scanning Electron Micrographs of etched GaAs surface 500°C, y_{CH_3I} = 0.015, 45 minutes, a) 10,000X, b) 5000X.

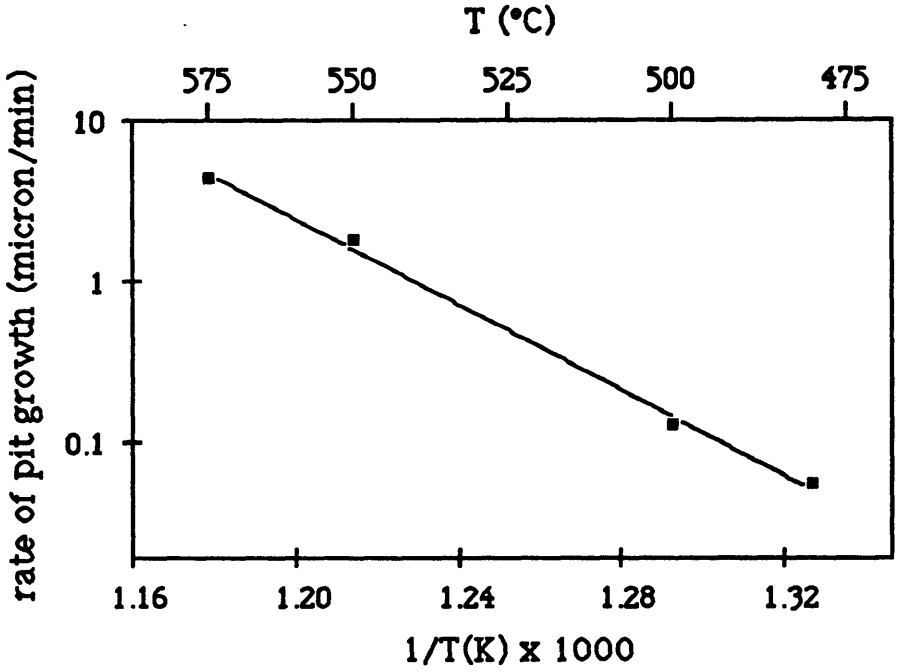

Figure 3.11: Arrhenius plot of etch pit growth rate (based on length). Etch conditions, y_{CH_3I} = 0.015, 2100 sccm H_2.

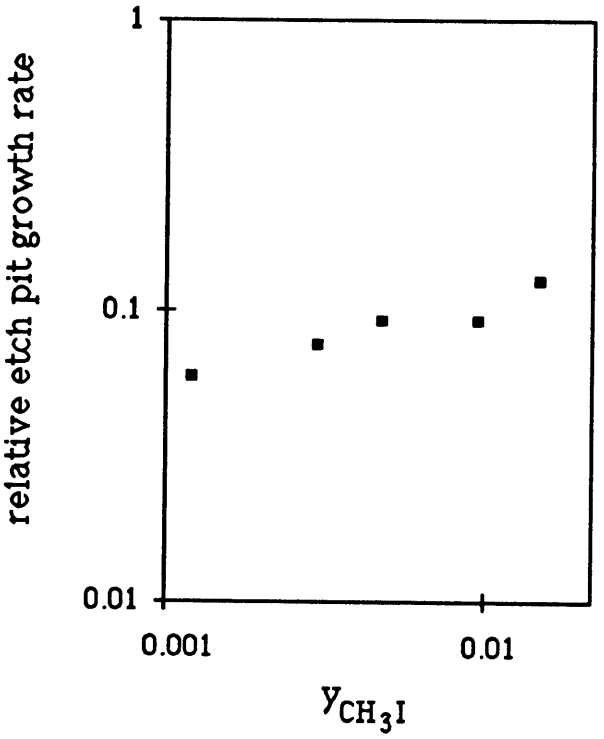

Figure 3.12: Etch pit growth rate as a function of y_{CH_3I}. Etch temperature 500°C.

kcal/mol. Figure 3.12 shows the CH_3I concentration dependence of etch pit growth rate. The apparent reaction order for etch pit growth as a function of y_{CH_3I} was determined from this picture to be 0.27. This relatively small reaction order suggests that surface saturation kinetics are controlling the rate of etch pit growth. Based on these data alone, the possibility of additional rate controlling resistances cannot be ruled out, however.

The bulk surface roughness, unlike the etch pits, is more difficult to quantitate from optical and SEM photomicrographs. Analysis has therefore limited to subjective observations from optical photomicrographs. The appearance and magnitude of the surface roughness was comparatively studied as a function of various reactor operating conditions. Direct comparisons between samples was considered valid for cases where the etched depths of the samples were equal. It was observed that the surface roughness improved with decreasing temperature at a fixed mole fraction of CH_3I. Furthermore, for fixed etch temperature and etch depth, surface roughness improved with increasing mole fraction of CH_3I. These results are summarized in Figure 3.13 which shows three regimes of surface morphology (good, fair, and poor) as a function of temperature and etch rate (i.e. y_{CH_3I}) for a total etched depth of 1000Å. It is important to note that the etch times are also decreasing in order to maintain a constant etched depth with increased y_{CH_3I}. Etched surfaces remained specular at temperatures of 480°C for etching times up to 1 hour (depths up to 0.9 microns) and at 500°C for etching times up to 15 minutes (depths up to 0.5 micron). Above

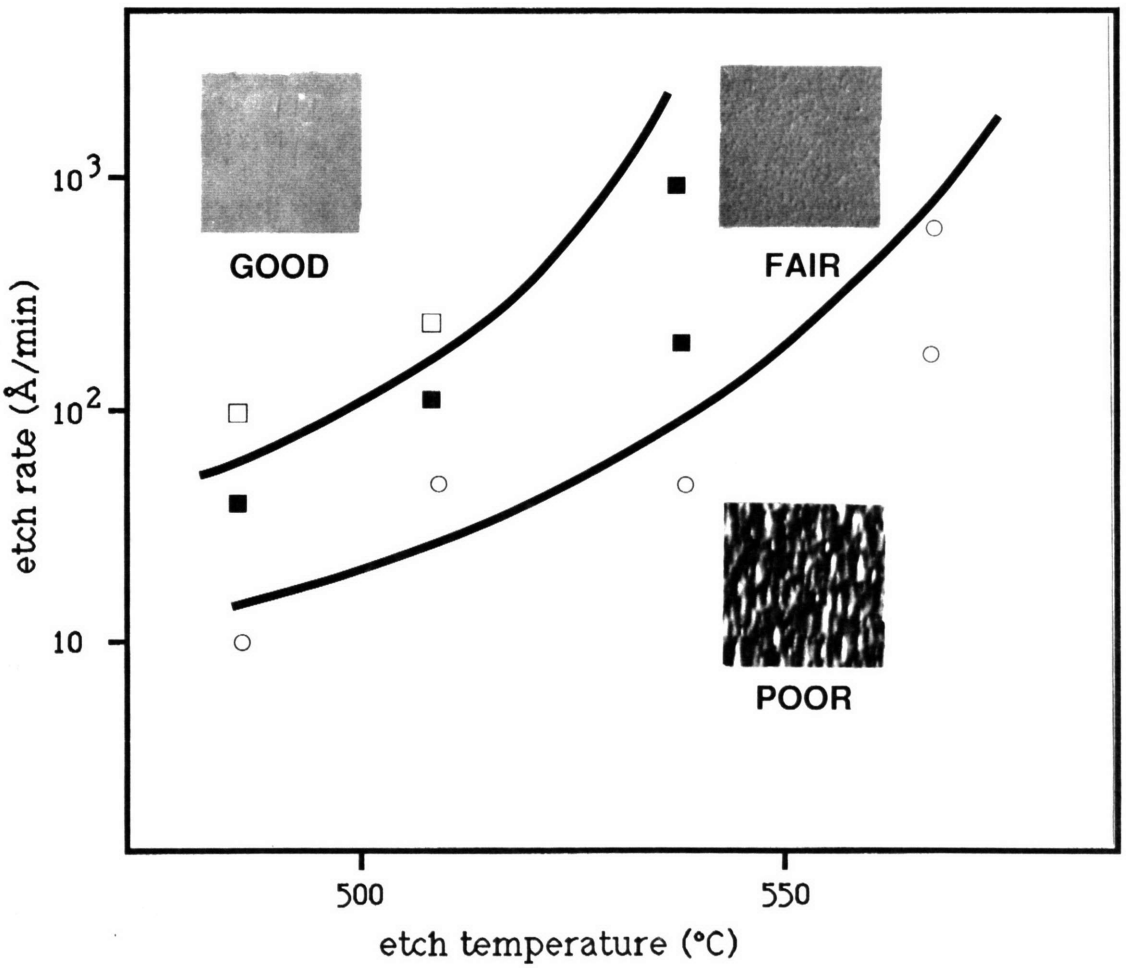

Figure 3.13: Surface morphology as a function of temperature and etch rate (etched depth = 1000Å).

520°C, surfaces were generally degraded in times as short as 5 minutes (depths up to 0.35 micron). AES was performed on samples with different morphologies (i.e. good vs. poor) and it was determined that the surface stoichiometric ratios of gallium and arsenic were unchanged from that of untreated GaAs.

In the vapor etch studies using chlorine containing compounds discussed in Chapter 2, it was consistently shown that smooth etched surface morphologies could only be obtained under conditions where the supply of etchant from the gas phase was rate limiting. In most cases this was observed only at high temperatures. At lower temperatures, etch rates were surface kinetically limited and etched surface morphologies were degraded. This observation suggests a causal relationship between surface kinetic limitations and degraded etched surfaces. The nature of surface reactions which would lead to increased surface roughness is not clear, however. CH_3I vapor etching provides another example of a relationship between rate limiting surface resistances and degraded surface morphologies. Although etch rates are primarily controlled by the decomposition of CH_3I in the gas phase, a surface rate controlling resistance has been observed at higher temperatures. It is also at these higher temperatures (>550°C) that the most degraded etched surfaces are formed. It is proposed that the rate controlling surface reaction is also responsible for the degraded surface morphologies. At temperatures below 520°C, this surface reaction is relatively fast compared to the gas phase decomposition of CH_3I while at higher temperatures, the surface reaction becomes relatively slow in comparison. This would

be the case if the activation energy of the surface reaction were less than 42.5 kcal/mol, the value for CH_3I decomposition.

Etch pits have been attributed to the presence of edge dislocations in the crystal at the surface (Gatos, 1962). These dislocations create lattice strain which can locally enhance chemical reactivity. Further, the atomic level structure of dislocations is such that there are many more dangling bonds present within the dislocation than on the bulk of the wafer surface, the availability of which may contribute to the locally enhanced reactivity toward the etchant species. The fact that local rate enhancements are observed in the form of etch pits on the surface is another argument for the existence of a slow surface reaction step on the bulk surface. Otherwise, if the etch rate were controlled solely by the gas phase decomposition of CH_3I and all surface reactions were infinitely fast, no means would exist for surface reactivity differences to manifest.

3.3.3 Etching in the Horizontal Reactor - Carbon Deposition on Etched Surfaces

The problem of carbon incorporation into OMVPE grown GaAs has been the subject of several studies (Keuch et al, 1984, van de Ven et al, 1986). Carbon from methyl radical ligands attached to gallium in $(CH_3)_3Ga$ and arsenic in $(CH_3)_3As$ has been conclusively shown to incorporate as an electrically active impurity in OMVPE grown GaAs (Lum, et al, 1988). The specific mechanisms for carbon incorporation

into OMVPE grown GaAs have not been conclusively determined at this time. The link between methyl containing compounds and carbon incorporation has been confirmed and therefore must be of concern with the methyl containing CH_3I vapor etch.

Carbon has been observed to deposit on a number of GaAs samples etched with CH_3I. The information is limited, however, to qualitative observations and no attempt was made to quantify these data. Carbon deposits appeared as soot colored films or patches on the etched GaAs surface. These carbon deposits never formed on the Si_3N_4 mask. In most cases, the carbon deposits were very weakly attached to the underlying GaAs substrate, a simple rinse in water or air blast would usually suffice for complete removal of these carbon films. One carbon film removed in this fashion was examined by AES by first lifting the film off of the GaAs substrate in DI water and subsequently capturing the film onto a silicon wafer. The Auger spectrum of the film is shown in Figure 3.14. It is nearly pure carbon, probably amorphous or graphitic, and no gallium or arsenic appears in the spectrum indicating that the film contains <1% of these elements.

Throughout the course of this work, steps were taken in order to minimize the occurrence of the carbon deposition. Wafer surface preparation was found to have an influence on the occurrence of carbon deposition. Specifically, carbon deposition was always encountered when the pre-etched surface was suspected to have photoresist or other carbon containing residues. These problems

could be reduced or completely eliminated if steps were taken to insure that the initial surface was carbon free. For example, when photoresist residue was known to be present, it was found that cleaning of the wafer by several immersions in concentrated (97%) H_2SO_4 under ultrasonic agitation led to etched surfaces with less subsequent carbon deposition than samples that were not cleaned in this fashion. Even in the cases where carbon films were observed to form, little or no effect on the measured bulk etch rate was observed. These films are apparently quite porous and therefore does not act to mask the surface from the etching vapors.

In addition to surface precleaning, carbon deposition also depends on the conditions of reactor operation. As was the case with surface morphology degradation, high etch temperatures and long exposure times generally led to increased carbon deposition. By etching at low temperatures for short times, these deposits could be avoided. The possible link between carbon deposition and degraded surface morphology was examined and is presented in Figure 3.15. Figure 3.15a is an optical micrograph of the surface of a sample etched with CH_3I at 500°C for 45 minutes (etched depth = 9000Å) photographed at 1060X on an optical microscope. Figure 3.15b shows the same surface after rinsing in DI water. The dark spots which show up in 3.15a have been washed away. These dark spots are early stages of the carbon film formation. Figure 3.15c shows the same surface as 3.15b, only in this photograph the Nomarski interference filter was used which highlights the surface morphology features. The two surface morphology features discussed in section 3.3.2 are present on

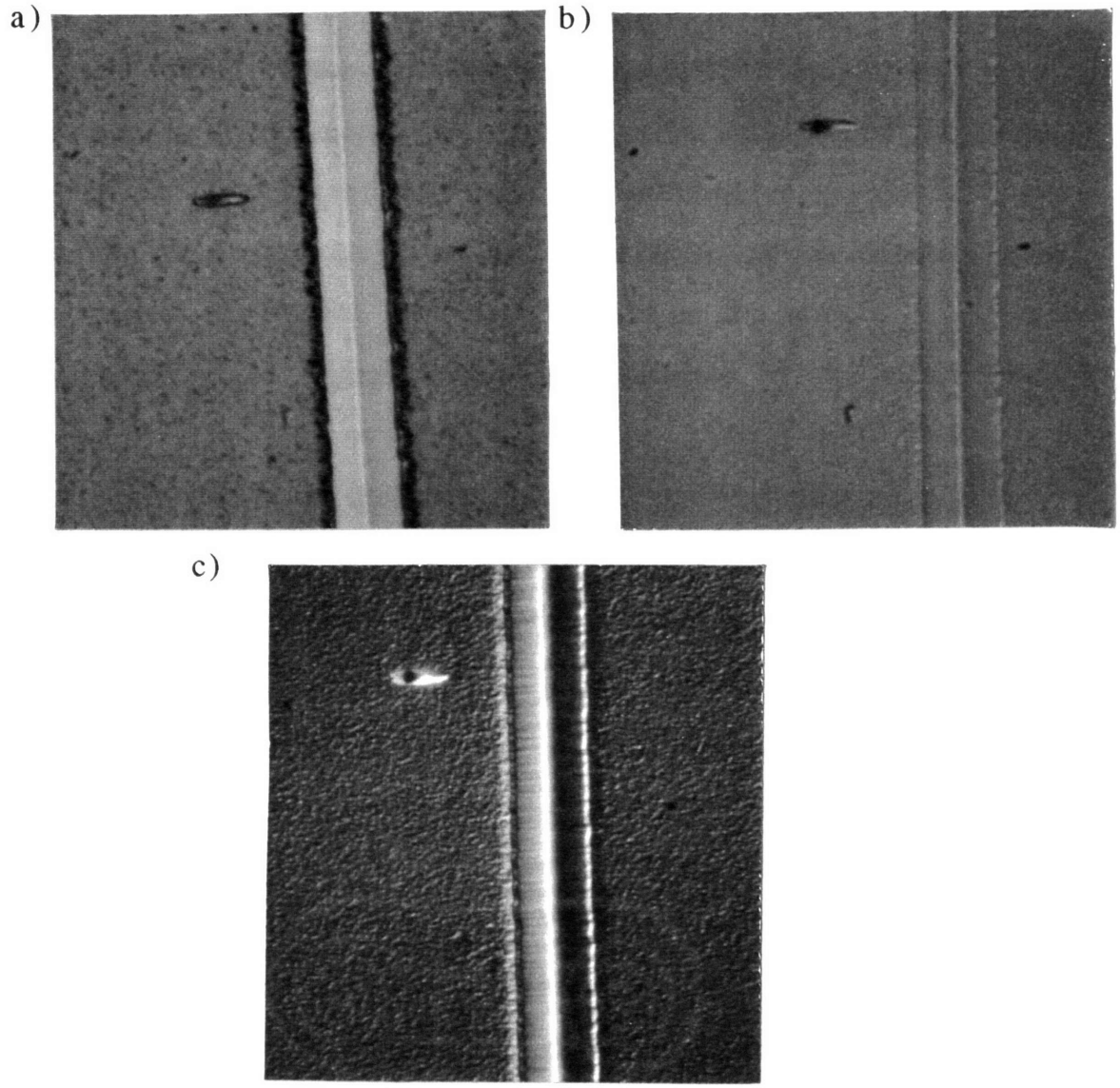

Figure 3.15: Photomicrographs of etched GaAs surface showing regions of carbon deposition. a) Surface etched at 500°C, 45 minutes, dark areas are carbon deposits. b) Same as a) after rinsing in DI water to remove carbon deposits. c) Same as b) with Nomarski interference on. (all photographs magnification X1060).

this sample, a single etch pit can be seen near the lower center of the photograph and the overall surface exhibits the same characteristic roughness. From Figure 3.15a, it is apparent that the carbon deposition is the greatest near the mask edge and around the edge of the etch pit. The rest of the surface is uniformly covered with spots of carbon. In Figure 3.15b, almost all of these carbon deposits have been washed away. One dark spot remains at the bottom of the etch pit, apparently the deposit here was unaffected by the water rinse.

From a processing perspective, it is important to emphasize the strong link observed between surface carbon deposition and surface preparations, especially when organic chemicals are used at any processing stage. Optimization of wafer cleaning procedures combined with operating the etch at low temperatures should completely eliminate carbon deposition of the forms discussed in this section, ie. soot-type films with poor substrate adhesion. Also of practical concern is the possibility of carbon chemically bound to the etched surface or chemically incorporated into the crystal near the surface. This issue is addressed in the next section.

3.3.4 OMVPE Growth of GaAs on CH_3I Vapor Etched Substrates

One of the potential applications for CH_3I vapor etching is as an *in situ* wafer cleaning step prior to OMVPE growth. The main requirements for such an *in situ* vapor etch are that the etched

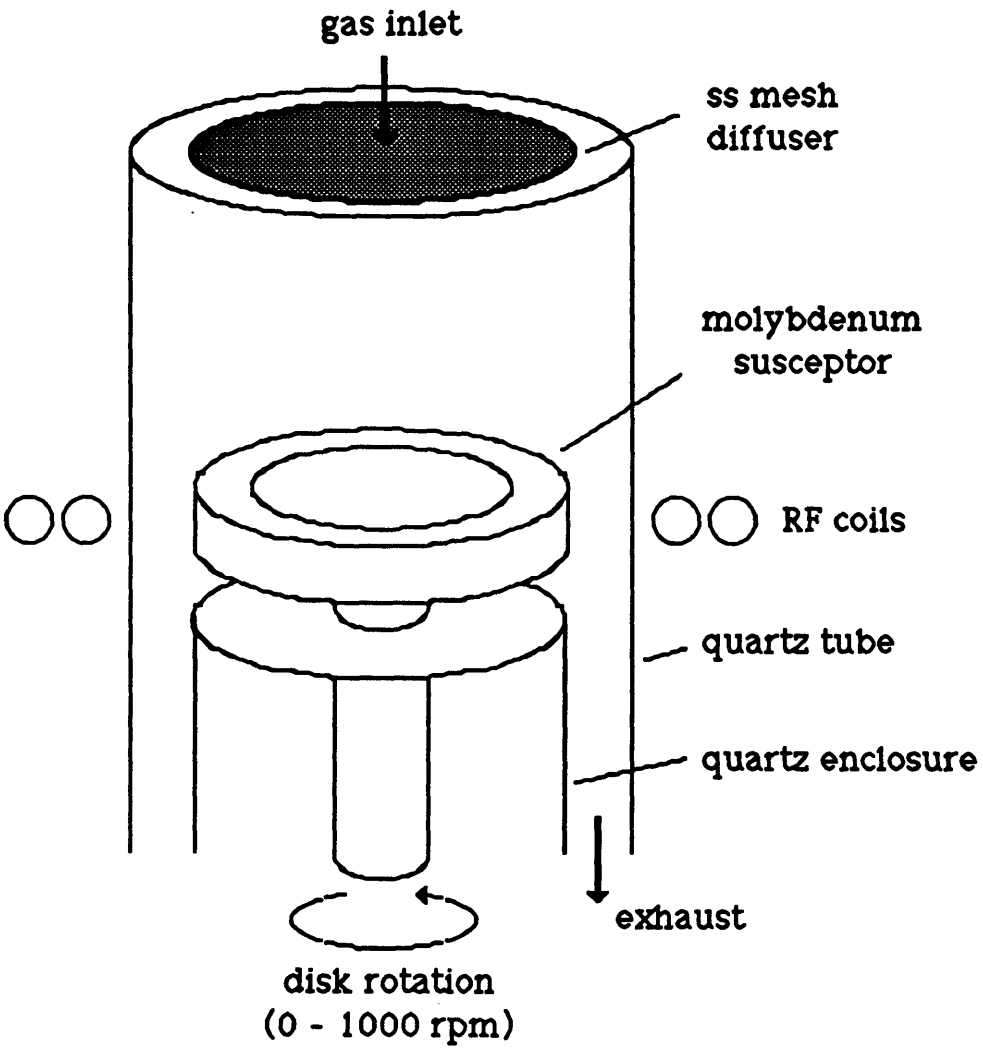

Figure 3.16: Schematic of vertical rotating disk reactor used for OMVPE growth of GaAs.

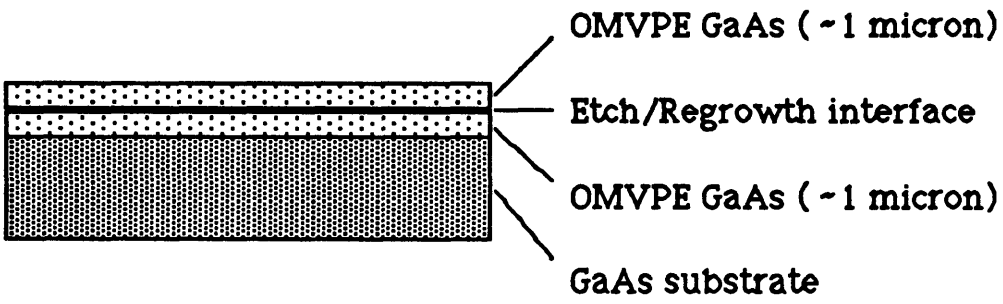

Figure 3.17: Test structure used for regrowth studies

surface remains smooth and free of any chemical contamination or surface states. Many of the factors which influence the surface quality have been discussed in the previous two sections. In this section, experiments involving OMVPE regrowth on CH_3I vapor etched GaAs surfaces are presented.

The procedure followed in these experiments is outlined in section 3.2.4. In short, several previously deposited OMVPE GaAs layers were subject to CH_3I vapor etching in the horizontal reactor system and then loaded into the vertical rotating disk reactor (schematically shown in Figure 3.16) for OMVPE growth of GaAs. The resultant structure is shown schematically in Figure 3.17. Etch temperatures from 460-520°C and CH_3I mole fractions (y_{CH_3I}) from 0.005 to 0.03 were studied. The interface between the two epitaxial layers was probed by capacitance-voltage (C-V) and SIMS analysis. In addition, the surface morphology of the re-grown epitaxial layers was examined using Nomarski interference microscopy.

Figure 3.18 shows a representative C-V profile of a sample for which an epitaxial GaAs layer was briefly exposed to air and then reloaded into the reactor for growth of the second epitaxial layer. The peak at 1 micron depth is due to electron accumulation at the regrowth interface. Electron accumulation can result from chemical impurities or electron traps at the interface and in this case, the interface contamination occured during the period of ambient exposure. The area under these peaks is used as a measure of total charge accumulation near the interface. Figure 3.19 shows the integrated

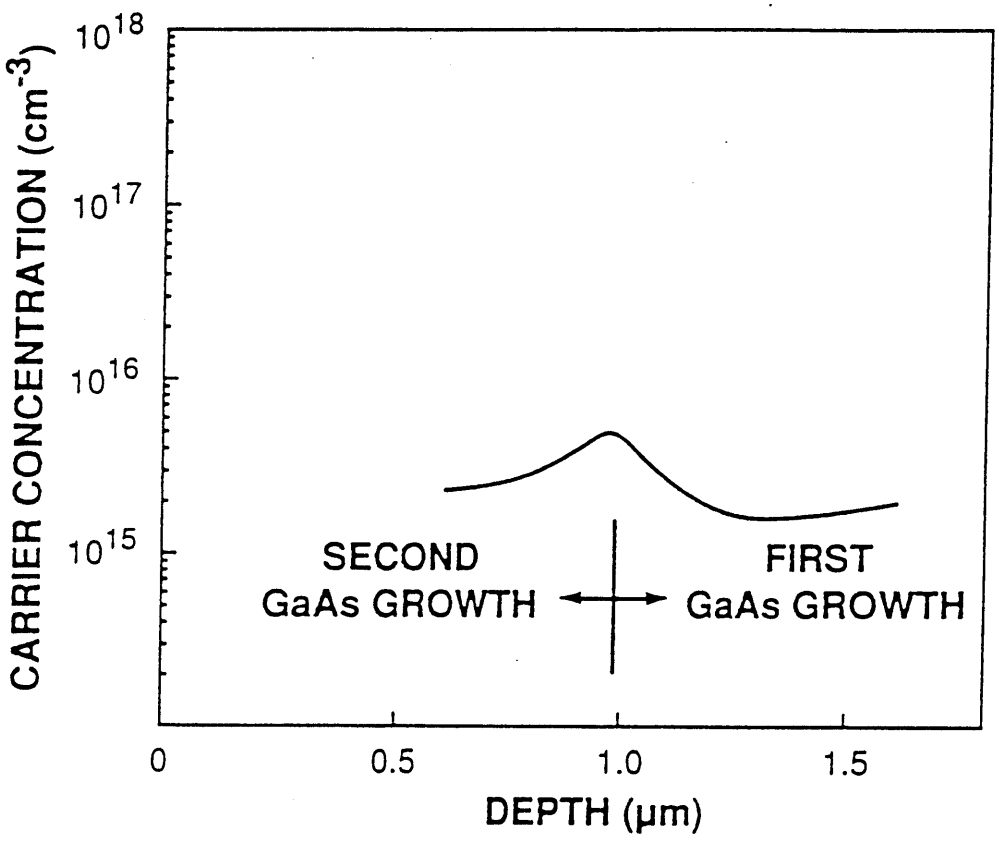

Figure 3.18: C-V profile for regrowth structure for which the interface was untreated (air exposed).

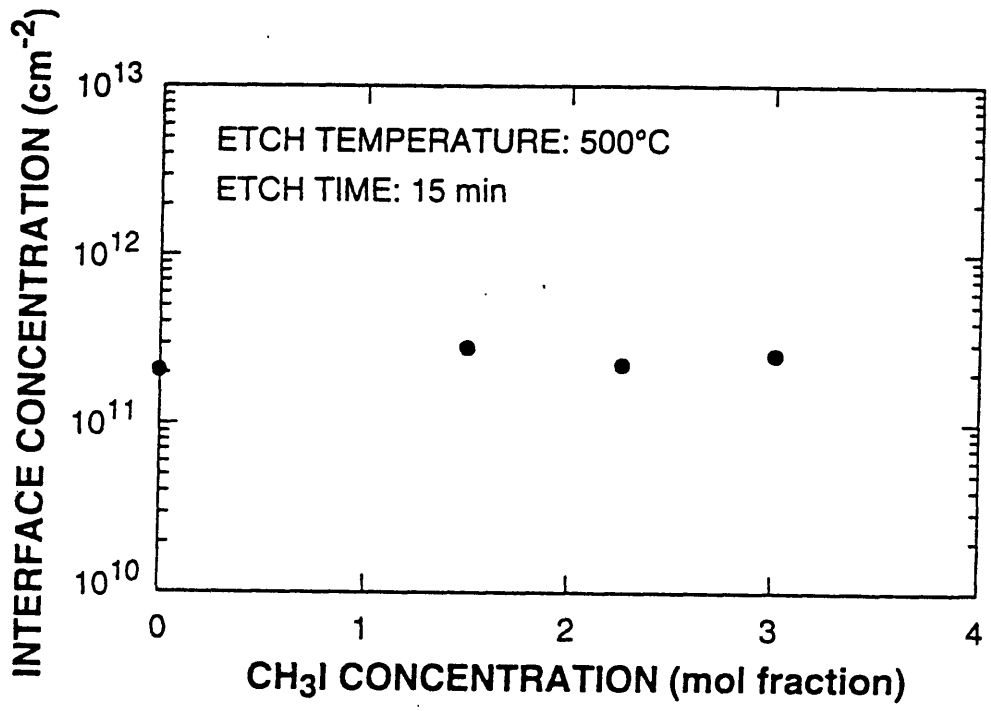

Figure 3.19: Total electron accumulation at etch/regrowth interface as a function of y_{CH_3I}. Etch conditions 500°C, 15 minutes.

total interface electron accumulation as a function of CH_3I concentration for an etch temperature of 500°C and an exposure time of 15 minutes. Similarly, Figure 3.20 shows the total electron accumulation as a function of etch temperature and etch time (either 15 or 30 minutes). From these two figures, it is apparent that the electrical charge characteristics of the etch/regrowth interface do not depend on etch temperature from 480 to 520°C, etch time up to 30 minutes, or CH_3I concentration up to 3.0 mol%.

The C-V measurement does not directly provide information about the chemical composition of the interface. Charge accumulation may occur as a result of chemical impurities or interface traps, but chemical impurities are not necessarily electrically active (Keuch, et al, 1986). It is therefore important to supplement C-V measurements with a SIMS depth profile of atomic composition in order to identify the chemical composition of the interface. This was done for several samples and the results are summarized in table 3.3. The major interfacial impurities detected by SIMS are oxygen, silicon, and carbon. It can be seen from table 3.3 that CH_3I vapor etching tends to reduce the amount of silicon impurity at the regrowth interface. The amount of carbon impurity depends on the etch temperature and remains undetectable for etch temperatures below 480°C.

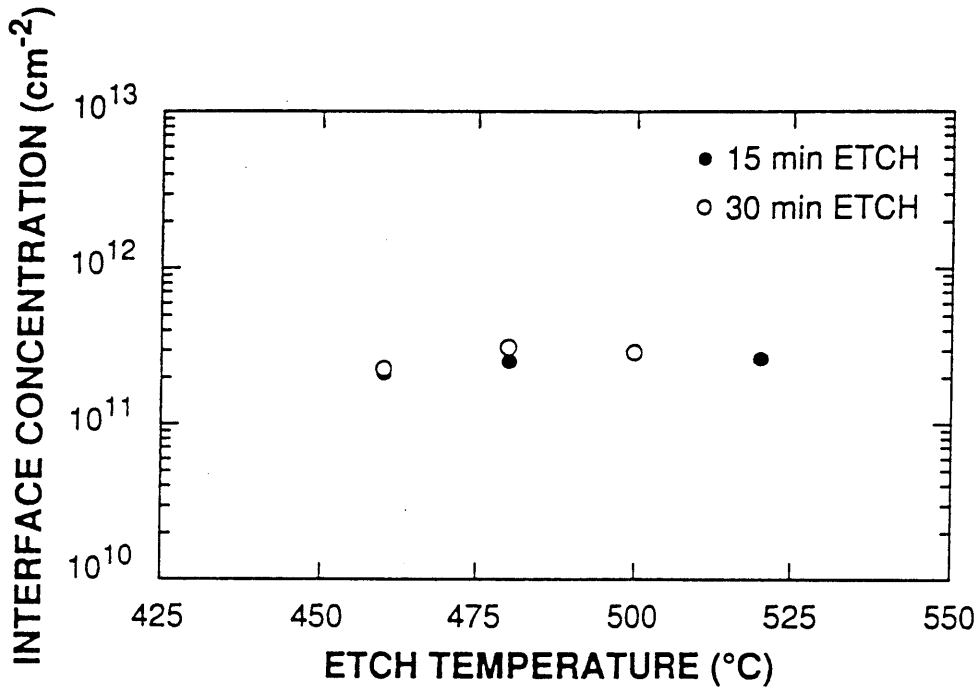

Figure 3.20: Total electron accumulation at etch/regrowth interface as a function of etch temperature and etch time, y_{CH_3I} = 0.015.

etch temp (°C)	etch depth (Å)	interfacial charge (cm^{-2})	SIMS Si (cm^{-3})	SIMS C (cm^{-3})	SIMS O (cm^{-3})
480	1000	$2.5x10^{11}$	$4x10^{16}$	nd	nd
500	2200	$2.7x10^{11}$	$6x10^{16}$	$4x10^{16}$	$4x10^{17}$
520	4400	$2.6x10^{11}$	$7x10^{16}$	$2x10^{17}$	$2x10^{17}$
no etch	0	$1.7x10^{11}$	$2x10^{17}$	nd	nd
H_2SO_4 rinsed	0	$5.2x10^{11}$	$1x10^{17}$	$2x10^{16}$	$3x10^{17}$

Table 3.3: Summary of etch/regrowth structures analyzed by C-V and SIMS depth profiling.

3.4 CONCLUSION

Vapor etching of GaAs and $Al_xGa_{1-x}As$ by CH_3I was demonstrated. Etch rates depend strongly on temperature, with an overall activation energy for the process near 45 kcal/mol. Observations of the etch rate dependence on CH_3I concentration and total gas flow rate led to the conclusion that the etching process occurs primarily under a condition of gas phase kinetic control with a secondary surface kinetic limitation which becomes more pronounced at temperatures above 525°C. The kinetically limiting step in the gas phase is the decomposition reaction of CH_3I but the surface kinetic limitation(s) is (are) not known. Surface reactions give rise to degraded surface morphologies at temperatures above 520°C and are additionally responsible for the sublinear dependence of etch rate on inlet CH_3I mole fraction at 550°C. At temperatures below 520°C, etched surfaces with specular morphologies could be maintained for etch depths up to 0.9 microns. In contrast to other vapor etch systems OMVPE regrowth on CH_3I vapor etched substrates revealed a lowering of both electrically active and chemical impurities at the etched surface/epilayer interface. Thus CH_3I vapor etching appears to be a promising alternative for use *in situ* of OMVPE systems.

Chapter 4

Vapor Etching of Patterned GaAs Substrates by CH_3I

4.1 INTRODUCTION

In situ vapor phase etching of three dimensional features would be a useful technique for fabrication of several opto-electronic and micro-electronic devices. One major advantage of *in situ* processing in optoelectronic device fabrication relates to the problem of $Al_xGa_{1-x}As$ oxidation from ambient exposure which can be detrimental to device performance. An example is the fabrication of a transverse junction buried heterostructure laser diode reported by Shimoyama et al (1988). Fabrication of this device involved several OMVPE growth steps interupted by masking and etching steps which were immediately followed by OMVPE regrowth. Shimoyama et al performed the etching *ex situ* which resulted in ambient oxidation of the exposed epilayers, especially the $Al_xGa_{1-x}As$ layers. To remove the oxide layer and improve the regrowth, they employed a short *in situ* HCl vapor etch step prior to OMVPE regrowth. If the entire etch step were performed *in situ* in the OMVPE reactor one would expect further improvement in device performance.

Two important phenomena can occur during vapor etching of materials partially covered by inert masks. First, localized etching enhancement near the mask can occur which is caused by the diffusion of etchant species from the inert mask to the chemically active surface. Enhancement will be observed in cases where the etching surface reactions are not solely rate limiting. Specific mechanisms of lateral transport are not known *a priori* but will involve some combination of surface and vapor phase volume diffusion. The second important etch characteristic is that as etching proceeds, sidewalls are formed at the mask/substrate interface. It is desirable for these sidewalls to have low reactivity toward the etch in order to minimize mask undercutting. These surfaces of these will usually possess different crystallographic orientations than the bulk substrate. It is therefore of interest to study the dependence of vapor etch rate on the orientation of the crystal.

4.1.1 Objective

The objective of this work is to study the etching of patterned GaAs substrates by CH_3I vapor. The problem is broken down into three component experiments (i) local etch rate enhancement due to the presence of inert masks is experimentally investigated as a function of mask size; (ii) etch rate as a function of crystallographic orientation is studied on bulk (111)Ga and (111)As GaAs substrates and compared to previous results from (100) surfaces (Chapter 3); (iii) etching of micro-facets of various orientations exposed on bulk substrates is studied. In the third case, surface reactivity differences

to drive diffusion processes. Finally, based upon these results, strategies for minimizing mask undercutting during CH_3I vapor etching are proposed and demonstrated.

4.1.2 Background

The phenomenon of growth or etch rate enhancement near inert masks has been observed by a large number of researchers in a number of different vapor growth and etching systems. Notable studies include Silvestri et al (1972) for germanium deposition near masks of SiO_2 and Oldham and Holmstrom (1967) and Takoudis et al (1989) for the vapor phase growth and etching of silicon. It is generally accepted that these enhancement effects result lateral transport of etchant or growth species from inert masks to chemically active surfaces. There are two potential mechanisms for this lateral transport, diffusion from the mask surface to the crystal and diffusion in the gas phase near the surface. Surface diffusion has been argued to be important in order to describe the observed saturation in rate enhancement with increasing mask width (Silvestri et al, 1972). Detailed numerical analysis of this problem has been undertaken for the OMVPE of GaAs from trimethylgallium by assuming that diffusion occurs in a two dimensional stagnant region above the substrate as well as on the surface (Coronell and Jensen, 1991). In this study, gas-phase diffusion effects where found to most strongly contribute to observed enhancements.

Crystallographic orientation dependence of surface reactivity has been observed in many semiconductor systems. On silicon single crystals, etch rates are generally slower on the more atomically dense crystal faces; the (111)Si surface is the slowest etching. In the III-V and II-VI binary semiconductor materials, however, the situation is quite different since the two constituent elements are chemically different, as reported by Gatos (1962) for several binary semiconductor compounds. On the basis of experimental findings, he argued that the difference in reactivities between the two (111) faces in zinc-blende semiconductor materials can be explained by simple chemical considerations. For the III-V compounds, the (111)A surface in ideal unreconstructed form is terminated in group III atoms (gallium, indium, aluminum) which are triply bonded to the underlying surface. In this configuration, the surface is devoid of any free electrons and is therefore relatively unreactive toward oxidizing agents (electron acceptors). In analogous fashion, the (111)B surface (in unreconstructed form) is terminated by group V atoms (arsenic, phosphorous, antimony) triply bonded to the surface. In this case, the unbonded orbitals are filled with two electrons each and therefore the reactivity toward oxidizing agents is high. Although both of these surfaces are expected to undergo surface atom rearrangements (Chadi, 1989), this theory of their chemical behaviour adequately explains observations made in several wet chemical etching systems.

Another interpretation of reactivity differences between (111)A and (111)B surfaces of GaAs was presented by Furuhata et al (1990).

They examined the etching of GaAs surfaces by Cl_2 under vacuum conditions (1 $x10^{-3}$ torr). A strong orientation dependence on etch rate was observed between the (111)Ga and (111)As surfaces under certain reaction conditions. At low surface temperatures (<450°C), the (111)As was the fastest etching surface followed closely by the (100) and (110) surfaces with the (111)Ga surface etching much more slowly. These results were explained by considering the formation and evaporation of the volatile $GaCl_3$ species to be rate limiting at low temperatures. On the (111)Ga face, this reaction is strongly inhibited due to the gallium atoms being triply bonded to the underlying surface. Conversely on the (111)As surface, surface gallium atoms are only singly bonded to the surface, hence there are more bonds available to react with chlorine to form $GaCl_3$. Naturally this implies that the formation and evaporation of arsenic species was rapid, even on the (111)As surface (where arsenic atoms are triply bonded to the underlying surface). At higher temperatures (>450°C), little difference in surface reactivity was observed. In this case, It was proposed that the volatility of GaCl is high enough that the formation of $GaCl_3$ is no longer necessary. This theory emphasizes the steric and kinetic effects that can occur on these surfaces, but is less general than Gatos' theory discussed above.

4.2 EXPERIMENTAL PROCEDURE

4.2.1 Lateral Diffusion Studies

For studying the etch rate enhancement near inert masks, wafers of (100) GaAs misoriented 2° to the (110) with various width stripes of silicon nitride were prepared by the following procedure. The wafers were first coated with 1000Å of plama enhanced chemical vapor deposition (PECVD) silicon nitride from SiH_4 and NH_3. The wafer was spin coated with photoresist over the nitride layer and the stripe pattern was transfered from a mask to the resist using conventional ultra-violet photolithography. There were two specific patterns used for this study. One had sets of 9 parallel stripes of decreasing width centered over a 200 micrometer period. The widths of the stripes were 5, 10, 20, 30, 40, 50, 60, 80, and 100 micrometers and the nitride thickness was 1000Å. A representative picture of a portion of this sample is shown in Figure 4.1. The second pattern had stripes of the same width but the stripes were centered over a 250 micron period and each stripe width was repeated three times before the next width appeared in the pattern. The sample was then placed in a stock solution of buffered hydrofluoric acid which etched away the exposed silicon nitride, leaving behind photoresist coated lines of silicon nitride on the GaAs surface. The remaining photoresist was then removed by conventional methods. The wafer was then cleaned by degreasing with succesive rinses of trichloroethylene, acetone, methanol, and deionized water, then placed in concentrated (97 wt%)

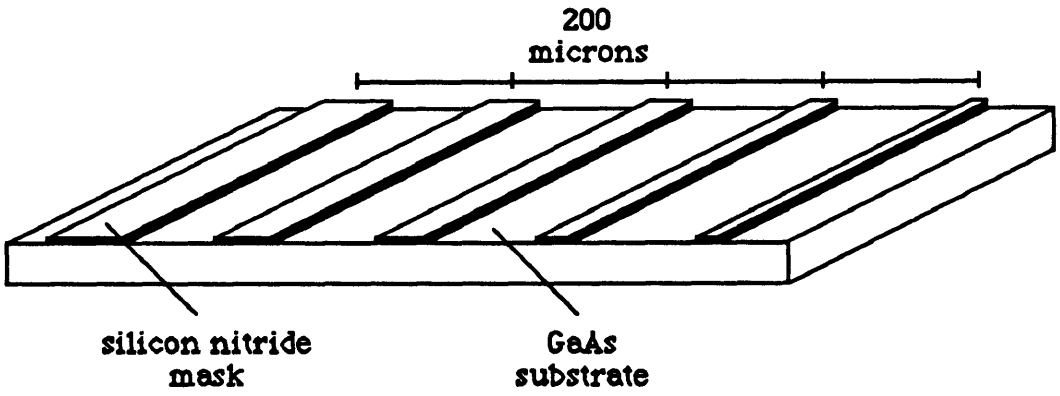

Figure 4.1: Schematic of masked GaAs substrate used for lateral diffusion experiments.

H_2SO_4 for two minutes, rinsed again in deionized water and then placed in concentrated (38 wt%) HCl for two minutes, rinsed again in deionized water and then loaded into the reactor where the vapor etching experiment was performed.

4.2.2 (111)A and (111)B GaAs Etch Rate Studies

The (111)Ga and (111)As GaAs used for these etch rate studies were undoped wafers supplied by American Xtal Technology. As in the previous section, the samples were initially covered with 1000Å PECVD silicon nitride which was removed from half of the wafer using photolithography.

4.2.3 Microfacet Etch Studies

For most of these experiments, bulk n^+ (100) GaAs wafers with a 2° misorientation to the (110) were used and it was desired to expose micro facets of either (111)Ga or (111)As orientations. This was accomplished using the procedure reported by Bailey et al (1989). Stripes of photoresist were patterned directly onto a sample of (100) GaAs either parallel or perpendicular to the (011) direction using photolithography. The resulting pattern had numerous parallel lines of photoresist 400 microns wide separated by 5 micron openings. The sample was then placed in a solution of 5 parts by volume H_2SO_4 (97 wt%), 1 part H_2O, and 1 part H_2O_2 (30%) which had been aged for at least 24 hours. This solution etched the exposed GaAs forming either a "V" groove (stripes perpendicular to the (011) direction) or a

"dovetail" groove (stripes parallel to the (011) direction) as shown in Figure 4.2a, b. Although the initial opening in the photoresist was only 5 microns in width, undercutting of the photoresist mask resulted in 20 micron openings after 3 minutes of etching. During this wet etch procedure, the solution was not agitated and care was taken to ensure that it remained stationary. These precautions assured that uniform grooves were produced across the whole sample. This becomes important in the subsequent analysis of the data where "after etching" grooves are compared to different "before etching" grooves. In addition to microfacets exposed on (100) GaAs substrates, a few (111)As substrates were used. With the resist stripes oriented parallel to the (110) direction, the so called "lambda" grooves are formed (Bailey et al, 1989). An example of a "lambda" groove cross section is shown in Figure 4.2c. The "lambda" groove is an interesting structure due to the fact that all three orientations of interest are present on one sample, i.e. the bulk sample is (111)As and the groove has both (111)Ga and (100) facets present

The reactor used for the vapor etching was described in detail in Chapter 3. For these experiments, vapor etch mixtures of 1.7 mol% CH_3I carried in a stream of 2100 sccm hydrogen were used. Etch temperatures were varied in the range of 480°C to 600°C. Etch depths were measured using a mechanical stylus after removal of any remaining silicon nitride in hydrofluoric acid. Etch times were chosen long enough to ensure that enough material had been

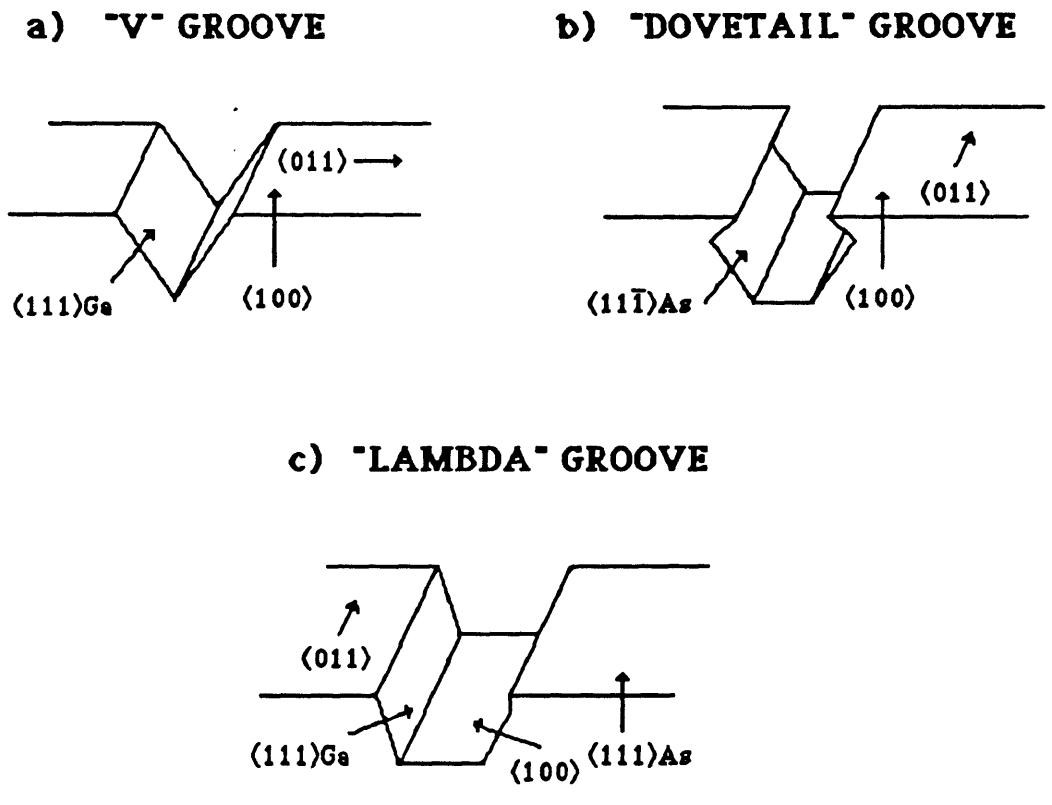

Figure 4.2: Groove structures prepared by photolithography and wet chemical etching. a) "V" groove produced on (100)GaAs, b) "dovetail" groove produced on (100)GaAs, c) "lambda" groove produced on (111)As GaAs.

removed to improve the accuracy in this measurement (>3000Å etched depth). In some cases, horizontal cross sectional photographs of etched samples were taken either with Nomarski interference microscopy (up to 1060X) or with a scanning electron microscope (>10,000X). In these cases, the samples were cleaved after etching and the photographs were taken from the newly exposed interface. These photographs were used to analyze etch depths of the micro-facets by comparing different cross sections before and after vapor etching.

4.3 EXPERIMENTAL RESULTS AND DISCUSSION

4.3.1 Inert Mask Effects on Vapor Etching

In the investigations of CH_3I vapor etching of (100) GaAs substrates half masked with Si_3N_4 reported in Chapter 3, an enhancement of etching near the mask/substrate interface was consistently observed. In these experiments, the masks were large (millimeters in width) and the enhancement was observed over a distance of 200 - 300 microns. A typical etch profile for these samples is shown schematically in Figure 4.3. The trench etched depth as shown in this figure was always between 1.5 - 3.0 times greater than the bulk etched depth (ie. far from the mask edge). It is hypothesized that this rate enhancement is due to the diffusion of etchant species from the masked region to the unmasked region. If this hypothesis is true,

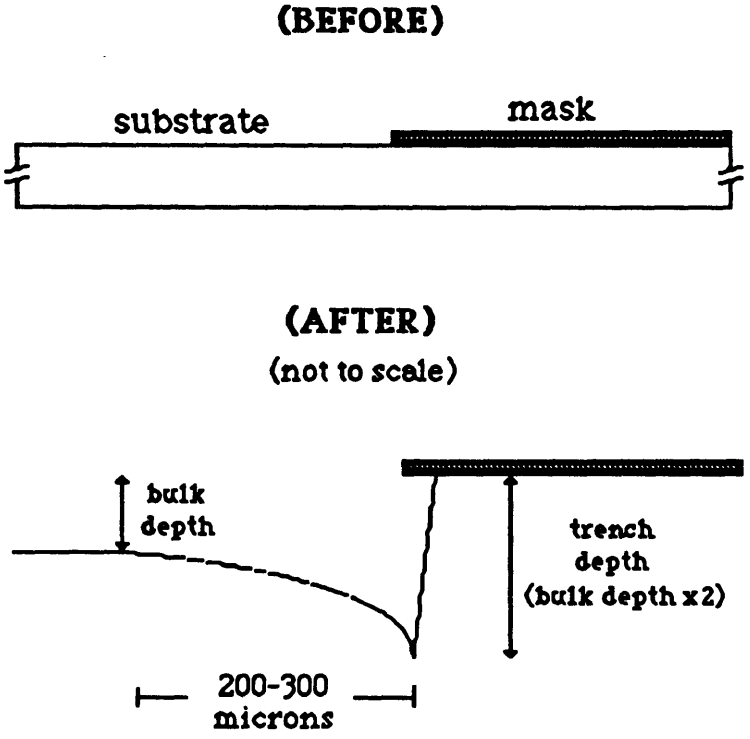

Figure 4.3: Typical etch profile near an inert mask (bulk etching sample)

one would expect the magnitude of the etch rate enhancement to depend on the size of the stripes, approaching zero for very narrow stripes. To further investigate this effect, etching experiments were performed on the patterned samples with different stripe width masks (Figure 4.1).

Figure 4.4 illustrates a typical result from one of these experiments. In general the etch profile was not uniform between the masks and for this reason the enhancement factor (E_f) is taken as the "trench depth" divided by the unperturbed etch depth. The unperturbed etch depth was taken as the etch depth between the two smallest stripes (i.e. the 5 and 10 micron stripes). Although the etch profile was convex in shape, the etch depth at the center was never observed less than 90% of the "trench depth".

The experimental results are summarized in Figure 4.5 which shows the enhancement factor (E_f) as a function of stripe width divided by the open area width (x_m) for two samples. For small stripes (<30 microns, x_m<0.15) the enhancement factor was 1.0 indicating that no measurable enhancement occured. In addition, the etch profile was uniform between neighboring masks. For larger stripes (>30 microns, x_m>0.15), enhancement factors clearly depend on x_m. In this case the concave etch profiles mentioned above were observed.

The data in Figure 4.5 clearly demonstrate a link between mask size and the degree of enhancement observed. It is proposed that the

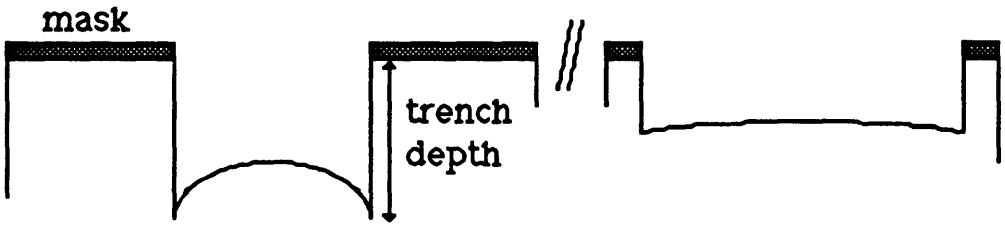

Figure 4.4: Typical etch profile near an inert masks (variable linewidth experiments)

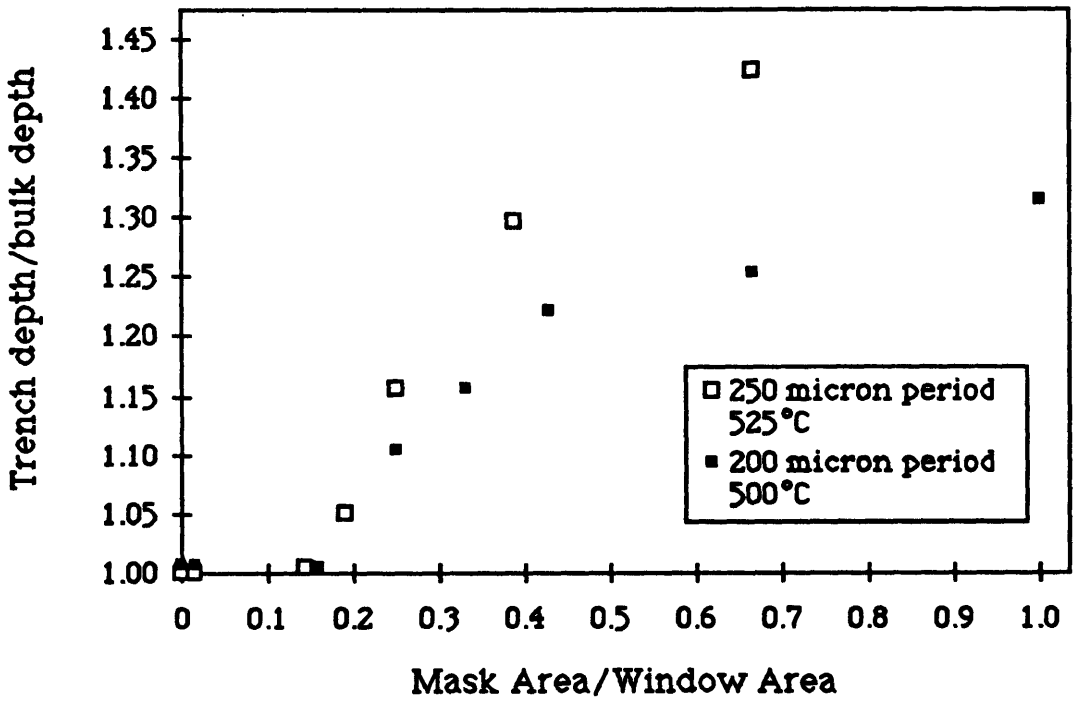

Figure 4.5: Etch rate enhancement due to inert mask as a function of mask/window ratio.

enhancement is caused by the diffusion of active etchant species from the inert mask to the reactive GaAs surface. Two diffusion processes could be occurring, gas-phase "volume" diffusion and surface diffusion and, under the right circumstances, either or both of these processes could lead to the observed enhanced etching near masks. With volume diffusion, an etch rate enhancement will arise due to there being little or no flux of etchant species to the mask compared to the exposed GaAs. This can lead to the formation of a lateral concentration gradient in the gas phase near the mask/substrate boundary resulting in enhanced etching near this boundary. With surface diffusion, etchant species adsorbed on both the exposed GaAs and the mask can diffuse along the surface. For etch rate enhancement to occur, the surface lifetime of adsorbed etchants must be longer on the mask than on the GaAs surface.

It is now shown that a model of gas phase "volume" diffusion will describe these experimental results. A 2-dimensional model of diffusion of the etchant species (iodine atoms) through a stagnant gas film will be considered. For the stagnant film assumption to be valid, the Peclet (Pe_m) number near the wafer surface must be less than 1. In our experiments, the length scale (L) of interest is the size of the mask period, 0.02 cm, diffusion coefficients (D) are around 1 - 5 cm^2/s and the average gas stream velocity (V) in the reactor is 20 cm/s. The Peclet number (VL/D) near the surface is therefore between 0.08 and 0.4, slightly less than 1. The stagnant film assumption is further supported by the experimental observation

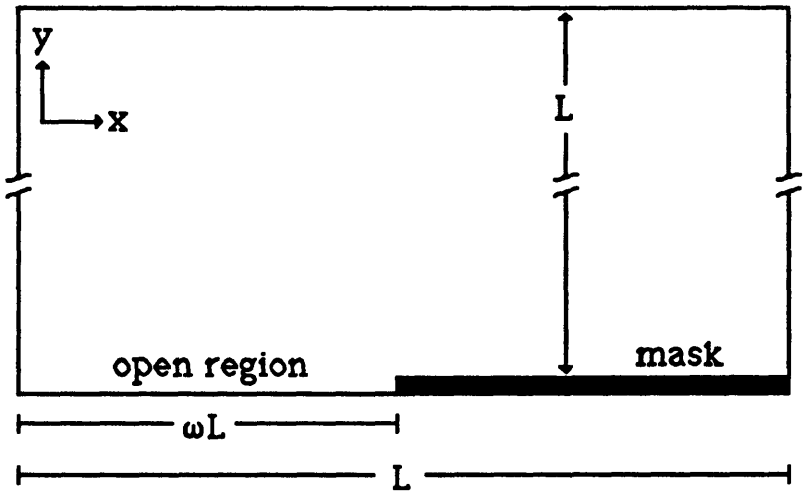

Figure 4.6: Domain for computation of volume diffusion effects of masks.

that the magnitude and shape of these etch profiles does not depend on how these wafers were oriented relative to the flow direction (ie. parallel or perpendicular with the mask upstream or downstream). Additionally, in their model of OMVPE of GaAs on patterned substrates, Coronell and Jensen (1991) also made this assumption, considering it to be valid for distances within 100 microns of the wafer surface.

A model for the two dimensional transport of a single species through a stagnant gas over a heterogeneous, periodic surface is now formulated. It is necessary to solve the diffusion equation in two dimensions:

$$\nabla^2 C = 0 \qquad (4.1)$$

where C is the dimensionless concentration of the etchant species (ie. iodine atoms). The domain on which this equation is solved is shown in Figure 4.6. Equation (4.1) is solved subject to the following boundary conditions

$$\frac{\partial C}{\partial \hat{x}} = 0 \qquad \hat{x} = 0,\ 1;\ \text{all } \hat{y} \qquad (4.2)$$

$$\frac{\partial C}{\partial \hat{y}} = 0 \qquad \hat{y} = 0,\ \omega < \hat{x} < 1 \qquad (4.3)$$

$$\frac{\partial C}{\partial \hat{y}} = Da_s C \qquad \hat{y} = 0,\ 0 < \hat{x} < \omega \qquad (4.4)$$

$$C = 1 \qquad \hat{y} = 1;\ \text{all } \hat{x} \qquad (4.5)$$

In these equations, ω is the open surface area to mask area ratio, $\hat{x} = x/L$, $\hat{y} = y/L$, $Da_S = k_S L/D_I$ and L is one half the period of the mask structure (ie. 100 or 125 microns) and D_I is the diffusion coefficient of iodine atoms (assumed equal to 3 cm^2/s). The assumption of constant concentration at $\hat{y} = 1$ (4.5) is reasonable since we don't expect the inhomogeneous surface to have significant effect on the concentration field at this distance from the surface. The exposed surface boundary condition (4.4) represents a first order surface reaction, the rate constant k_s is unknown and is therefore adjusted to give the best fit to the data. In the limit as k_s approaches infinity, boundary condition (4.4) is replaced with

$$C = 0 \qquad \hat{y} = 0,\ 0 < \hat{x} < \omega \qquad (4.4a)$$

Equation (4.1) was solved on a square domain (L x L) subject to boundary conditions (4.2) - (4.5) by using a simple finite difference approximation on a 50 x 50 square grid. The value of k_s which gives this curve is 180 cm/s, corresponding to a surface Damkohler number ($Da_S = k_S L/D_I$) of 1.2 (based on a diffusivity, D of 3 cm^2/s, L = 0.01 cm). The results are shown in Figure 4.7 as predicted maximum trench depth as a function of the parameter ω. This figure also shows the experimental data points from the 200 micron period sample (L = 100 micron). The agreement between these predicted values and the data is quite reasonable. Figure 4.8 shows the predicted etch profiles

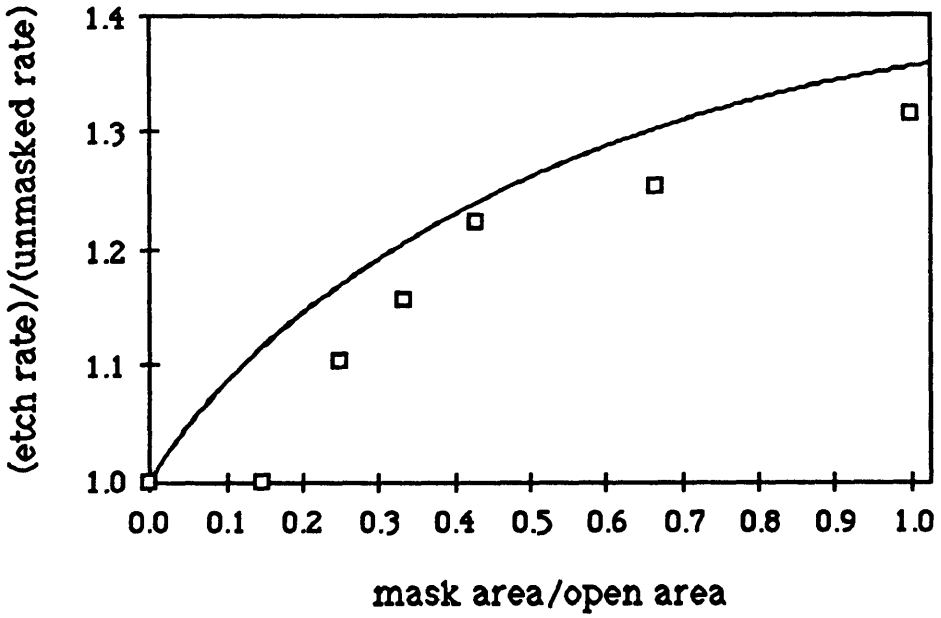

Figure 4.7: Predicted trench depth enhancement (solid curve) compared to experimental data (open squares) (200 micron period sample)

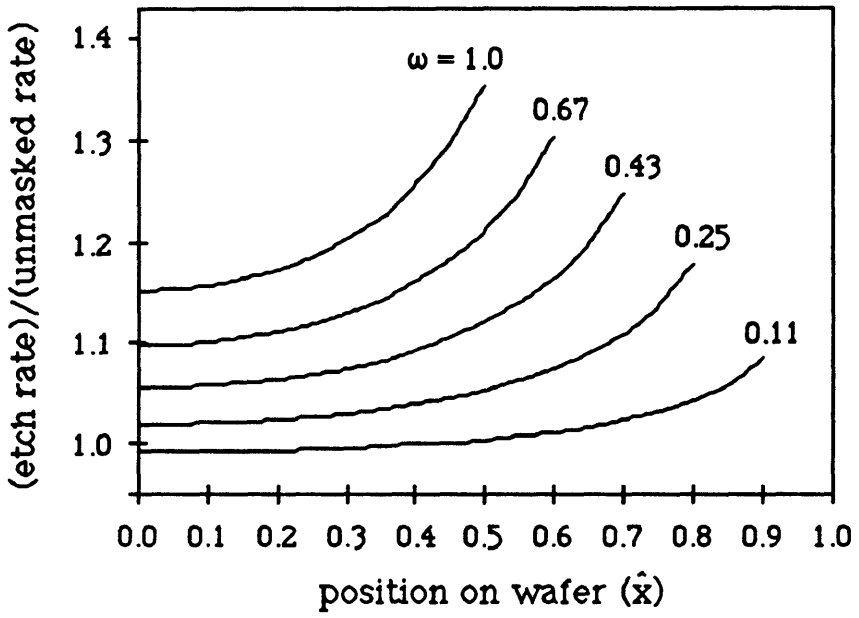

Figure 4.8: Predicted etch profiles for several mask fractions, mixed boundary condition case (Da_s = 1.2).

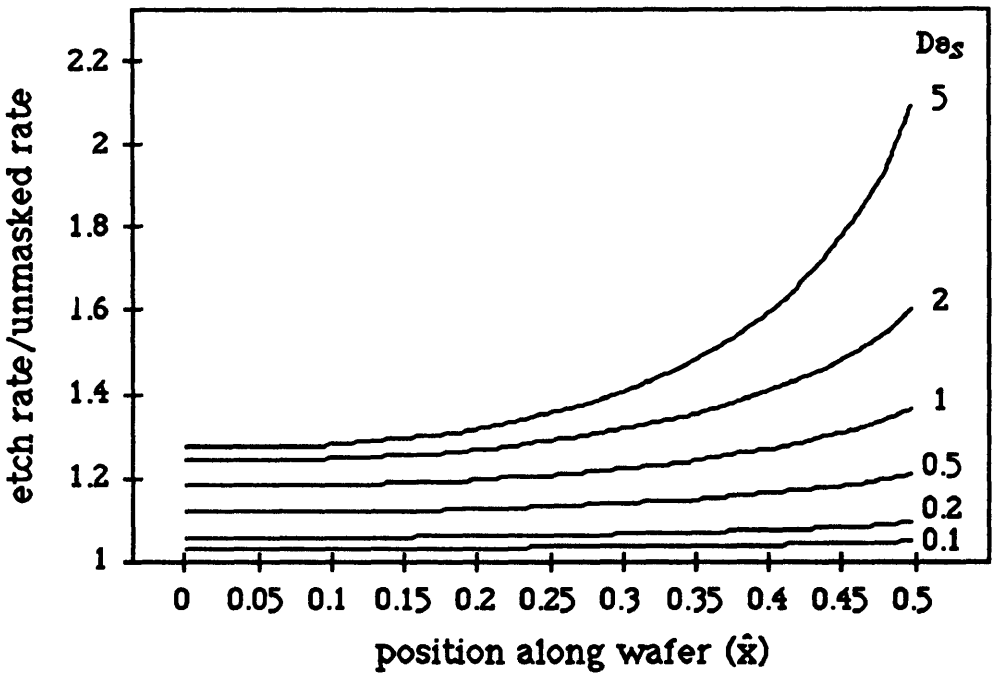

Figure 4.9: Predicted dependence of etch profiles on assumed value of Da_S. Mask area/open area (ω) = 1.0.

for several different mask/window ratios for Da_s = 1.2. The values are also in excellent agreement with the experimentally measured profiles (not shown), exhibiting variations on the order of 10% across the etched surface. Figure 4.9 shows the effect of assumed Da_s on the predicted etch profile for ω = 1 (half mask). This model does not predict the disappearance of the trench at low mask/window ratio's, however. This discrepancy may be due to inherent errors the Dektac measurement which is generally considered to be only 5% accurate for these etch depths.

In equation (4.5), it is assumed that the concentration has a constant value at a distance L above the substrate. This assumption is examined by replacing (4.5) by the following boundary condition

$$C = C_0 \qquad \hat{y} = \beta;\ \text{all}\ \hat{x} \qquad (4.5a)$$

the value of ß was then varied and the results are shown in Figure 4.10 as etch rate/unmasked rate for a mask area to open surface area ratio of 1.0 and Da_s = 1. It can be seen in this figure that the magnitude of the predicted etch rate enhancement depends on the value of ß but the shape of the etch profile depends on ß only for ß < 1. As ß is increased beyond a value of 2.5, the stagnant film begins to break down. Small values of ß may lead to a breakdown of the constant concentration assumption at the upper boundary. Nevertheless, this analysis emphasizes that the assumed position of the upper boundary has a significant impact on the computed

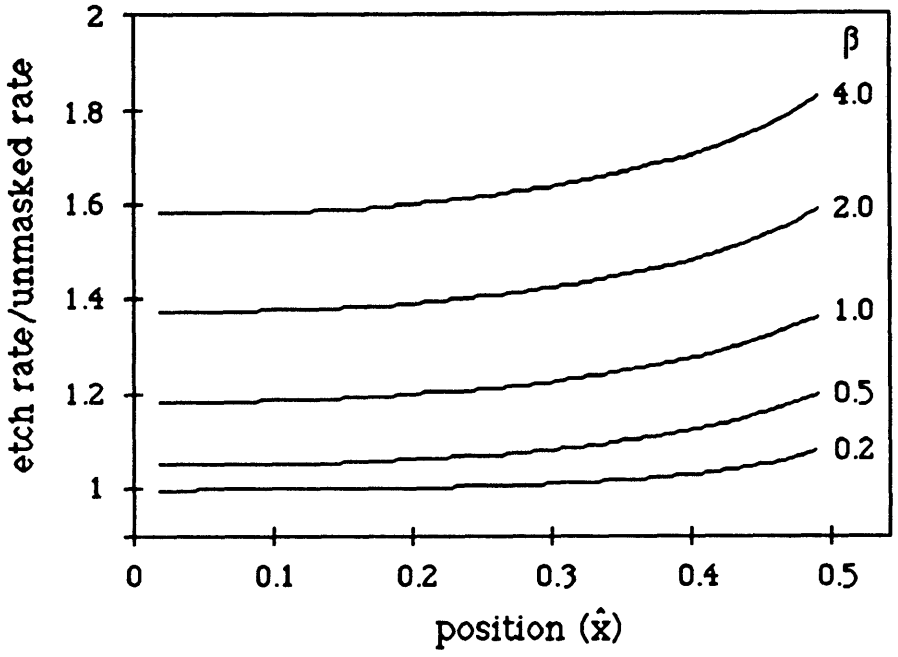

Figure 4.10: Predicted dependence of etch profiles on assumed value of β. Mask area/open area = 1.0, Da_s = 1.0.

solution, limiting the usefulness of this calculation for quantitative determination of k_s.

It is also instructive to examine the model results under the assumption of an infinitely fast surface reaction. This is done using boundary condition (4.4a) in place of (4.4) (and ß = 1). The etch profiles predicted by this pure volume diffusion model are shown in Figure 4.11 and clearly fail to match the data of Figure 4.4, predicting maximum trench depths of up to 400% of the bulk etched depths. This result is in strong conflict with our experimental observations of trench depths closer to 30%.

It can be concluded from this analysis that the observed etch rate enhancement near inert surfaces is represented well by a model of coupled gas phase volume diffusion with a first order surface reaction. Although a finite surface reaction rate is predicted by this analysis, these results do not contradict our previous assertion in Chapter 3 that the etch rates in the horizontal reactor are controlled by gas phase reactions. This surface reaction rate is fast compared to other processes occuring in the bulk gas stream. For example, Da_s based on this k_s (180 cm/s) and the height of the reactor (h), 1.5 cm is 150 times greater than on the smaller length scale (0.01 cm) considered in this formulation. In addition, the ratio $(k_s h)/(k_{decomp(CH_3I)})$ at 500°C is on the order of 10^4, indicating that the gas phase decomposition of CH_3I in the bulk gas (to produce iodine) is much slower than this surface reaction. The value of this

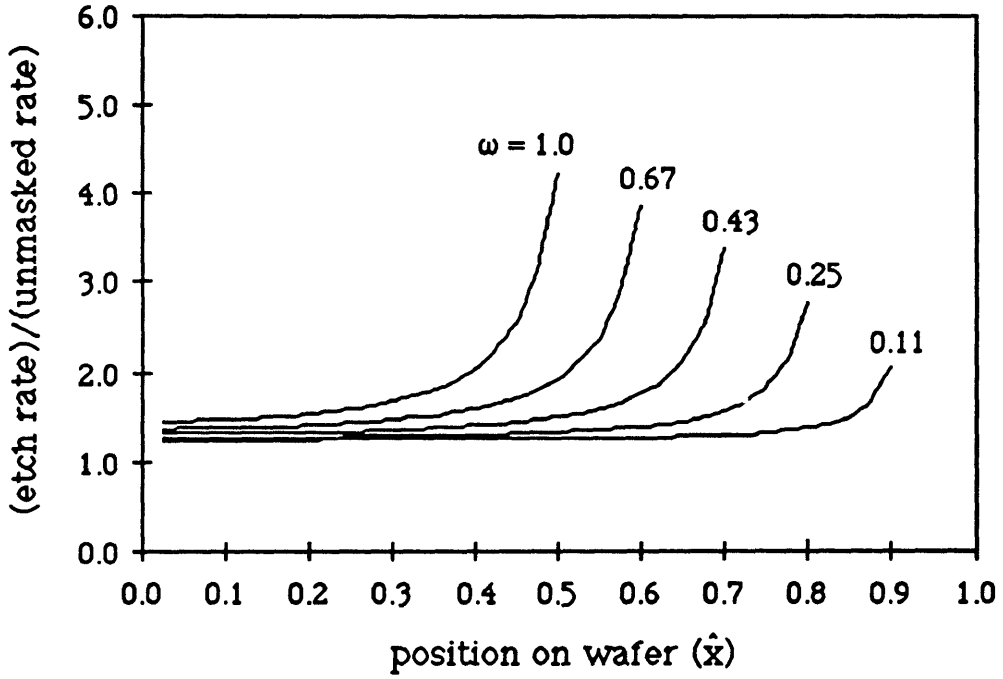

Figure 4.11: Predicted etch profiles, pure volume diffusion model (Da_s very large).

dimensionless ratio also serves to justify the omission of a volume production term in our model formulation.

4.3.2 Vapor Etching of Bulk Substrates of (111) GaAs by CH_3I

The results of CH_3I vapor etching of GaAs wafers exposing the (111)Ga and (111)As orientations are presented in Figure 4.12, an Arrhenius plot comparing etch rates of (111)Ga, (111)As, and (100) GaAs substrates as a function of temperature. From this figure, it is clear that the (111)Ga is the fastest etching facet especially at lower temperatures. At 504°C, the ratio of the rates on (111)Ga:(100):(111)As is 3.0:1.8:1.0 and at 555°C the ratio is 1.7:1.5:1.0. The activation energies were found by a least squares fit to the data to be 50 kcal/mol for the (111)As, 45 kcal/mol for 100 and 43 kcal/mol for the (111)Ga surfaces. The etch rates appear to be converging to the same value at high temperatures, consistent with our previous observation that the gas phase decomposition of CH_3I to form active etchant species is the rate limiting step in the etch process. However, if the gas phase kinetics were solely rate controlling, one would expect little variation between etch rates on these different substrate orientations. It is therefore apparent that there is an additional surface effect operating in series with the vapor phase production of active etchant species. This surface effect serves to lower the reactivity of the surface toward the etchant

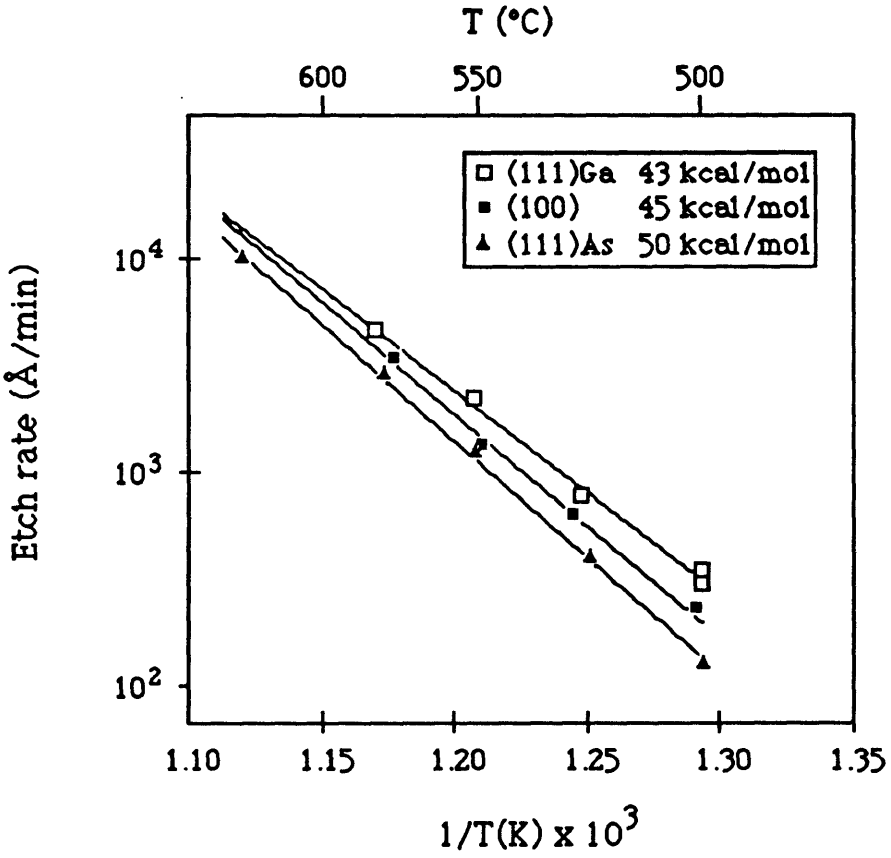

Figure 4.12: Arrhenius plot comparing etch rates of the three GaAs bulk substrate orientations studied; (111)Ga, (100), (111)As.

species and is most apparent on the (111)As surface and least so on the (111)Ga.

The surface morphology of (111)As and (111)Ga etched substrates is shown in Figure 4.13. The (111)As face is characterized by the formation of etch pits with a three-fold symmetry as can be seen in Figure 4.13a for a sample etched at 500°C to a bulk depth of 600Å in 5 minutes. The number and size of these pits increases with time, leading to the formation of a completely faceted surface. The etch pits are sharply faceted and these facets are close to (110) orientations. A typical surface for the vapor etched (111)Ga sample is shown in Figure 4.13c,d for samples etched at 500°C to a total depth of 10,000Å and at 575°C to a depth of 13,000Å. Although etch pits on these surfaces exhibit a three fold symmetry, the edges are very rounded and the etch pit is nearly circular. Away from the etch pits, the surface is roughened but shows no apparent symmetry or faceting. This roughening is also more apparent at higher etch temperatures although the number of etch pits does not increase significantly with increasing temperature.

Let us consider these results in light of the two discussions of surface reactivity presented above. Gatos (1962) proposed that surface reactivity differences were due to differences in the electronic nature of the bonds on the surface. The observation that the surface reactivity order is (111)Ga>(100)>(111)As would be consistent with Gatos (1962) proposition that the etch chemistry is reducing in nature due to the higher reactivity toward the electron depleted

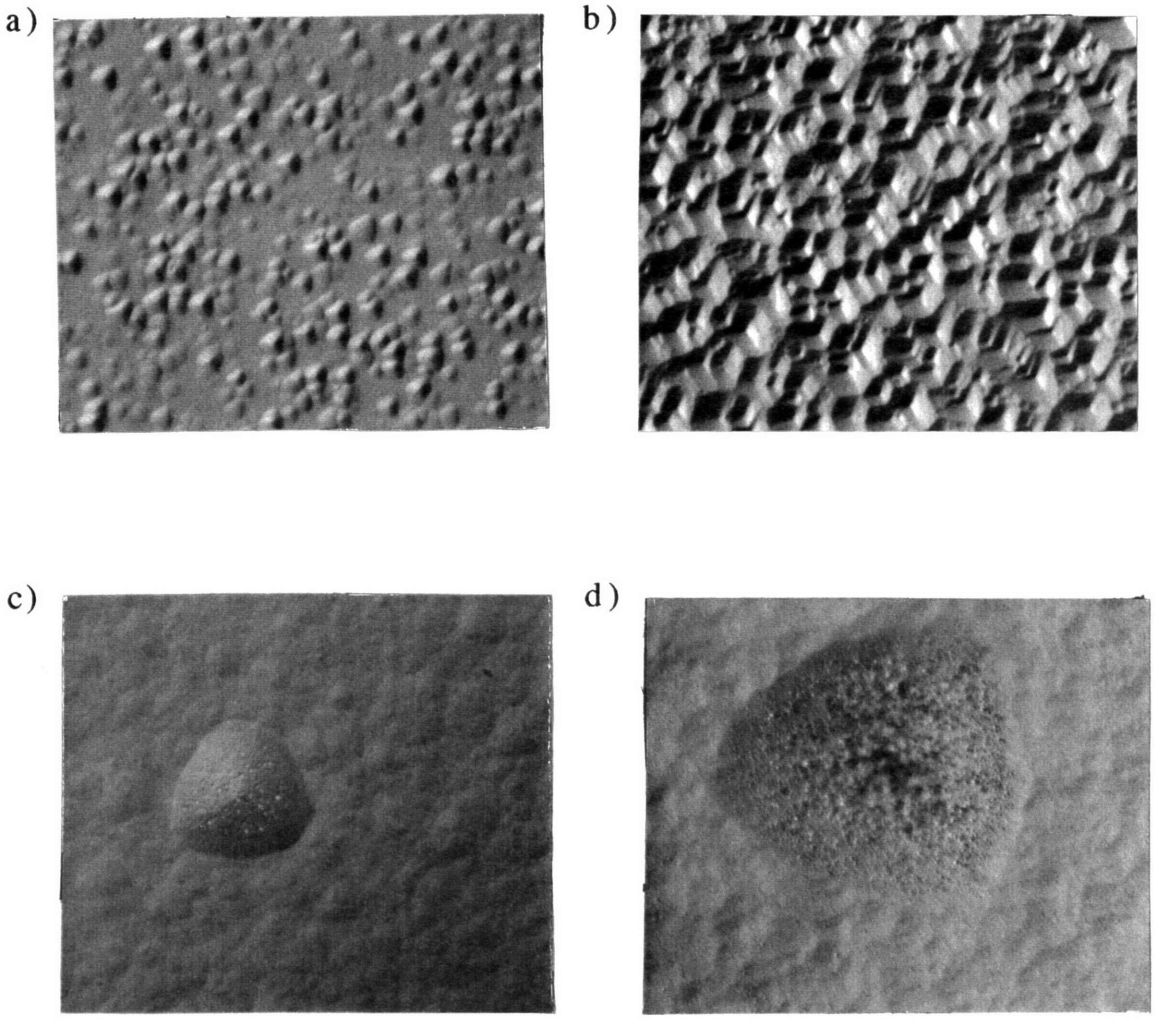

Figure 4.13: Surface morphologies of etched GaAs surfaces (Nomarski interference micrographs, 1060X). a) (111)As etched at 500°C for 5 minutes.(600Å) b) (111)As etched at 500°C for 45 minutes (6000Å). c) (111)Ga etched at 500°C for 30 minutes (10,000Å). d) (111)Ga etched at 580°C for 3 minutes (13,000Å).

(111)Ga surface. We expect that the etchant species are iodine and/or methyl free radicals which are generally not expected to be strongly reducing (iodine atoms are expected to behave as electron acceptors or oxidizing agents). These surface reactivity differences are also in contrast to Furuhata's (1990) results for the chlorine vapor etching of GaAs discussed above. By similar reasoning (to Furuhata), it follows that it is the removal of arsenic from the surface which is additionally limiting etching on the (100) and (111)As when compared to the (111)Ga surface in our experiments. However, Furuhata observed a sharp break in his Arrhenius plot for his slow etching (111)Ga surface indicating two different operating regimes, a surface reaction limited regime (at low temperatures) and a mass transport regime. No such break is evident in our data, however, suggesting that the CH_3I vapor etch occurs in a mixed kinetic regime over a wide range of operating conditions. The arsenic removal step is a strong candidate for the slow surface reaction since arsenic removal will be most difficult from the (111)As surface, due to the fact that arsenic atoms are attached to the underlying surface with three bonds. In our experiments, however, this arsenic removal limitation never appears as the sole kinetic limitation. A possible explanation for this comes out of the GaAs molecular beam epitaxy (MBE) literature. Foxon and Joyce (1977) observed that the sticking coefficient of arsenic on (100)GaAs surfaces depends strongly on the amount of available gallium on the surface. Conversely, at high arsenic coverages (ie. little available gallium), the sticking coefficient of arsenic approached zero. Based on this idea, the following mechanism for etching is proposed. Iodine atoms produced by the

gas phase decomposition of CH_3I react with gallium atoms on the surface forming the volatile product GaI. The rate of this reaction is proportional to both the amount of iodine available to the surface from the gas phase and the amount of gallium available on the surface. Arsenic desorbs without chemical assistance, it will tend to accumulate on the surface, blocking gallium from the reactive vapors and effectively passivating the surface. The extent of arsenic accumulation is limited, however, and will tend to saturate due to the strong dependence of the arsenic sticking coefficient on the arsenic surface coverage. Under steady state etching conditions, the arsenic coverage will tend to a constant value which will be determined by the surface orientation, the etch rate and the surface temperature. We expect that this steady state value will be higher on surfaces where arsenic is more strongly bound (ie. (111)As>(100)>(111)Ga) consistent with our observations of surface reactivity differences. It is finally interesting to note that the vapor etching of the (111)As surface produced the most sharply faceted structures of the three surfaces studied. The bulk (111)As surface is unstable under CH_3I vapor etching apparently due to its low reactivity. Faceting behaviour has also been observed when OMVPE growth of GaAs was performed on the (111)As surfaces from trimethylgallium and arsine (Reep and Ghandi, 1984).

bulk orientation	groove type	facet orientation	etch temp. (°C)	bulk etched depth (microns)	facet/bulk
100	V	(111))Ga	480	1.0	2.8
100	V	(111)Ga	520	0.9	2.5
100	V	(111)Ga	530	1.3	2.8
100	V	(111)Ga	576	2.7	2.9
100	dovetail	(111)As	576	2.8	ND
masked	V	(111)Ga	530	2.7	5.7
111As	lambda	(111)Ga	500	0.25	0.06
111As	lambda	(100)	500	0.25	0.14
masked	lambda	(111)Ga	500	0.25	0.06
masked	lambda	(100)	500	0.25	0.14

Table 4.1: Comparison of etched depths of micro-facets exposed on bulk substrates of GaAs versus the bulk etched depth.

4.3.3 CH_3I Vapor Etching of Faceted Structures of GaAs; Interactions Between Surface Heterogeneities and Lateral Diffusion Processes

Results for CH_3I vapor etching of faceted structures is presented in Table 4.1. In this table, results are presented as ratios of etched depths versus the bulk surface etch rate for the GaAs various substrate orientations. Etching of the (111)As surface exposed in the "dovetail" groove structure could not be measured due to its low rate. It is interesting to note how the "dovetail" structure evolves as shown in Figure 4.14(a,b). The overhang was completely etched away, and a new facet was exposed. This facet is inclined approximately 36° (144°) to the (100) plane, corresponding closely to the (211)As orientation.

A typical evolution of a "V" groove structure with (111)Ga sidewalls is shown in Figure 4.15(a,b). The initial "V" opens up laterally, forming a structure with sidewalls of approximately the same starting angle and a bottom which is apparently (100) in character but is somewhat curved. The curvature of the bottom is most likely due to kinetic effects; as a new (100) surface is exposed by the receding sidewalls, it begins to undergo etching in the downward direction. The sidewall facet angle also changed as the etching proceeded and, therefore, the (111)Ga facet was not preserved. In reporting etch rates of these sidewalls, an average value was taken between the initial and final sidewalls. The sidewall angles only changed by a few degrees and therefore these sidewalls are still

a)

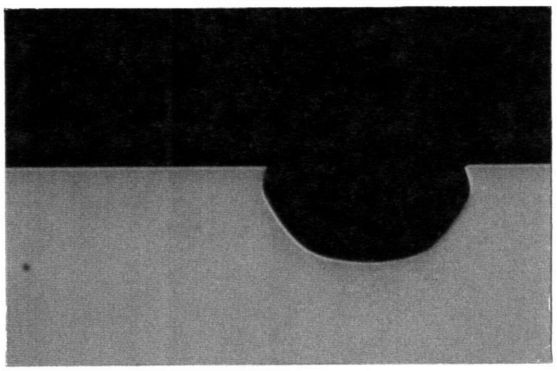

b)

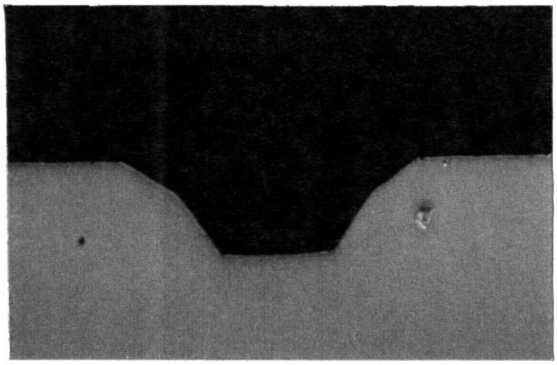

Figure 4.14: Evolution of "dovetail" structure, a) initial groove shape, b) groove shape after CH_3I vapor etching at 575°C, 8 minutes, y_{CH_3I} = 0.015.

a)

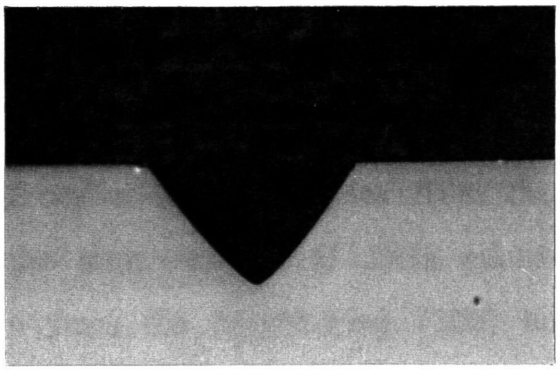

b)

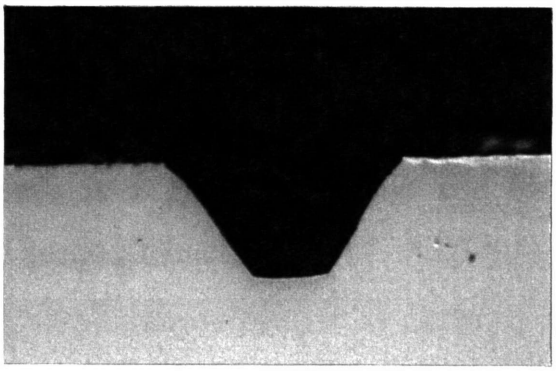

Figure 4.15: Evolution of "V" groove structure. a) initial groove shape. b) groove after CH_3I vapor etching at 480°C, 120 minutes, y_{CH_3I} = 0.015.

chemically similar to the (111)Ga facet. Vapor etch rates of these (111)Ga surfaces were consistently 2.5 - 2.8 times higher than the bulk substrate (100) etch rate. The rate increase did not depend on temperature, suggesting that diffusion processes rather than kinetic are causing the observed rate enhancement. This diffusion is the lateral diffusion of active etchant species from the less reactive (100) bulk substrate to the more reactive (111)Ga micro-facets. Due to additional diffusion from the neighboring (100) bulk substrate, a net etch rate enhancement on these (111)Ga micro-facets occurs when compared to the reactivity ratios of the (111)Ga/(100) bulk substrates. At 504°C, the bulk (111)Ga/(100) etch rate ratio was 1.7:1 and at 555°C the ratio was 1.1:1, both smaller than the (2.5 - 2.8):1 ratio observed in these experiments. It is less obvious what the cause of the changing facet angle is. The bottom of the sidewall recedes more quickly than the top, the sidewall tending to become more vertical. Possibly the intersection of the sidewall with the bottom of the groove is a good nucleation site for subsequent two dimensional step propagation.

The vapor etching of the "lambda" groove structures exposed on the (111)As substrates allows for comparison between the slow etching (111)As facet and the faster etching (100) and (111)Ga facets which could not be observed on the "dovetail" structure. Under etching, the "lambda" groove maintained its basic structure and the sidewalls receded laterally. This structure is not symmetric, however and it is therefore difficult to properly superimpose "before" and "after" cross sectional images. In order to overcome this difficulty, a "lambda"

groove sample was prepared with a silicon nitride mask over the bulk (111)As surface. The position of the mask served as a marker for the original positions of each of the two receding sidewalls. The etching conditions were the same as for the unmasked sample and the etch rate of (111)Ga:(100) etch rate ratio was thus determined to be 2.5:1.0. From these two experiments, it was determined that the ratio of etched depths (111)Ga:(100):(111)As was 18:7.4:1. Compared to the ratio on bulk samples of 3.0:1.8:1.0, enhanced selectivity is again observed. In fact, the cross sectional images from the masked and unmasked "lambda" groove samples were nearly identical, indicating that the (111)As bulk surface is effectively inert.

4.3.4 Mask Alignment Strategies, Orientation Effects and Etch Anisotropies

Considering the results presented in the previous three sections, a strategy for aligning parallel line masks on (100) GaAs substrates is proposed which should minimize mask undercutting. It would be desirable to promote the formation of a sidewall facet with the (111)As orientation on the (100) surface. The (111)As is the slowest etching facet and as we have seen, this slowness will be exaggerated in this situation where the bulk of the surface is more reactive. Orientation of stripes parallel to the (110) direction on the (100) surface should promote the appearance of (111)As facets much in the same fashion as the wet chemical etch preparations of the samples used in this study (ie. the "dovetail" groove). Conversely, stripes oriented perpendicular to the (110) should exhibit a large

degree of undercutting due to the high reactivity of the (111)Ga sidewalls that will be exposed. Cross sectional SEM images of two such samples are shown in Figure 4.14. Figure 4.14a is an image of the undercutting which occured with Si_3N_4 stripes oriented parallel to the (011) direction after etching with CH_3I vapor (500°C, 1.5 mol% CH_3I, 20 minutes). The sidewalls exposed are sloped 45°, smaller than the expected angle between (100) and (111)As of 56.7° and the ratio between the etched depth and the undercut distance (measured at the top of the slope) is 1:1. This undercutting ratio is larger than was expected based on the previously determined reactivity ratio between (100) and (111)As of 7.4:1. One possible explanation for the discrepancy is the possibility of poor mask adhesion near the mask/substrate boundary augmented by the difference in the coefficient of thermal expansion between GaAs and Si_3N_4. Figure 4.14b shows the undercutting which occured with Si_3N_4 stripes oriented perpendicular to the (011) direction after etching with CH_3I vapor (525°C, 1.5 mol% CH_3I, 10 minutes). In this case, formation of the (111)Ga facet is not necessarily expected due to its high reactivity. As can be seen from the Figure, the undercut ratio of 2.5:1 is very close to the ratio of (111)Ga to (100) etch rates (table 4.1) of 2.5:1 at 520°C. The exposed sidewall is close to a (011) orientation.The results shown in Figure 4.16 are in general agreement with expectations based on the results shown in Table 4.1. The undercut depths were close to the expected values but the undercut shapes were not anticipated. Clearly the orientation of masking stripes on (100)GaAs parallel to the (011) direction is superior to a perpendicular orientation if the goal is to minimize

mask undercutting effects. If near vertical sidewalls are required, however, the perpendicular orientation is preferred but substantial mask undercutting is expected.

a)

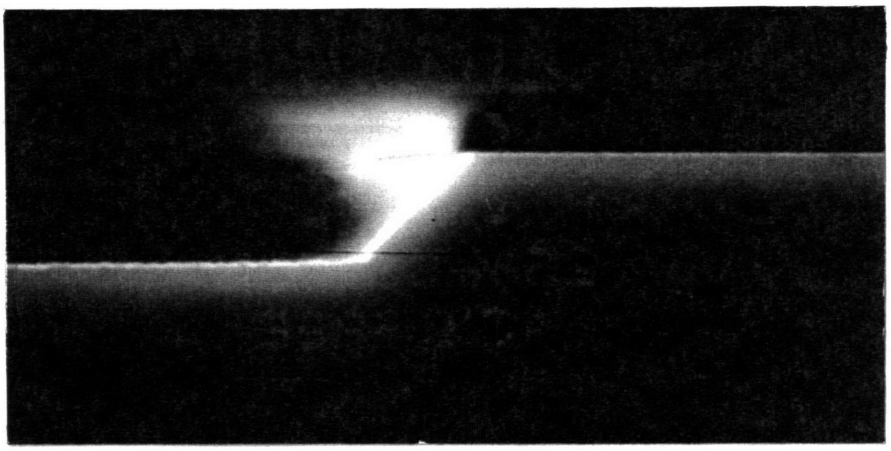

b)

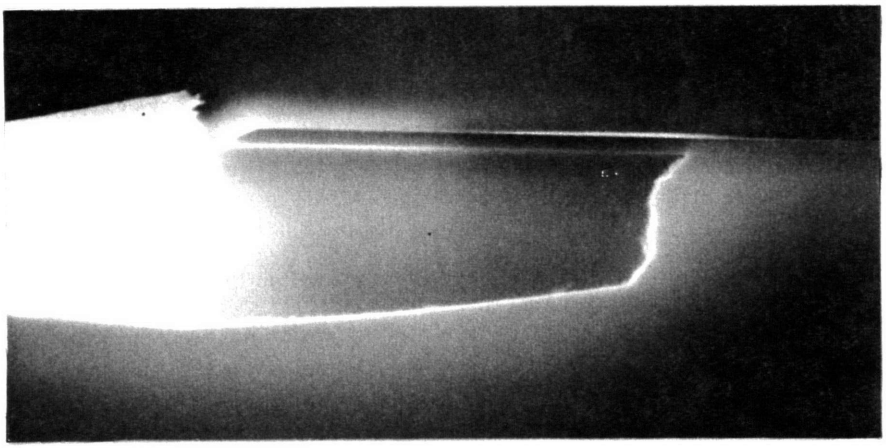

Figure 4.16: SEM cross sections of undercutting by CH_3I vapor etching on patterned (100)GaAs substrates. a) mask stripes oriented parallel to the (011). b) mask stripes oriented perpendicular to the (011).

4.4 CONCLUSIONS

This chapter presented experimental data and analysis relevant to the problem of applying CH_3I vapor etching to patterning of masked substrates of GaAs. It was shown that lateral diffusion from inert surfaces to reactive ones can locally enhance etching by as much as a factor of three over bulk surfaces but for most practical mask sizes (<100 microns) the enhancement will be no more than 30%. Differently oriented bulk samples were found to etch at different rates, the (111)Ga surface was the fastest, followed by the (100) and the (111)As. In situations where surfaces of different orientations are in close proximity, diffusion processes were observed to enhance differences in surface reactivity by as much as a factor of 18. For etching of masked substrates of (100) GaAs, it was determined that orienting mask stripes parallel to the (110) direction promoted the formation of slow etching sidewalls inclined at a 45° angle to the surface. This mask alignment minimizes mask undercutting and is, therefore, of technological importance.

Chapter 5

The Mechanism of CH_3I Vapor Etching of GaAs

5.1 INTRODUCTION

In Chapter 3, CH_3I vapor etching of GaAs was demonstrated to be a promising technique for *in situ* substrate cleaning prior to OMVPE. Additionally, it was shown in Chapter 4 that the anisotropic features of this etch on GaAs can be utilized to minimize undercutting of mask stripes when etching three dimensional structures. The CH_3I vapor etch process has been understood to occur primarily under a condition of gas phase kinetic control, ie. the etch rate is limited by the extent of CH_3I decomposition in the gas phase. This hypothesis is explored by experimental study of CH_3I decomposition in the horizontal reactor used in previous vapor etching studies. It has additionally been proposed that the etchant species in the vapor etching reaction are iodine free radicals produced from CH_3I decomposition. A test of this hypothesis is performed by comparing experimental etch rates in a vertical rotating disk reactor to those predicted by a detailed numerical simulation of the vapor etch process, including heat, mass, and momentum transfer and chemical reactions.

#	reactants	products	$\log_{10}A$	E^*/R	B	ref
1	$CH_3I + M$	$CH_3 + I + M$	15.4	21439.36	0	1
2	$I + CH_3I$	$I_2 + CH_3$	14	9964.771	0	1
3	$I_2 + M$	$2I + M$	13.99	15299.45	0	1
4	$2I + M$	$I_2 + M$			0	*
5	$2CH_3$	C_2H_6	14.1	0	-0.4	2
6	$CH_3 + H_2$	$CH_4 + H$	11.93	5485.657	0	2
7	$I + H_2$	$HI + H$	12.75	16809.26	0	3
8	$2H + M$	$H_2 + M$	17	0	-0.6	2
9	$CH_3 + CH_3I$	$CH_4 + CH_2I$	12.5	5083.04	0	1
10	$I + CH_3I$	$HI + CH_2I$	13.25	17614.49	0	est.
11	$2CH_2I$	$C_2H_4I_2$	14.1	0	-0.4	1
12	$H + HI$	$H_2 + I$	13.7	352.2899	0	3
13	$H + CH_3I$	$H_2 + CH_2I$	14.5	6039.255		est.
14	$H + I_2$	$HI + I$	14.6	0	0	4

Table 5.1: Elementary reactions considered for the decomposition of CH_3I in H_2. Constants are for rate expression of the form $k = AT^B\exp(E^*/RT)$, T in kelvins. (References: 1) Saito et. al., 1980, 2) Tanaka and Komeno, 1988, 3) Sullivan, 1962, 4) Handbook of Bimolecular and Termolecular Reactions, date.). Rate constants for reactions 10 and 13 were estimated by analogy to related H-abstraction reactions from methane taken from reference 4. Rate of reaction 4 can be determined from thermodynamics (reverse of reaction 3).

5.2 GAS PHASE CHEMICAL REACTION SET

In order to simulate the gas phase chemistry in CH_3I vapor etching, it is first necessary to determine a set of reactions to fully describe the decomposition chemistry. We have proposed that free radicals, particularly iodine atoms, produced during the decomposition are the etchant species. Therefore the reaction set must include details about reactions which both produce and consume free radicals, especially iodine atoms. Values for rate parameters have been found from several sources and in some cases have been estimated based on analogies to similar reactions for which the parameters are known.

The thermal decomposition of CH_3I diluted in Ar and other noble gasses has been studied in a shock tube over the temperature range 1050 - 1500°K (Saito, et. al., 1980, 1984). These are the only known studies to date of the thermal decomposition of CH_3I. Based on the reaction sequence proposed in this work, an elementary reaction sequence was constructed which additionally considers reactive effects of a hydrogen carrier. These reactions and their associated rate parameters are shown in Table 5.1 and are listed here

$$CH_3I + M \rightarrow CH_3 + I + M \quad (5.1)$$

$$I + CH_3I \rightarrow I_2 + CH_3 \quad (5.2)$$

$$I_2 + M \rightarrow 2I + M \quad (5.3)$$

$$2I + M \rightarrow I_2 + M \quad (5.43$$

$$2CH_3 \rightarrow C_2H_6 \quad (5.5)$$

CH_3 +	H_2	→	CH_4 +	H	(5.6)
I +	H_2	→	HI +	H	(5.7)
2H +	M	→	H_2 +	M	(5.8)
CH_3 +	CH_3I	→	CH_4 +	CH_2I	(5.9)
I +	CH_3I	→	HI +	CH_2I	(5.10)
$2CH_2I$		→	$C_2H_4I_2$		(5.11)
H +	HI	→	H_2 +	I	(5.12)
H +	CH_3I	→	H_2 +	CH_2I	(5.13)
H +	I_2	→	HI +	I	(5.14)

This reaction set is based upon one proposed for the decomposition of CH_3I (Saito, et al, 1980) with additional reactions included to account for the effects of the hydrogen carrier gas as a reacting species. Rate constants are reported in Table 5.1 and were obtained from a number of sources as listed in the table. The rate parameters for reaction (5.10) and (5.13) were estimated from analogy to the related hydrogen abstraction reactions from ethane.

For calculation of iodine atom concentrations, it has been determined that the reduced reaction set (5.1 - 5.4) predicts concentrations within an order of magnitude of the full reaction set (at atmospheric pressure). This determination was made by comparing predicted iodine atom concentrations from integration of the full reaction set to that from integration of reactions 1-4 only.

5.3 MASS SPECTROMETER STUDY OF CH_3I DECOMPOSITION

The decomposition of CH_3I was studied in the horizontal reactor system used previously for vapor etching experiments by sampling the gas stream with a capillary tube (150 micron ID). Other than the fact that there was no GaAs wafer present in the reactor, the experimental conditions were identical to those used for vapor etch studies. A gas sample from the reactor was delivered into the mass spectrometer through a two stage, differentially pumped system illustrated in Figure 5.1. In this arrangement, the low pressure side of the capillary tube is held at roughly 100 - 200 millitorr by a roughing pump (2-stage, rotary vane). The drop in pressure from 100 - 200 millitorr to the high vacuum (~10^{-5} torr) is accomplished by several small orifices in a gold foil, in this case 12 - 25 micron diameter holes. These orifices are roughly aligned line-of-site to the ionizer of the mass spectrometer. It is expected that only stable species are detected by this type of sampling arrangement, the gas residence time in the capillary tube is on the order of 1 second and it is therefore expected that free radicals and condensable vapors will not be (reliably) detectable with this sampling arrangement. The total response time of the mass detector to a change in the inlet feed gas composition was on the order of several seconds. The mass

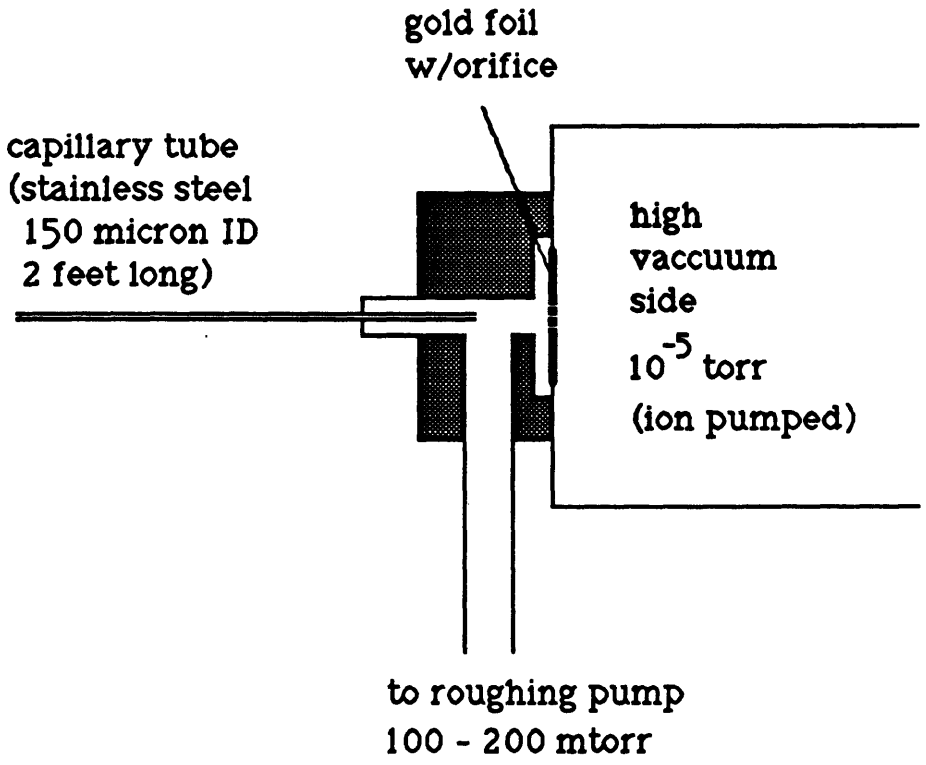

Figure 5.1: Schematic of mass spectrometer configuration for sampling gasses at atmospheric pressure.

spectrometer used was a UTI model 100C and was outfitted with a dynode electron multiplier for ion detection.

Using this gas sampling system, the decomposition of CH_3I was studied as a function of susceptor temperature. For these experiments, the capillary tube was placed so that it just rested on the back end of the bare molybdenum susceptor allowing for sampling of the gas at the susceptor surface. The total flow of hydrogen to the reactor was 1000 sccm and $y_{CH_3I} = 0.01$. Data were recorded after allowing the mass 142 signal to reach a stable value, usually 2 minutes after the inlet gas composition was switched (from pure H_2 to the test mixture). Electron multiplier currents were individually recorded at the mass numbers of interest. The peak heights were generally observed to fluctuate by +/- 5% or less and this is the assumed error in the measurement.

The room temperature spectrum for a stream of 0.7 mol% CH_3I in hydrogen is shown in Figure 5.2. In this figure, the peaks are normalized to the mass 142 signal (CH_3I mw = 142). The absolute electron multiplier reading at mass 142 was 1.3×10^{-7} amps. The practical sensitivity of the electron multiplier is 1×10^{-11} amps and therefore concentrations on the order of 1 ppm are detectable with this probe. Another feature of this spectrum is the mass 15 peak which is nearly 7 times as high as the mass 142, parent peak. The mass 15 signal originates from the CH_3^+ ion from the cracking of CH_3I in the ionizer, its abnormal height relative to the higher masses is due to mass number dependence of the electron multiplier gain, ie.

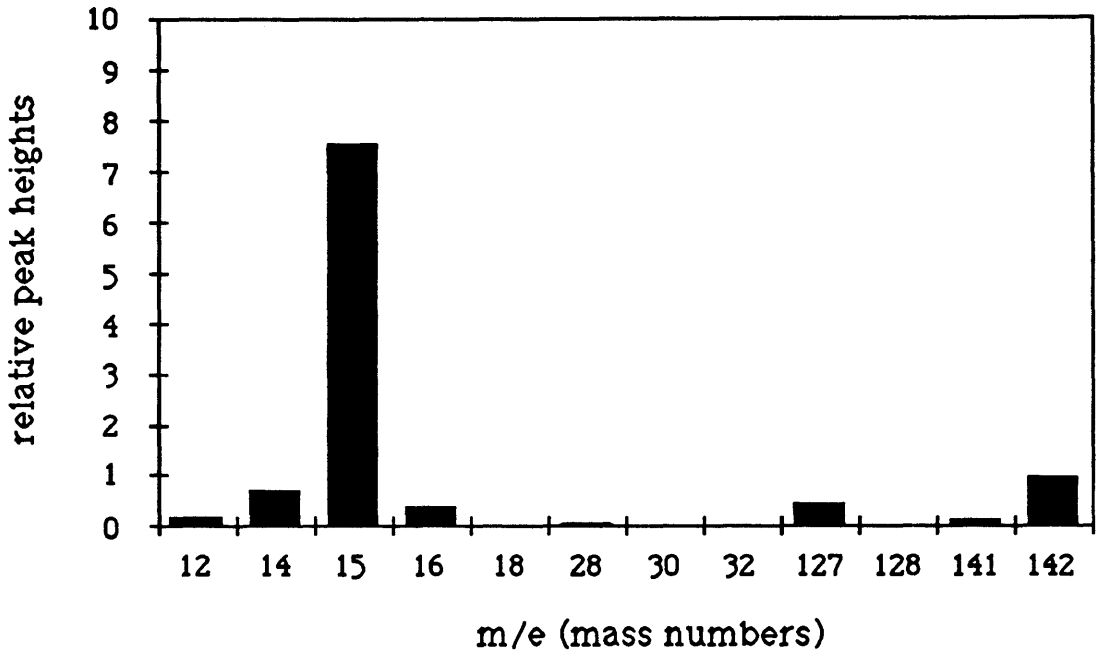

Figure 5.2: Room temperature mass spectrum of 0.7% CH_3I in H_2. Background levels subtracted out. Multiplier gain not compensated for.

Susceptor Temperature	mass 142 amps x 10^8	128/142 x100	127/142 x10	15/142	16/142
295	12.99	2.94	4.61	7.55	0.38
604	8.30	2.98	4.34	7.17	0.40
769	7.60	3.16	4.47	7.04	0.46
817	7.20	3.15	4.58	7.30	0.58
856	6.80	3.09	4.56	7.58	1.10
894	5.60	3.39	4.64	8.27	2.05
932	5.00	3.40	4.39	8.54	3.78
963	2.80	3.93	4.10	12.21	9.00
993	0.52	7.31	4.92	50.96	61.73

Table 5.2: Decomposition data for CH_3I in hydrogen (0.7%). Peak heights as a function of susceptor temperature (K).

the amount by which the electron multiplier amplifies a given ion current signal is larger for smaller m/e ratios.

Table 5.2 lists several data for the CH_3I decomposition experiments. The values reported in this table have background levels subtracted off and are scaled to the current value recorded at 142 amu, the "parent" peak for CH_3I. Deviations in these entries from the corresponding room temperature value are therefore understood to be products of the CH_3I decomposition *in the reactor* as opposed to being products of decomposition *in the ionizer.* Products from decomposition in the reactor are first seen to arise at 16 amu at 856°K, at 15 amu at 894°K, and at 128 amu at 993°K. The 16 amu peak is most likely due to methane (CH_4) formed by the reaction of CH_3 (from CH_3I decomposition) with either H_2 or CH_3I (reactions 6 and 9 respectively). Likewise, the peak at 128 amu is likely due to HI formed by the reaction of I (from CH_3I decomposition) with H_2 or CH_3I (reactions 7 and 10 respectively). It is not clear what the mass 15 signal is due to; one known contribution, from cracking of CH_4 in the ionizer, will not account for the entire signal. It is also important to note that some expected stable products of CH_3I decomposition were not detected, specifically I_2, and C_2H_6. It is expected that I_2 will condense prior to the gas sample reaching the mass spectrometer whereas the C_2H_6 level is probably below the detection limit.

The data for 16 and 142 amu are plotted as a function of temperature in Figure 5.3. The CH_3I (mass 142) signal is seen to drop slightly as temperature increases for low temperatures ($T < 650°C$)

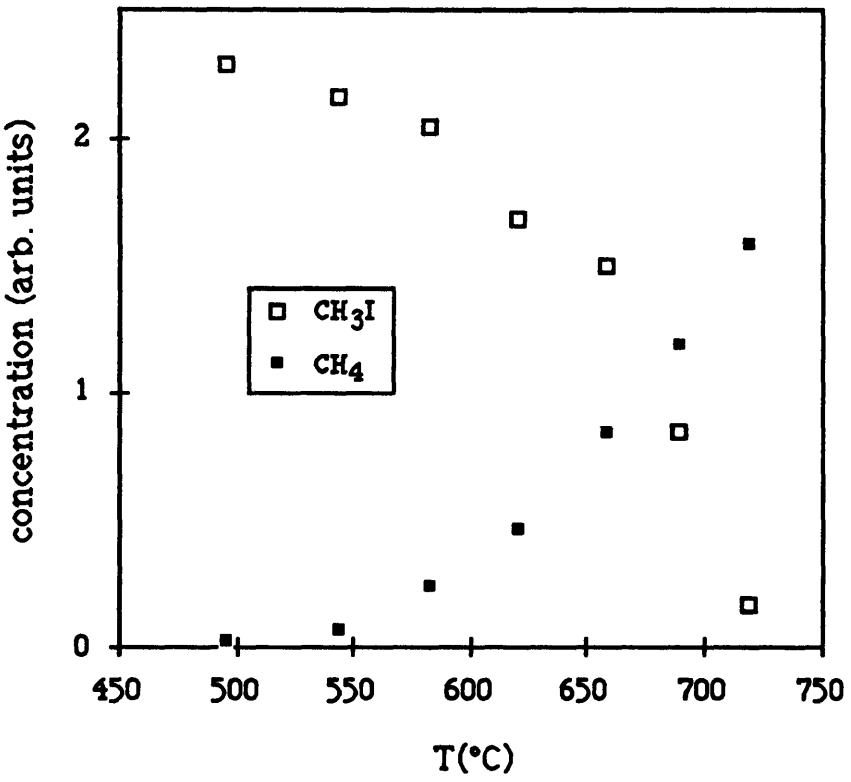

Figure 5.3: Measured mass 142 (CH_3I) and mass 16 (CH_4) versus temperature.

and then to drop more sharply at higher temperatures (T > 650°C). The sharper high temperature drop in mass 142 corresponds with the rapid increase of the mass 16 signal and it is at these temperatures that the decomposition reaction is occuring. The gradual decline in the mass 142 signal at lower temperatures is not due to decomposition but is instead due to thermal diffusion (the Soret effect), which will cause a lowering of the CH_3I concentration at the hot susceptor surface and from the lowering of the total gas density as temperature increases as given by the ideal gas law.

For purposes of comparison, the decomposition of CH_3I was simulated by a time integration of the full set of 14 difference equations generated from the 14 chemical reactions in Table 5.1. For this integration, a constant gas temperature was assumed equal to the surface temperature and the time of reaction was taken to be the average residence time in the reactor over a 2 cm distance, roughly 0.2 seconds. In other words, the horizontal reactor is approximated as an isothermal plug flow reactor. The results of these integrations are shown in Figure 5.4 which shows predicted concentrations of CH_4 and CH_3I as a function of temperature. Comparison of Figure 5.3 to Figure 5.4 reveals qualitatively similar behavior, the sharp decline in CH_3I concentration coincides with the sharp rise in CH_4. However, the decomposition temperature predicted by the isothermal plug flow model is almost 150°C lower than that found experimentally. The isothermal plug flow representation is clearly a poor approximation for describing the actual reactor. Clearly the effects of the non-uniform temperature field on reaction rates and replenishment of

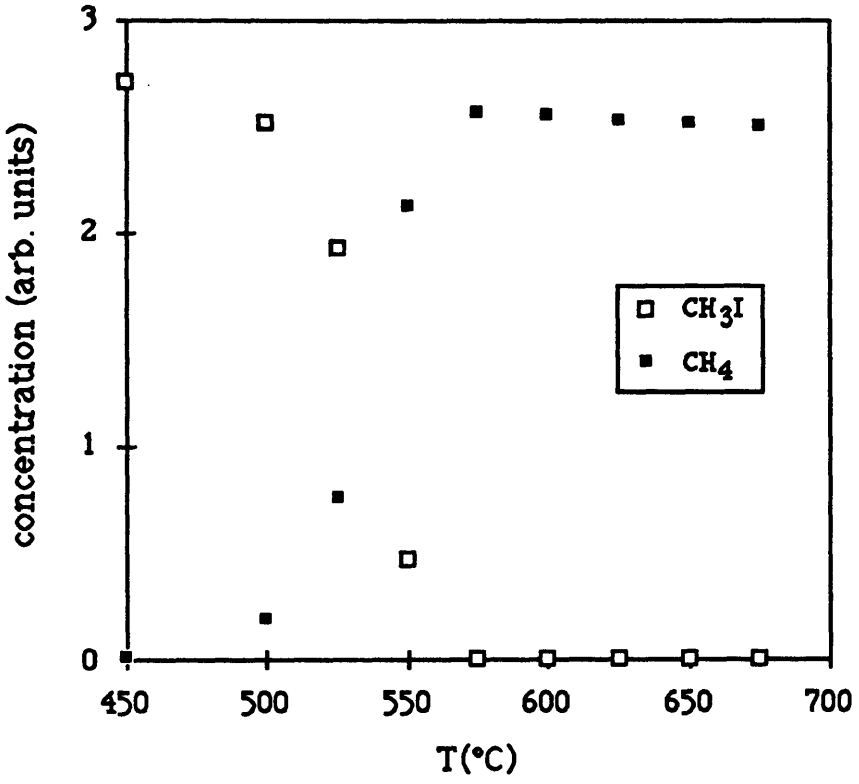

Figure 5.4: Predicted CH_3I and CH_4 concentrations based on full reaction model, isothermal plug flow assumption, 1 slpm, H_2 carrier, 2 cm distance. (compare to mass spec decomp. data).

CH_3I to the hot region near the susceptor surface by diffusion from the colder gas above are important, necessitating the use of a more detailed description of the reactor physics in order to accurately represent the chemistry.

5.4 ETCH PRODUCT ANALYSIS

Information about stable etch products will give some insight into the mechanism of CH_3I vapor etching of GaAs. Expected products are methylated and/or iodated species of gallium and/or arsenic formed from the reaction of the solid GaAs with CH_3 or I radicals. The low vapor pressure of gallium metal (bp = 2403°C) at our typical etch conditions means that it is necessary that a volatile compound of gallium be formed during the etch process. Arsenic, on the other hand, has several volatile forms at these temperatures, As_2 and As_4 being the two most stable vapor forms (T_{subl} = 613°C). Therefore, arsenic may form volatile compounds during etching or it may evaporate as the element.

Initial attempts to study etch products were conducted by examining the exhaust gas from the reactor with the mass spectrometer system described in the previous section. This analysis was limited to detecting stable, volatile etch products (the trimethyl or dimethyl-iodo compounds of gallium and arsenic only). The results of these studies were inconclusive inasmuch as no gallium or arsenic containing species were found in the m/e range from 0 - 300 AMU. A

significant amount of deposits were observed on the reactor walls downstream of the etching region of the reactor after several reactor runs. Since no volatile etch products could be detected, the primary etch products are either liquids or solids at room temperature and would be present in these deposits. These deposits were broadly classified as one of two different types, a dark brown-black deposit was observed on the reactor tube wall above and directly behind the susceptor. Further downstream, a deposit which was yellow/orange in color was observed. Both of these deposits were removed from the reactor and analyzed by AES. This analysis was necessarily obscured by the fact that the samples were exposed to air prior to being introduced into the vacuum system for AES analysis.

The AES spectrum of the brown-black deposit is shown in Figure 5.5. The deposit is primarily arsenic with the expected oxygen impurity from the ambient exposure. The small amount of carbon in this spectrum is also due to sample contamination from ambient exposure.

Close inspection of the second, yellow/orange deposit revealed that it was made up of small liquid droplets, most of which contained pieces of a solid material. The AES spectrum of the droplets revealed them to contain gallium, iodine, oxygen, and carbon as is shown in figure 5.6. The iodine signal in the drops was strongest on the solid regions and weakest in the liquid region. Additionally, the iodine signal was obscured due to the main oxygen peak having the same energy.

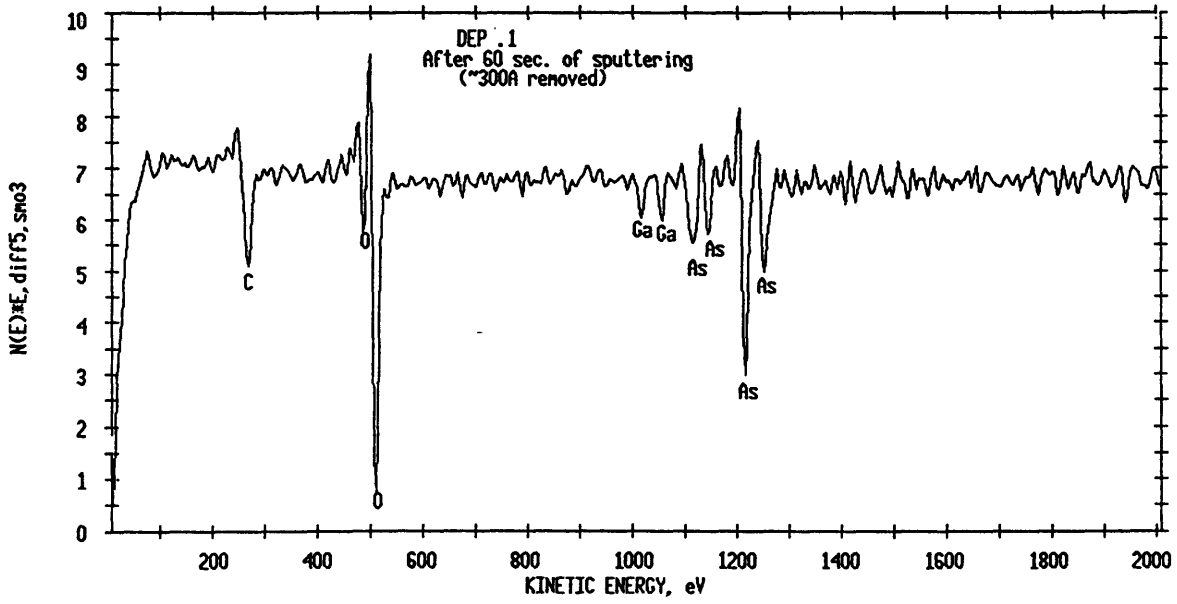

Figure 5.5 AES spectrum of arsenic containing wall deposit

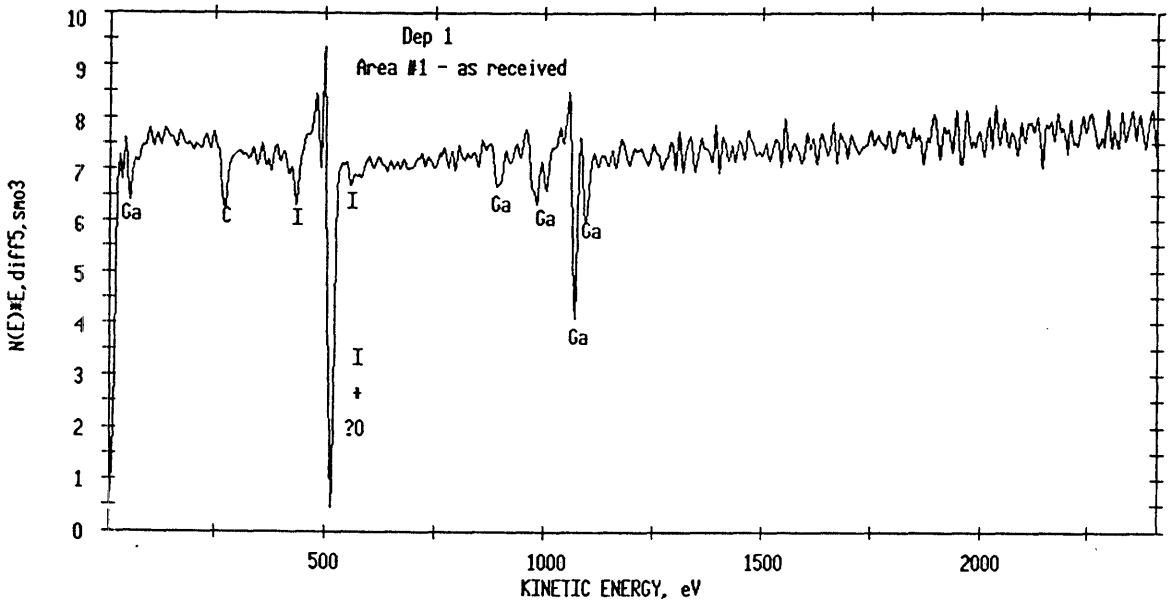

Figure 5.6: AES spectrum of gallium containing wall deposit

This result leads to the following tentative conclusion. The primary etch product is GaI (gallium mono-iodide). This compound has been previously isolated and is known to be unstable in air. It would not be unusual for this compound to disproportionate to $GaI_{3(s)}$ and $Ga_{(l)}$, a process that may be accelerated in air (see reference on GaCl disproportionation). This would explain our results as meaning that the liquid is gallium metal (mp = 30°C) with solid particles of GaI_3 suspended within.

The following etching reaction is proposed based on these results

$$2GaAs_{(s)} + 2I_{(v)} \text{ -----> } 2GaI_{(v)} + As_{2(v)} \qquad (5.15)$$

This reaction is allowed thermodynamically ($\Delta G_{r(500°C)}$ = -3 kcal/mol). This is the overall reaction which will be tested in the next section. Etching reactions involving methyl radicals should not be completely ruled out, but these are clearly not dominant. Furthermore, the evidence argues against the formation of purely methylated compounds (ie. $Ga(CH_3)_3$, $As(CH_3)_3$) which are volatile should have been detected on the mass spectrometer.

5.5 CH_3I VAPOR ETCHING IN THE VERTICAL ROTATING DISK REACTOR: COMPARISON OF MODEL WITH EXPERIMENT

5.4.1 Introduction

In section 5.3, it was found that simple, isothermal models for the chemical reactions in the horizontal reactor system led to significant errors in predicting bulk decomposition rates. This result emphasizes the need for incorporating detailed physics and chemistry into a fully integrated model in order to accurately predict species concentrations and surface reaction rates. It is important to incorporate effects of heat, mass, and momentum transfer as well as detailed chemistry. The field of chemical vapor deposition has in recent years seen development of many detailed models for describing the flow and temperature fields in these types of reactors (for an excellent review of the subject see Jensen et al, 1991 and references therein). The best of these models have incorporated high levels of detail including effects of thermal diffusion and radiative heat transfer. The current state of development couples these models with detailed gas phase and surface chemical reactions. The equations for these systems are non-linear and require numerical techniques such as finite elements or finite difference in order to obtain approximate solutions.

For the purposes of this section, we are interested in simulating the CH_3I vapor etch chemistry in the vertical rotating disk reactor

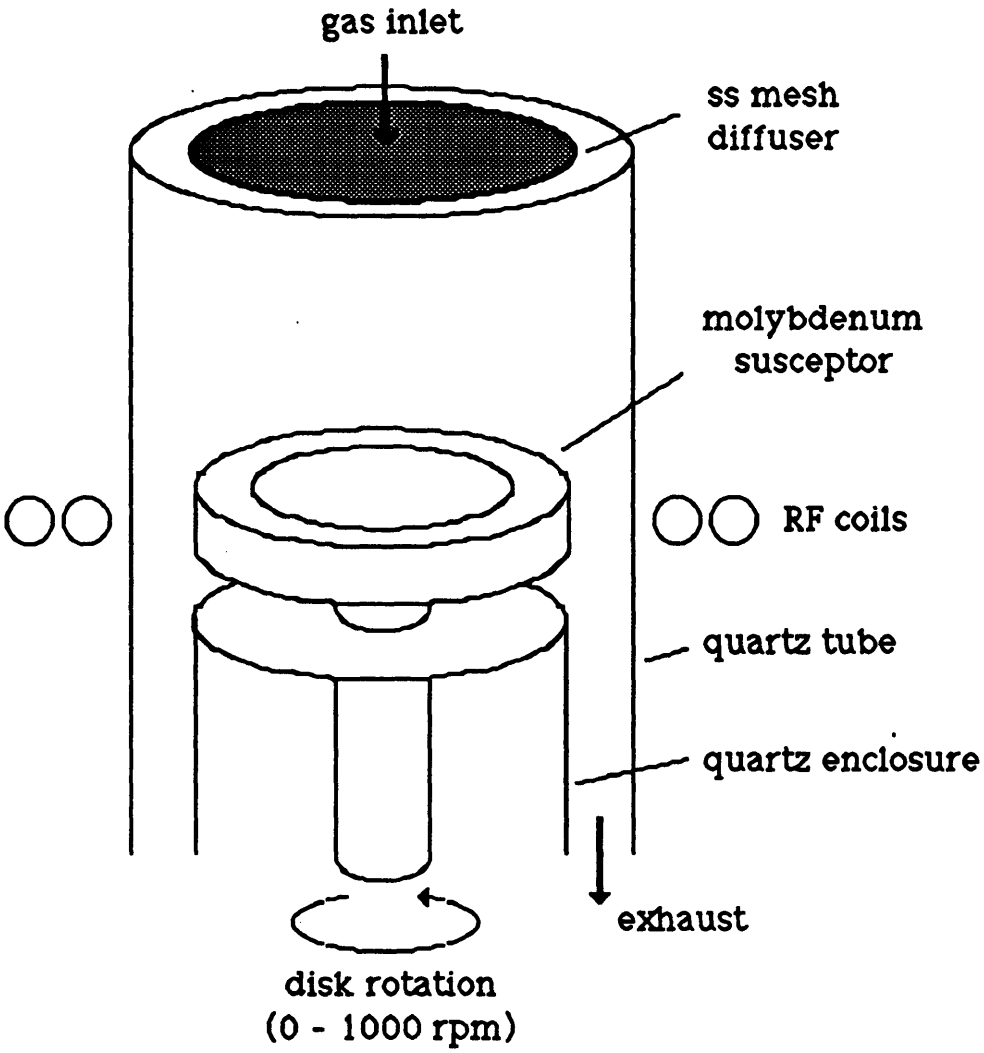

Figure 5.7: Schematic of vertical rotating disk reactor.

system. A schematic of this reactor is shown in Figure 5.7. There are several reasons for choosing this reactor over the horizontal reactor used for much of the experimental work to date on this subject. First, the vertical rotating disk reactor has radial symmetry and can therefore be accurately represented in two spatial dimensions. Second, an existing model for the vertical rotating disk reactor system was available which has been demonstrated to accurately predict growth rates of GaAs from trimethylgallium (TMGa). Finally, the vertical rotating disk reactor is technologically important as a state-of-the-art OMVPE reactor system and it is therefore desired to investigate vapor etching in this system

5.4.2 Details of Numerical Model

The computer model for the vertical rotating disk reactor system used in this chapter is the model developed by Patnaik et al (1987) with minor modifications. This model was modified to handle a multi-component, multi-reaction system. In brief, it is a finite element representation in two space dimensions of the vertical rotating disk reactor geometry. The model is based on the full equations for momentum, heat, and mass transfer and includes radiative heat transfer and thermal diffusion. It has been demonstrated to accurately predict OMVPE growth rates of GaAs from trimethylgallium under conditions of mass transport rate limitation (Patnaik, 1989). It has further been used to establish reactor operating regimes which avoid the onset of buoyancy driven,

recirculating flows which are undesirable for reproducible, controllable OMVPE growth.

The approach used to do the calculations takes advantage of the fact that the bulk of the gas in the reactor is hydrogen with a reactant (CH_3I) present in dilute amounts. This allows heat of chemical reaction effects to be ignored and decoupling of the flow/temperature calculation from the reaction/mass transfer computation. In practice, the flow and temperature fields are computed first and serve as inputs to the reaction/mass transfer model. As an independent test of this component of the model, computed reactor wall temperatures have been compared to experimentally measured values (5.4.3).

The main goal of this modelling work is to test the mechanism for CH_3I vapor etching of GaAs that has been deduced from the experimental evidence in Chapter 3 and the etch product analysis in section 5.4. Restated, the mechanism that has been argued is one where free radicals produced by the decomposition of CH_3I react with solid GaAs to form vapor products. Based on the etch product analysis, it was deduced that iodine atoms are the primary etchant species with one iodine atom removing one molecule of GaAs (equation 5.15). Coupling this surface iodine consumption reaction with the gas phase production of iodine atoms requires an assumption as to the surface reaction probability of iodine atoms. At high surface reactivities, the assumption of zero surface concentration is valid. However, it was shown in Chapter 4 that this

may not be the case, a situation of mixed control between the gas phase production and diffusion of etchant species to the surface and the surface reactions must be considered in general. Therefore, the following commonly used expression for describing finite surface reaction rates (R_{sur}) is employed

$$R_{sur(i)} = \frac{\sigma_i y_i P}{\sqrt{2\pi m_i RT}} \qquad (5.16)$$

which is simply an assumed surface reaction probability σ_i (between 0 and 1) multiplied by the surface collision frequency, a result derived from kinetic theory (m_i is the molar mass of species i). The value of σ_i will generally depend on temperature and surface coverage. Because σ_i's are generally not known, it is important to test the sensitivity of computed solutions to variations in these assumed values. The surface boundary condition for each component (i) is obtained by balancing equation (5.2) to the gas phase supplied flux to the reacting surface for each component (i):

$$\frac{\partial C_i}{\partial y} = \frac{R_{sur(i)}}{D_i} \qquad (5.17)$$

Where C_i and D_i are respectively the concentrations and diffusivities of species i. It is important to note that the desorbing products are not included in these calculations. In other words, that the iodine atoms are simply considered to disappear at the surface according to the kinetics described above. Desorption limitations have not been observed in our experiments to date so this assumption should

suffice. Values for species diffusion coefficients used in these calculations are estimated using standard methods (requiring values of Leonard-Jones parameters for each species). Values for thermal diffusion coefficients are estimated using the technique reported by Holstein (1988).

5.4.3 Verification of Computed Temperatures: Comparison of Measured Reactor Wall Temperatures with Model Predictions

Verification of computed temperature fields has been done directly by measuring internal hydrogen gas temperature by 2-D Raman spectroscopy in a horizontal OMVPE reactor (Fotiadis, et. al., 1990). As it is the internal gas temperatures that we are interested in, this type of direct gas temperature measurement would be ideal. However, we lack the sophisticated apparatus required to gather such measurements and therefore chose a simpler albeit less direct approach. The outer reactor wall skin temperature is an accessible measurement and the model computes these values as well. Therefore we can compare the predicted wall temperatures to the measured values and will take this to be an indirect verification of the internal gas phase temperatures.

For the experimental measurements of wall skin temperature, a chromel-alumel thermocouple junction was directly contacted with the reactor wall and held in place by a thin quartz rod. The

thermocouple junction itself was formed by welding two pieces of chromel and alumel wire into a bead which was then flattened out. With this arrangement, conduction of heat away from the junction is not expected to be significant. RF heating of the thermocouple junction did occur, but by switching off the RF power, the wall thermocouple temperature was observed to relax to a stable value rapidly when compared to the rate at which the susceptor cooled. It is this relaxed value which is reported to be the wall temperature. The susceptor temperature is measured by a thermocouple which is directly inserted into the bottom of the susceptor (molybdenum). This is the same thermocouple referenced to when reporting etch/growth temperatures in the vertical reactor and has been previously verified to be accurate by comparison to surface optical pyrometer measurements. During these experiments, a constant flow of hydrogen to the reactor was maintained at 10 slpm and the disk was rotated at 450 rpm. Wall skin temperature measurements were taken at several different positions above the top of the susceptor. Simulations were performed at these same reactor conditions and under the additional assumption that the reactor wall top and bottom were constantly at room temperature.

The results of these experiments are shown in Figure 5.8 which also shows the corresponding computed wall temperatures.. Excellent agreement is demonstrated, and the computed internal gas temperatures are thus indirectly confirmed.

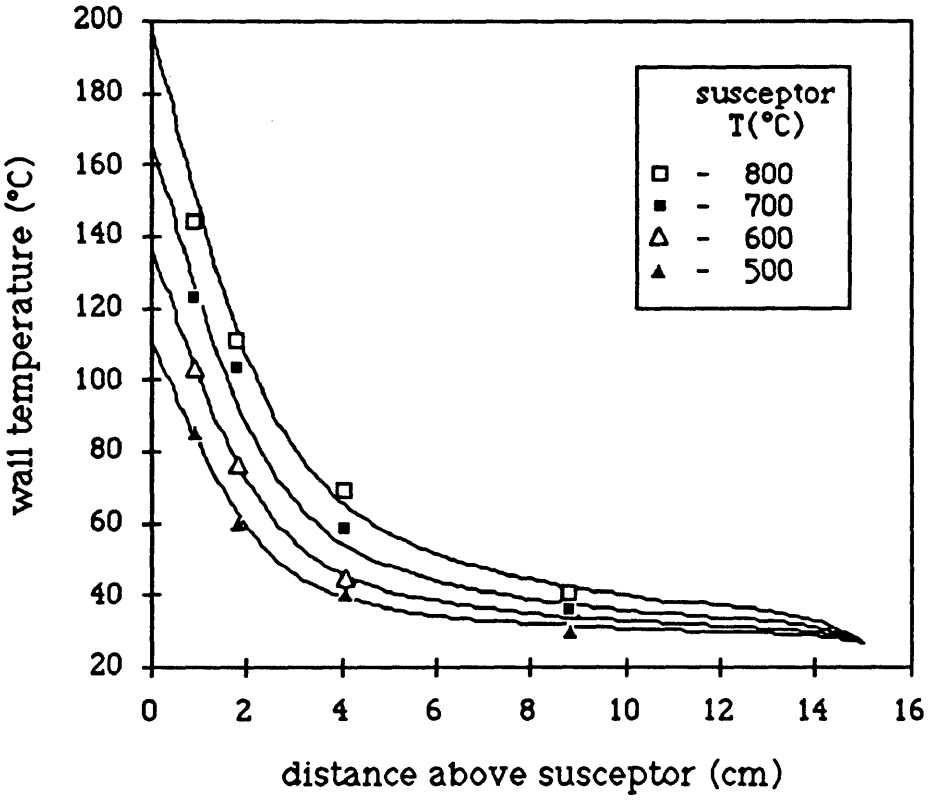

Figure 5.8: Wall temperatures predicted by vertical reactor model (solid curves) versus measured wall temperatures (symbols).

5.4.4 Vapor Etching Rates: Comparison of Model with Experiment and Other Predictions

Vapor etching in the vertical rotating disk reactor was experimentally investigated under a number of experimental conditions. For all of these experiments, the total hydrogen flow to the reactor was 10 slpm, the reactor pressure was 0.2 atm, and the susceptor was rotated slowly at 20 rpm. Etching was performed on GaAs epilayers which were grown over an $Al_xGa_{1-x}As$ marker layer; the etched depth being determined by the difference of the remaining epilayer thickness from the original thickness. In general, for similar etch temperatures and CH_3I mole fractions, etch rates in the vertical reactor were roughly 25 times lower than for the same conditions in the horizontal reactor (Chapter 3). These differences are easily understood in the context of the gas phase decomposition control of the reaction. The initiation reaction (reaction 1 in Table 5.1) operates under the low pressure limit and therefore decomposition rates are expected to be roughly 5 times lower due to the lower operating pressure of the vertical reactor compared to atmospheric pressure operation of the horizontal reactor system. The lower pressure also causes concentration of CH_3I to be a factor of 5 lower than in the horizontal system for the same inlet mole fraction.

The results of these experimental studies are shown in Figures 5.9 and 5.10 and are compared to etch rates predicted by the model described in sections 5.4.1 and 5.4.2. For these calculations, the value assumed for σ_I was the largest possible, 1.0. As can be seen from

these figures, the quantitative agreement between the experimentally measured and predicted etch rates is quite good. The error bars shown in these figures represent errors inherent in the Dektak measurements of etch depth and are fairly large because of the small etched depths (~1000 - 2000 Å total material removed) compared to the accuracy of the Dektak (+/- 200Å).

The dependence of the predicted etch rates to the assumed value of σ_I is shown in Figure 5.11. There are two regimes shown in this figure. At high assumed values for σ_I , the predicted etch rate does not depend on the assumed value of σ_I and the rate is understood to be limited by gas phase processes. At lower values, the rate drops linearly with decreasing σ_I and this is a mixed surface/gas phase control regime. More detailed experimental studies are necessary in order to determine the exact value of σ_I and some factors which contribute to this number are discussed in Chapter 6.

The predicted effect of susceptor rotation rate on the etch profiles is shown in Figure 5.12 for two values of σ_I , 10^{-5} and 1.0. For both cases, it can be seen that high rotation rates (500 rpm and above) are required to improve the etch rate uniformity across the susceptor from a 30% variation at 20 - 100 rpm to less than 20% at 500 rpm. The etch rate decreases overall, due to the reduction in thermal boundary thickness at high rotations and the subsequent reduction in CH_3I decomposition.

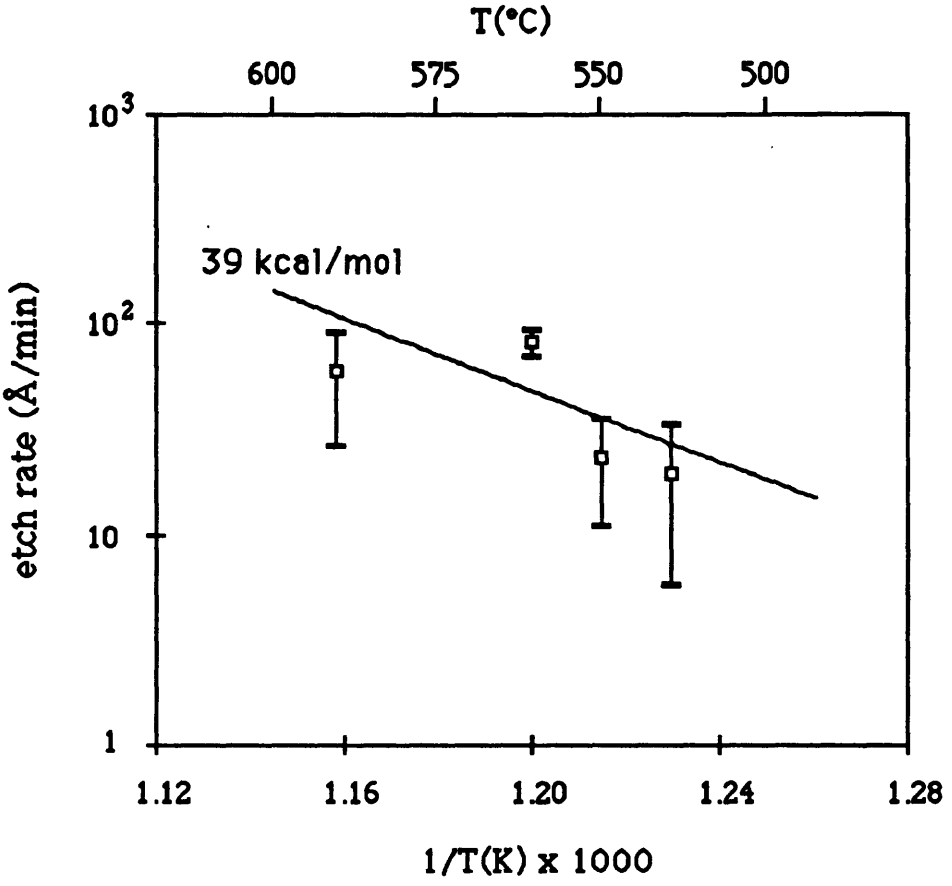

Figure 5.9: Predicted temperature dependence of etch rate in vertical reactor (solid line) vs. experimental data (squares w/error bars). Etch conditions, y_{CH_3I} = 0.01, 10 slpm H_2, 0.2 atm. Assumed value for σ_I =1.0.

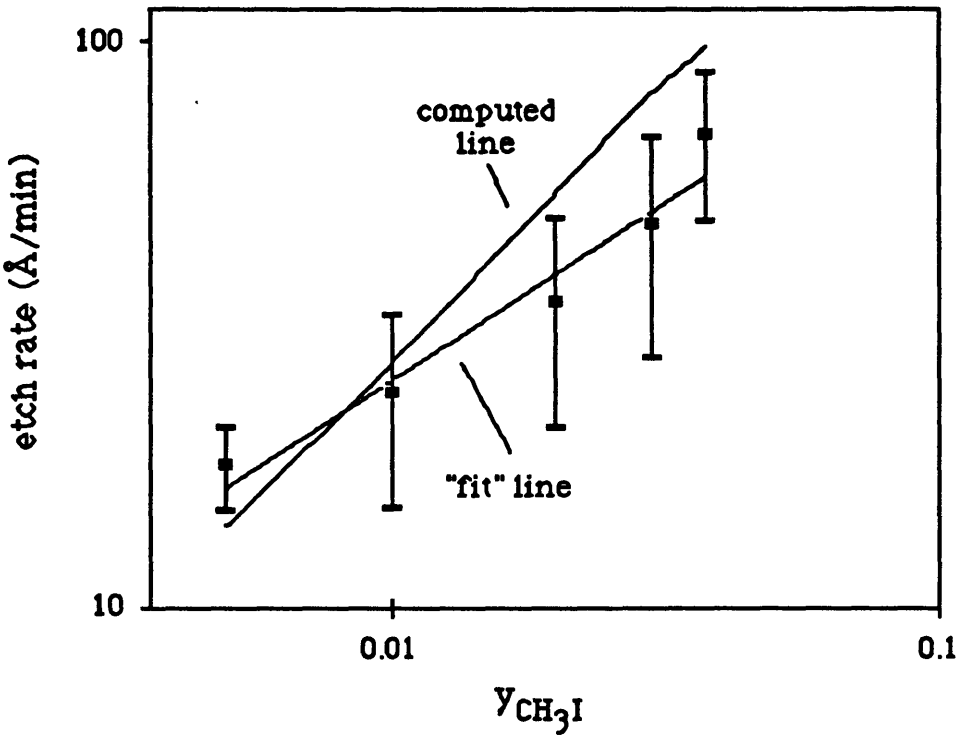

Figure 5.10: Predicted etch rates compared to experimental etch rates in the vertical reactor as a function of CH_3I concentration. Etch conditions, 550°C, 0.2 atm, 10 slpm H_2.

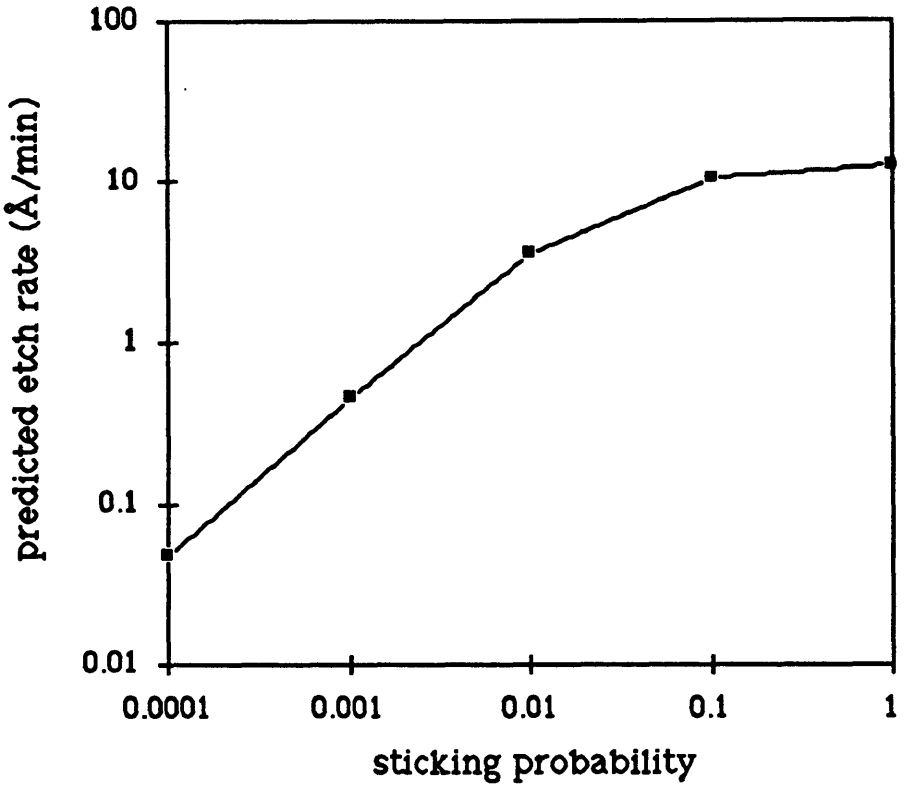

Figure 5.11: Predicted etch rate as a function of assumed iodine sticking probability, σ_I. Etch conditions, 525°C, y_{CH_3I} = 0.01, 10 slpm H_2, 0.2 atm.

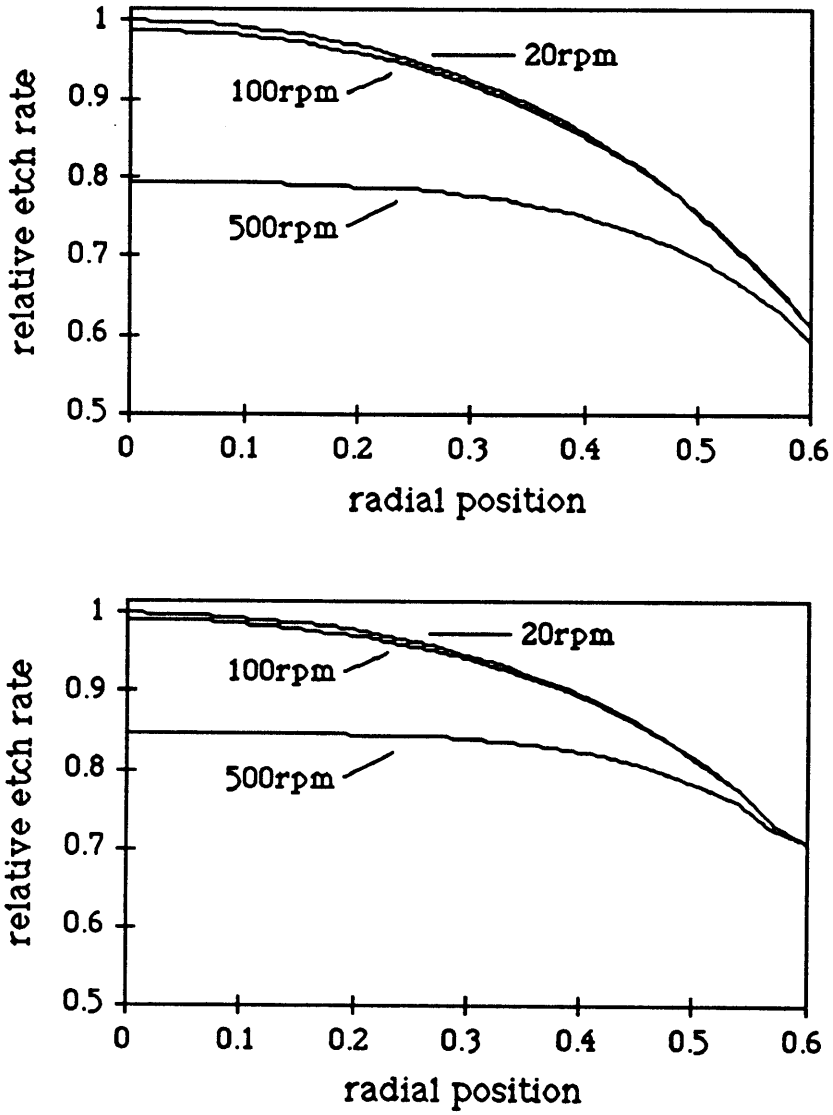

Figure 5.12: Predicted effect of disk rotation rate on etch rate and uniformity. Conditions 525°C, y_{CH_3I} = 0.01, 10 slpm H_2, 0.2 atm, σ_I = 10^{-5} (top), σ_I = 1.0 (bottom).

In addition to checking solution sensitivity to variations in σ_I , the sensitivity of predicted etch rates to variations in D_I and k_1 were examined. Parameters for determining iodine atom diffusion coefficient could not be found and the actual diffusivities used are those previously used for diffusion of Ga-atoms in hydrogen (Patnaik. 1987). It is therefore important to check the sensitivity of computed solutions to variations in this diffusivity. The sensitivity to value of k_1 (reaction 5.1) was additionally confirmed to correspond exactly to variations in inlet CH_3I concentration. Therefore, the etching reaction order is also determined in this analysis. The sensitivity to variations in these parameters is illustrated in Figure 5.13, which shows the computed etch rate at the susceptor center as a function of the given parameter value (base value = 1.0) on a log-log plot. Sensitivity is checked for two different values of σ_I, 10^{-5} and 1.0 since it is expected that the solution structure is different in the two regimes shown in Figure 5.11.

The results in Figure 5.13, in addition to providing a measure of confidence in the computed solutions also gives some insight into the structure of the I-atom concentration field near the surface. For σ_I = 10^{-5}, increasing D_I results in a decrease in the predicted etch rate. This counter-intuitive result is due to the fact that iodine atoms are produced within the thermal boundary layer *close to the surface.* There are therefore two diffusion driving forces, the surface reactivity which sets up a flux to the surface and diffusion away from the surface due to the fact that I-atom concentration drops to zero in that direction. For low surface reactivities, the second process

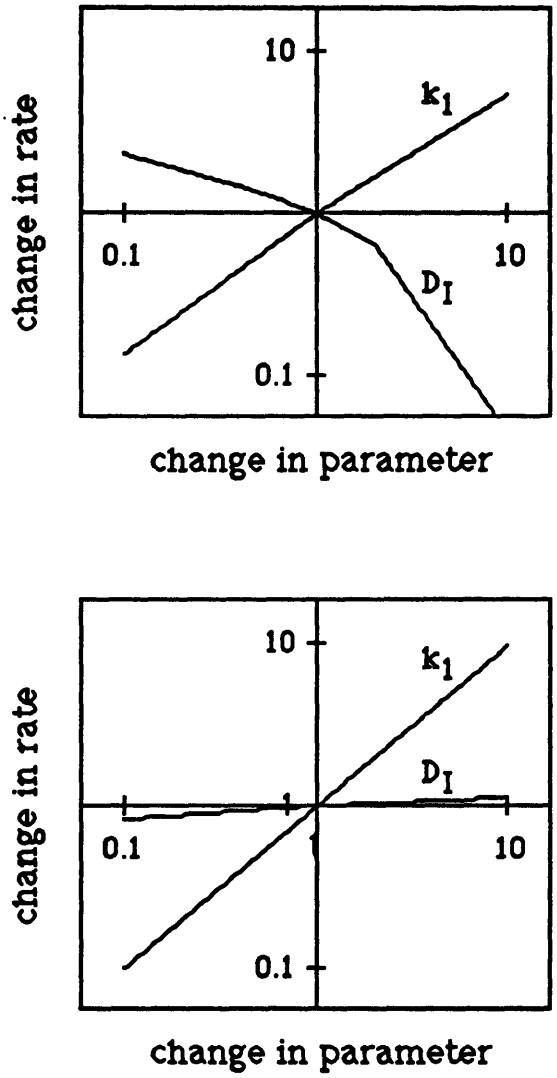

Figure 5.13: Sensitivity of predicted etch rates to variations in both k_1 and D_I. Conditions 525°C, y_{CH_3I} = 0.01, 10 slpm H_2, 0.2 atm, σ_I = 10^{-5} (top), σ_I = 1.0 (bottom).

dominates. For high surface reactivities (σ_I = 1.0), little dependence of the solution on the assumed value for D_I is seen. In this case, a balance between the two diffusion processes exists. This analysis is confirmed by examining the position above the susceptor surface where the I-atom concentration is its maximum. For low surface reactivities, the maximum is very close to the surface. As D_I is raised, the maximum moves away from the surface but decreases in absolute magnitude. At high surface reactivities, the maximum is relatively high above the surface and a very sharp concentration gradient is set up near the surface.

Another observation from Figure 5.13 is a lowering of etching reaction order in y_{CH_3I} from 0.97 for σ_I = 1.0 to 0.80 for $\sigma_I = 10^{-5}$. The cause of this effect is not entirely clear but could be due to the same competitive diffusion process discussed above. The possible connection between this observation and the experimentally observed sublinear reaction orders in the horizontal reactor system (Chapter 3) should not be ignored. However, the horizontal reactor is not expected to exhibit boundary layer structures *per se*. Nevertheless, iodine atom concentrations are expected to exhibit a maximum near the surface and competitive diffusion would be expected to occur - the magnitude of the effect in the horizontal reactor cannot be deduced from this analysis of the vertical reactor, however.

5.5 CONCLUSIONS

In this chapter the mechanisms operating to control etch rates of GaAs by CH_3I vapor were examined. First, the decomposition reaction of CH_3I was studied in the horizontal reactor previously used for vapor etching experiments by mass spectroscopic monitoring of stable gas species within the reactor. The main stable product of CH_3I decomposition in H_2 was CH_4 and a small HI signal was detected at high temperatures. At typical etch temperatures (in the range from 450 - 550°C), the decomposition of CH_3I was not substantial and was not detectable until temperatures in excess of 600°C were reached. Comparison of these experimental results with an isothermal plug flow model of the decomposition chemistry showed that the plug flow reactor description of this reactor is qualitatively correct but quantitatively inaccurate - the predicted decomposition temperature was 150°C lower than that found experimentally. Second, an etching mechanism where iodine atoms produced from the gas phase decomposition of CH_3I was proposed based on a chemical analysis of the etch products and the experimental results previously discussed in Chapter 3. The proposed mechanism was confirmed by successful comparison of experimental etch rates with computed etch rates by a complete model description of the process in the vertical rotating disk reactor system. Etch rates in the vertical reactor are much lower than those previously observed in the horizontal reactor system due to the lowering of the gas phase decomposition of CH_3I at reduced pressures (0.2 atm vs. 1 atm). It was further shown that an increase

in the disk rotation should lead to improved radial uniformity of etch rate while decreasing etch rates overall.

Chapter 6

Vapor Etching of GaAs with CH_3I: Surface Reactions

6.1 INTRODUCTION

In previous chapters, the chemical vapor etching of GaAs by CH_3I was discussed and was shown to be a potentially useful process especially as a complementary, *in situ* process to crystal growth by OMVPE. The etching of GaAs is understood to occur primarily by the reaction of iodine atoms with GaAs to produce volatile gallium-iodide compounds, with arsenic evaporating in elemental form. Although the production of iodine atoms in the gas phase (by CH_3I decomposition) is the primary rate limitation, gas phase diffusion and surface reactions have been observed to influence the etching of micro-faceted structures and masked features. Additionally, it has been hypothesized that surface rate limitations are responsible for the degraded surface morphologies observed at higher etch temperatures, especially the formation of etch pits and for the sublinear dependence of etch rate on y_{CH_3I} (Chapter 3).

In this chapter, experimental results are presented on the effects of adding trimethylarsenic (TMAs) to the CH_3I etch mixture are presented. Addition of TMAs is shown to lower etch rates by

reducing the reactivity of the GaAs surface to iodine attack. A surface reaction model for etching is proposed which can account for both the effects of adding TMAs and the previously observed sublinear reaction order in CH_3I inlet concentration.

6.2 BACKGROUND

Although there have been a number of studies of different chemistries for vapor etching of GaAs, very few have examined the effects of adding other chemicals to the etch mixtures. In theory, by adding gallium and/or arsenic sources to the etch gas mixture, it should be possible to overcome any non-stoichiometric etching properties of a particular vapor etch. For example, if a particular etch removed arsenic preferentially to gallium, then gallium would be expected to accumulate on the surface, possibly coalescing into droplets and thereby causing an eventual breakdown in etched surface morphology. In this hypothetical situation, a source of arsenic added to the etch mixture would allow stoichiometric etching to be achieved.

Heynen and Balk (1980) specifically examined the effects of adding AsH_3 and GaCl to the HCl/H_2 etch of GaAs. It was found that adding AsH_3 decreased the etch rate weakly and had little apparent effect on the surface morphology. GaCl on the other hand decreased etch rates in a proportional fashion and improved etched surface morphology on the (100) and (111)Ga surfaces if some AsH_3 was also

present. Mirror like surfaces could be maintained with etch rates as high as 5500 Å/min by appropriate choice of $GaCl:AsH_3:HCl:H_2$ ratio, demonstrating that surface stabilization can be obtained at non-equilibrium conditions.

Bakin, et al. (1972) found that smooth surfaces could be maintained on GaAs (100) surfaces in the $AsCl_3$-Ga-H_2-As_4 chloride-vapor transport system only at conditions close to equilibrium (ie. close to no etching).

In neither of these two studies was it possible to elucidate the exact mechanism for etched surface morphology improvement. Nor is it possible to determine a general scheme for improving surface morphology based these two studies due to the conflicting results obtained regarding the nature of etching conditions required for obtaining smooth etched surface morphology. Therefore, it is not known *a priori* what effect addition of arsenic or gallium sources to a particular etch mixture will have on etched surface morphology or etch rates.

The arsenic source that is used in the present study is trimethylarsenic (TMAs, $(CH_3)_3As$). One study of TMAs adsorption on GaAs (100) surfaces has shown that no decomposition of the molecule occurs on the surface but rather it desorbs intact upon heating (Creighton, 1989). It is therefore expected that only the gas phase decomposition of TMAs will occur in these experiments. Although a number of researchers have studied the gas phase

decomposition of TMAs, there is some dispute as to the exact decomposition mechanism. Using a molecular beam mass spectrometer sampling system, Lee, et al. (1988) proposed a straightforward mechanism of sequential methyl radical scissions from the TMAs molecule, leading to the eventual formation of elemental arsenic. This mechanism is in agreement with that proposed in earlier work on TMAs decomposition in toluene (Price and Richard, 1970). Li, et al (1990), however, propose that the decomposition in hydrogen proceeds by the intermolecular elimination of methane via a 5-coordination transition state complex of TMAs with one H_2 molecule. This argument was made to account for the fact that the decomposition rate is higher in hydrogen (T_{decomp} = 535°C) vs. helium (T_{decomp} = 570°C) but no direct evidence for the proposed transition state was provided. Nevertheless, observed lower decomposition temperatures in hydrogen compared to inert gases is not uncommon since hydrogen will propogate free radical chains through the formation of H-atoms. H-atom abstraction of CH_3 ligands from the TMAs could also explain the observed lowering of decomposition temperature.

6.3 EXPERIMENTAL PROCEDURE

The general experimental method and apparatus employed in these studies was discussed in detail in Chapter 3. The reactor system was modified for these experiments by adding a trimethylarsenic (TMAs) bubbler to the available sources. The etch gas mixture consists of a

hydrogen carrier gas containing both trimethylarsenic (TMAs) and methyl iodide (CH_3I). The GaAs substrates employed are all n^+ (100) + 2° to (110) manufactured by AXT. Each wafer was half masked with silicon nitride. The reactor is of horizontal configuration operated at atmospheric pressure. All of the etched depths reported were measured at a distance 5 mm downstream from the front edge of the wafer (12mm from the front edge of the susceptor). A typical experiment involves heating the sample to the desired temperature under hydrogen flow, allowing this temperature to stabilize for at least five minutes and then first switching in the TMAs quickly followed by CH_3I. The time of exposure is chosen so that an ample amount of material is removed (>2000Å) to assure reasonable accuracy of subsequent etch depth measurements via Dektac profilometry. Etch rate is calculated by dividing the etched depth by the total exposure time.

Three different sets of experiments were performed. First, the effect of changing TMAs concentration at a constant inlet CH_3I concentration was examined. Second the effect of changing the temperature at a constant TMAs/CH_3I ratio was investigated. Finally, the effect of changing the CH_3I concentration at a fixed TMAs flow was studied. In these experiments, the effects of varying the particular parameter on the etch rate and on the etch profile near the mask are reported.

6.4 EXPERIMENTAL RESULTS AND DISCUSSION

6.4.1 Results

The effect of adding TMAs to the CH_3I/H_2 etch gas mixture on etch rate was studied as a function of changing TMAs concentration at two different temperatures. Figure 6.1 shows the results at a susceptor temperature of 504°C for etch mixtures of 38.4 sccm CH_3I, 2100 sccm H_2 and TMAs/CH_3I ratios ranging from 0 to 0.4. The etch rates shown in this figure have been normalized to the rate at TMAs/CH_3I = 0. The results are characterized by an initial steep drop in etch rate with small amounts of TMAs present. This suppression effect tapers as the TMAs flow is increased. The results for a susceptor temperature of 553°C are shown in figure 6.2 for an etch mixture of 38.4 sccm CH_3I, 2100 sccm H_2 and TMAs/CH_3I ratios from 0 to 1.2. A quantitatively similar trend is observed here as well, although the net decrease is proportionally lower than at 504°C. The curves shown in Figures 6.1 and 6.2 are represented by the surface reaction model which will be presented in the next section.

Results for the temperature dependence of the *etch rate* are shown in Figure 6.3 for a CH_3I flow of 38.4 sccm and a constant TMAs/CH_3I ratio of 0.086. The activation energy calculated via a least squares fit to the data is 57 kcal/mol. Previous results for etching of GaAs by CH_3I alone revealed activation energies on the order of 43 - 48 kcal/mol, significantly lower than this value.

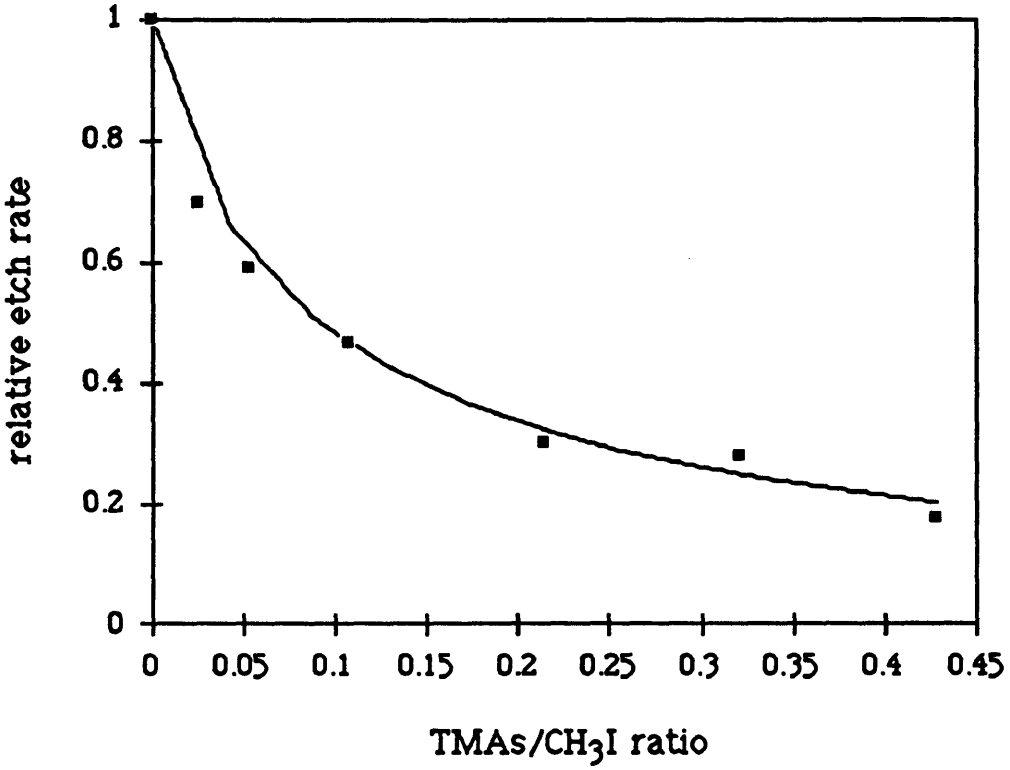

Figure 6.1: Effect of adding TMAs on CH_3I etching of GaAs. 504°C, 38.4 sccm CH_3I, 2100 sccm H_2.

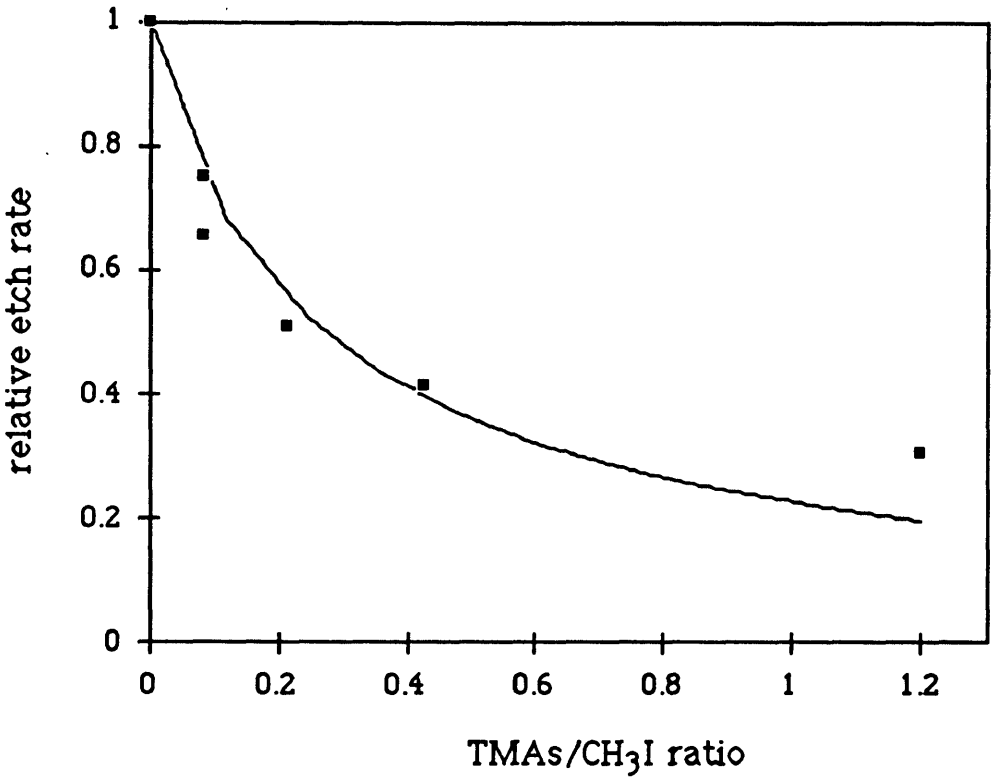

Figure 6.2: Effect of adding TMAs on CH_3I etching of GaAs. 553°C, 38.4 sccm CH_3I, 2100 sccm H_2.

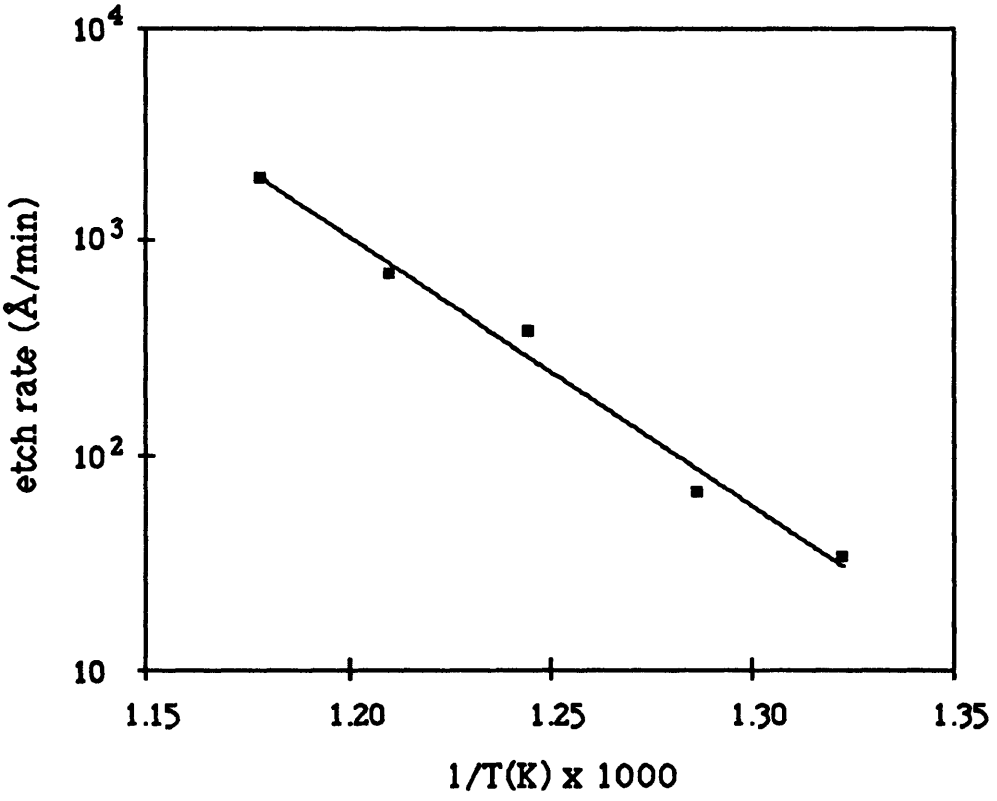

Figure 6.3: Temperature dependence of etch rate for CH_3I/TMAs mixture. Conditions: 38.4 sccm CH_3I, 2100 sccm H2, TMAs/CH_3I ratio of 0.086.

The effect of changing CH_3I flow at a constant TMAs flow of 3.3 sccm at a susceptor temperature of 550°C was also investigated. The etch rate order in CH_3I inlet concentration is calculated to be 0.83. It is interesting to note that the reaction order determined for this temperature for CH_3I alone was 0.68 (Chapter 3).

Another interesting feature was noted in these experiments which pertains to a discussion presented in Chapter 4. It relates to the non-uniform etch profiles observed near inert masks in the CH_3I vapor etching of GaAs. When TMAs was added to the etch mixture, it was observed that these non-uniformities decreased in proportion to the amount of TMAs. This result is illustrated in Figure 6.4. It is further apparent from this figure that the trench etch rate is decreasing faster than the bulk etch depth and therefore the potential for achieving uniform etch profiles near masks can be realized.

6.4.2 Discussion

Based on the experimental results just presented and the previously discussed results from Chapters 3 and 4, a model for the effects of adding TMAs to the CH_3I/H_2 etching system is now developed. The addition of TMAs to the vapor etch mixture CH_3I/H_2 could potentially have several effects on the etching chemistry. TMAs will serve as an additional source of methyl radicals in the gas phase but more importantly it a source of arsenic.

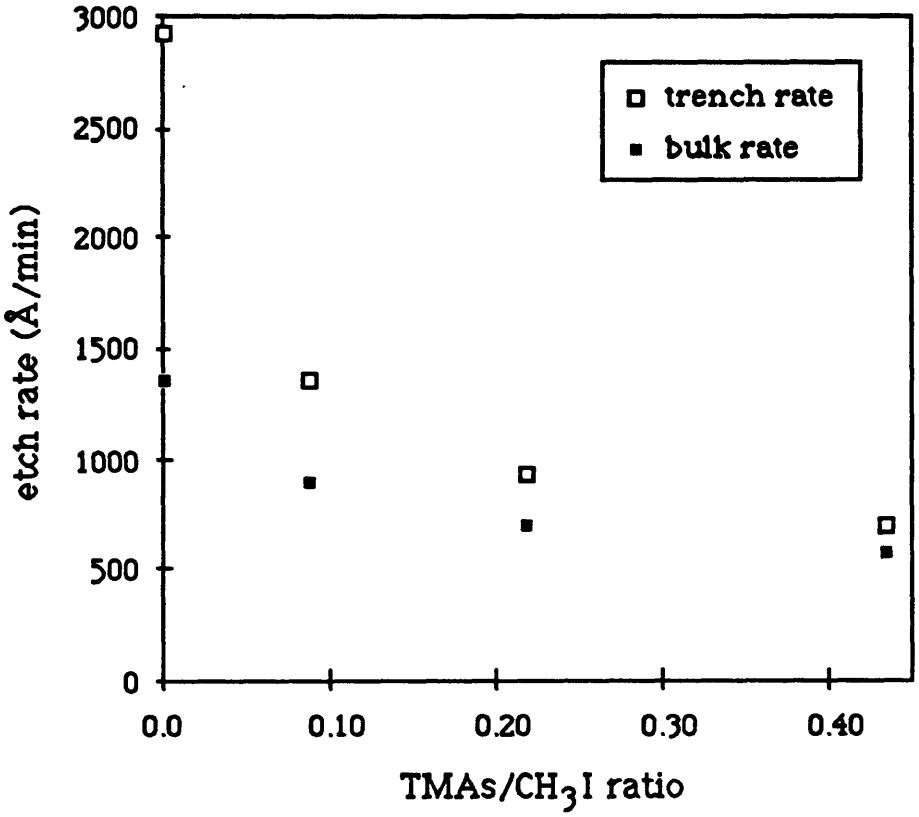

Figure 6.4: Effect of TMAs addition on etch profile near inert masks. Conditions: 553°C, 38.4 sccm CH_3I, 2100 sccm H_2.

Some initial experiments were performed to determine if TMAs alone would etch GaAs at an appreciable rate. No etching was observed for several concentrations and temperatures studied. The possibility that the etch rate suppression effect is due to gas phase reactions cannot immediately be ruled out. However, the fact that reaction order in · remains close to first order suggests that this is not the case. Further, the etch profile improvement with increasing TMAs is consistent with a decrease in surface reactivity as was shown in Chapter 4 (Figure 4.9).

Although other researchers have determined conditions under which etched surface morphology was improved by addition of gallium and arsenic containing compounds, no such improvement was observed in these studies. Nor was the morphology any more degraded. It has been previously hypothesized that surface reaction limitations may be responsible for the degraded surface morphologies that occur at the higher etch temperatures (Chapter 3). It may be that a rate limiting surface reaction is responsible for degraded etched surfaces observed in Chapter 3 but the general classification that any surface reaction limited etch process will result in degraded surfaces is clearly too broad.

Based on these results, the following model for the surface chemistry is proposed

$$I_{(v)} + Ga_{(s)} \rightarrow GaI_{(v)} + As_{(s)} \qquad (6.1)$$

$$2As_{(s)} \rightarrow As_{2(v)} + 2Ga_{(s)} \qquad (6.2)$$

$$As_{(v)} + \quad Ga_{(s)} \quad \rightarrow \quad As_{(s)} \qquad (6.3)$$

With corresponding rate constants k_1, k_2, and k_3. For the purposes of this model, $Ga_{(s)}$ represents a surface gallium atom available for reaction with the gas phase reactions (ie. a gallium "site") and $As_{(s)}$ represents a surface arsenic atom available for reactions with the gas phase (an arsenic "site"). Thus reaction (6.1) represents the reaction of an iodine atom in the gas phase to abstract a surface gallium site resulting in the ejection of GaI to the gas phase, leaving behind an available surface arsenic site. Reaction (6.2) is a pure surface reaction. Because arsenic atoms are expected to evaporate from the surface in a dimeric (As_2), or tetrameric (As_4) form (Foxon, et al, 1973, Hou, et al, 1989), at least two $As_{(s)}$ sites are needed. In the development of equations which follows, it will be assumed that As_2 is the form of arsenic which evaporates from the surface and that its rate of evolution will be in proportion to the square of the $As_{(s)}$ surface concentration, which is to say that the ability of one surface arsenic atom to "find" another is the rate limiting step. Reaction (6.3) is analogous to reaction (6.1) with the exception that no volatile product is formed. It is assumed that the decomposition of TMAs supplies arsenic atoms (As) in the gas phase to the surface. From reaction (6.1), an expression for the etch rate can be written

$$r_{etch} = k_1 [I_{(v)}] n_{Ga} \qquad (6.4)$$

where n_{GaAs} is the number of available gallium sites per unit of surface area. Equation (6.4) can be rewritten in dimensionless form

$$\frac{r_{etch}}{k_1 \Phi P/RT} = x_{Ga}\, y_I \qquad (6.5)$$

In this equation, Φ is the concentration of total ($As_{(s)}$ + $Ga_{(s)}$) surface sites (#/area), x_{Ga} is the gallium fraction of the total surface sites (n_{Ga}/Φ), y_I is the mole fraction of iodine atoms in the gas phase at the reacting surface and P is the total pressure. Applying conservation of total surface sites to reactions (6.1) - (6.3), x_{Ga} can be solved for in terms of k_1, k_2, k_3, y_I, y_{As}, and Φ from the following equation (assuming steady state gallium surface coverage)

$$0 = -k_1[I]n_{Ga} + 2k_2(\Phi - n_{Ga})^2 - k_3[As]n_{Ga} \qquad (6.6)$$

or in dimensionless form

$$0 = -k_1' y_I x_{Ga} + 2k_2'(1-x_{Ga})^2 - k_3' y_{As} x_{Ga} \qquad (6.7)$$

Where $k_1' = k_1RT/\Phi P$, $k_2' = k_2/\Phi^2$, and $k_3' = k_3RT/\Phi P$ are the normalized rate constants (units of inverse time). The "bimolecular" surface reaction kinetics which are assumed for the surface formation of As_2.(reaction 6.2) is the source of the quadratic term in equation (6.7). Although equation (6.7) is quadratic in x_{Ga}, only one of the two roots is physically allowed ($x_{Ga} < 1$). Substituting the expression thus derived for x_{Ga} into equation (6.5) gives the final solution

$$\frac{r_{etch}}{k_1 \Phi P} = (1 + \frac{K}{2} - \frac{\sqrt{(K^2+4K)}}{2})y_I \qquad (6.8)$$

with

$$K = \frac{k_1' y_I + k_3' y_{As}}{2k_2'} \qquad (6.9)$$

Equation (6.8) has the property that for K = 0, the dimensionless etch rate is simply y_I and x_{Ga}=1. If K is very large, x_{Ga} drops to zero and so does the rate. Equation's (6.8) and (6.9) can be used to fit curves to the data presented earlier in this chapter by varying one of two constants, k_1'/k_2' and k_3'/k_2'. and this is the model on which the curves fit to the data in Figures 6.1 and 6.2 arise. In order to perform these fits, it is assumed that y_I and y_{As} (at the surface) are directly proportional to the inlet concentrations of CH_3I and TMAs respectively. The fit is then performed by first varying k_1'/k_2' to reproduce the experimentally determined reaction orders for the given temperature from Chapter 3. In this case, at 500°C, the reaction order in y_{CH_3I} is 0.83 and at 550°C it is 0.68. Once is determined, k_3'/k_2' is fit by a generalized least squares technique to the data points and the curves shown in the figures are generated. One important result of this fit is that given the parameters fit by this technique, the the rise in the observed reaction order for the CH_3I/TMAs mixture from 0.68 to 0.83 in y_{CH_3I} at 553°C is predicted. In fact, if this model is correct, it should be possible to recover a first order etch rate dependence in y_{CH_3I} if large amounts of TMAs are

introduced. Since the exact values of y_I and y_{As} are not known, the values of the fitting parameters are relative and no real quantitative physical insight is possible. If y_I and y_{As} could be exactly determined, more direct verifications of this model would be possible.

6.5 CONCLUSIONS

Some aspects of surface chemistry related to the vapor etching of GaAs by CH_3I have been investigated. It has been determined that the addition of trimethylarsenic (TMAs) to the CH_3I etch chemistry causes a lowering of etch rates due to competitive reaction for surface gallium between arsenic from TMAs decomposition and iodine from CH_3I decomposition, where only the latter reaction leads to etching. This lowering of etch rate is accompanied by an improvement in the non-uniformity of etch profiles near inert masks and the potential for etching uniformly near masks is realized through the addition of TMAs. TMAs addition does not appreciably influence etched surface morphology. A general model for surface chemistry has been developed to explain these results and the previously observed sublinear etch rate dependence on CH_3I concentration. Further understanding and verification of this model will require additional experiments and a more exact coupling with the gas phase chemistry to determine exact levels of arsenic and iodine at the surface.

Chapter 7

Summary and Future Work

The main objective of this thesis, to develop a viable vapor etch process for use *in situ* of OMVPE reactor systems has been primarily achieved. As a bulk wafer cleaning agent, the results were extremely promising as it was shown that mirror smooth etched surfaces could be maintained without the introduction of any detectable impurities onto the etched surface. In addition the etching of AlGaAs was demonstrated and the rates did not depend on the aluminum fraction in these materials. The etching of masked substrates exhibited several undesirable characteristics, however. Not surprisingly, undercutting of masks occured although this could be minimized by appropriate parallel stripe orientation (to promote the appearance of slow etch facets). For etching of features other than parallel lines, the differences in surface reactivity will manifest leading to directionally dependent mask undercutting. The other undesirable feature of etching masked substrates is the non-uniformity in etched depth which is observed near the mask/substrate boundary. It was shown that this effect is due to gas phase diffusion effects which transport etchant species from the inert mask to the reactive GaAs surface. However, by adding trimethylarsenic (TMAs) to the etch mixture, these non-uniformities can be controlled although bulk etch rates are reduced as well due to surface kinetic limitations.

The understanding which was gained into the etch mechanism is also interesting. The conclusion that the CH_3I vapor etch of GaAs occurs under a gas phase kinetic limitation is a unique result in the albeit limited body of vapor etching literature for this material. The fact that CH_3I does not react with the GaAs surface is apparently the key reason that smooth etched surfaces can be obtained at significantly lower temperatures than for compounds previously studied. For these other compounds, smooth surfaces could only be obtained at high temperatures where the otherwise rate limiting surface reactions become fast enough to force a gas phase diffusion limitation. The sole exception to this is Cl_2 etching, although no studies of Cl_2 etching in a flow system have been reported at this time and the data are limited to experiments performed under high vacuum conditions where smooth surfaces were obtained under flux limited conditions. Although rough surface morphologies tend to correlate to conditions where surface reactions are rate limiting, this work has shown that certain surface kinetic barriers (as imposed by adding TMAs) have no effect on etched surface morphology. Thus the causes of surface destabilization are not at all clear and there is certainly room for more investigations into these effects.

In the CH_3I vapor etch system it was observed that rough morphologies and carbon deposition tended to correlate. It may be of value to examine etching using other iodine containing compounds such as ethyl- or propyl- iodide since it is known, for example, that less carbon is incorporated into OMVPE GaAs when triethylgallium is substituted for trimethylgallium. HI vapor etching was studied

(Appendix A) in the course of this work and etched surfaces were consistently rough; however, source purity was an issue and it is not clear if an impurity in the HI source was causing the morphology degradation. Also, HI is a corrosive chemical so its applicability is further restricted.

8 BIBLIOGRAPHY

Arnot, H. E. G., Watt, M., Sotomayor-Torres, C. M., Glew, R., Cusco, R., Bates, J., Beaumont, S. P., 'Photoluminescence of Overgrown GaAs-GaAlAs Quantum Dots', Superlattices and Microstructures, **5**, 459-463, 1989.

Bakin, N. N., Dedkov, V. D., Porokhovnichenko, L., P., 'Polishing GaAs Gas Etching', Inorganic Materials, **8**, 1206-1208, 1972.

Balooch, M., Olander, D. R., 'The Thermal and Ion-Assisted Reactions of GaAs(100) with Molecular Chlorine', Journal of Vacuum Science and Technology B, **4**, 794-805, 1986.

Bharadwaj, L., M., Bonhomme, P., Faure, J., Balossier, G., Bajpai, R., P., 'Chemically Assisted Ion Beam Etching of GaAs and GaSb using Reactive Flux of Iodine and Ar^+ Beam', SPIE Dry Etch Technology, **1593**, 186-192, 1991.

Bhat, R., Baliga, B., J., Ghandi, S., K., 'Vapor-Phase Etching and Polishing of Gallium Arsenide Using Hydrogen Chloride Gas', Journal of the Electrochemical Society, **122**, 1378-1382, 1975.

Bhat, R., Ghandi, S. K., 'The Effect of Chloride Etching on GaAs Epitaxy Using TMG and AsH_3', Journal of the Electrochemical Society, **125**, 771-776, 1978.

Bhat, R., Ghandi, S. K., 'Vapor-Phase Etching and Polishing of GaAs Using Arsenic Trichloride', Journal of the Electrochemical Society, **124**, 1447-1448, 1977.

Buchan, N. I., Kuech, T. F., Scilla, G., Cardone, F., Potemski, R., 'Carbon Incorporation in Metal-Organic Vapor Phase Epitaxy Grown GaAs from CH_xI_{4-x}, HI, and I_2', Journal of Electronic Materials, **19**, 277-281, (1990).

Buhaenko, D. S., Francis, S. M., Goulding, P. A., Pemble, M. E.,'The Interaction of H_2 with GaAs (100) Surfaces: A Model Study of MOVPE Substrate Preparation', Journal of Crystal Growth, **97**, 591-594, 1989.

Carter, A. J., Thomas, B., Morgan, D. V., Bhardwaj, J. K., 'Semiconductor Optoelectronic Device Fabrication using Dry Etching', Materials Research Society Symp. Proc., **144**, 683-688, 1989.

Chadi, D. J., 'Atomic Structure of Reconstructed Group IV and III-V Semiconductor Surfaces', Ultramicroscopy, **31**, 1-9, 1989.

Cheung, R., Thoms, S., Beamont, S. P., Doughty, G., Law, V., Wilkinson, C. D. W., 'sReactive Ion Etching of GaAs using a Mixture of Methane and Hydrogen', Electronics Letters, **23**, 857-858, 1987.

Coronell, D., G., Jensen, K., F., 'Analysis of MOCVD of GaAs on Patterned Substrates', Journal of Crystal Growth, **114**, 581-592, 1991.

Creighton, J. R., 'Adsorption and Decomposition of Trimethylarsenic on GaAs(100)', unpublished, presented at MRS Fall Meeting, Boston, MA,1989.

Dorschand, S., Daweritz, L., Berger, H., 'Investigations on the HCl Gas-Phase Etching of Differently Doped and Oriented GaAs Crystals', Crystal Research and Technology, **18**, 1359-1368, 1983.

Durose, K., Aylett, M. R., Haigh, J., 'Production of Etched Features in InP for Integrated Optoelectronic Applications by Laser Direct-Write Photochemical Etching', Chemtronics, **3**, 201-205, 1988.

El Jani, B., Grenet, J. Cl., Guittard, M., Senouci, B., 'In Situ Etching of GaAs Using $AsCl_3$ in MOVPE. I', Journal of Crystal Growth, **58**, 381-386, 1982.

El Jani, B., Guittard, M., Grenet, J. Cl., Gibart, P., 'In Situ Etching of GaAs Using $AsCl_3$ in MOVPE. II', Journal of Crystal Growth, **60**, 131-135, 1982.

Flanders, D. C., Pressman, L. D., Pinelli, G., 'Reactive Ion Etching of Indium Compounds using Iodine Containing Plasmas', Journal of Vacuum Science and Technology B, **8**, 1990-1993, 1990.

Foxon, C. T., Harvey, J. A., Joyce, B. A., 'The Evaporation of GaAs Under Equilibrium and Non-Equilibrium Conditions using a Modulated Beam Technique', Journal of Physical Chemistry of Solids, **34**,1693-1701, 1973.

Foxon, C. T., Joyce, B. A., 'Interaction Kinetics of As_2 and Ga on {100} GaAs Surfaces', Surface Science, **64**, 293-304, 1977.

Furuhata, N., Miyamoto, H., Okamoto, A., Ohata, K.,'Cl_2 Chemical Dry Etching of GaAs - Crystallographic Etching and Its Mechanism', Journal of Electronic Materials, **19**, 201-208, 1990.

Gatos, H. C., 'Crystal Structure and Surface Reactivity', Science, **137**, 311-322, 1962.

Givargizov, E., I., Babasian, R., A., 'Mechanisms of Etching of GaAs and GaP', Journal of Electronic Materials, **9**, 883-904, 1980.

Ha, J. H., Ogryzlo, E. A., Polyhronopoulos, S., 'Kinetics of the Reaction of Gallium Arsenide with Molecular Chlorine', Journal of Chemical Physics, **89**, 2844-2847, 1988.

Henry, L., Vaudry, C., Granjoux, P., 'Novel Process for Integration of Optoelectronic Devices using Reactive Ion Etching without Chlorinated Gas', Electronics Letters, **23**, 1253-1254, 1987.

Heynen, M., Balk, P., 'Vapor Phase Etching of GaAs in a Chlorine System', **53**, 558-562, 1981.

Holstein, W. L., 'Thermal Diffusion in Metal-Organic Chemical Vapor Deposition', Journal of the Electrochemical Society: SOLID STATE SCIENCE AND TECHNOLOGY, **135**, 1788-1793, 1988.

Hou, H., Zhang, Z., Chen, S., Su, C., Yan, W.,Vernon, M., 'Observation of Competing Arsenic Removal Channels in the Cl_2 + GaAs reaction', Applied Physics Letters, **55**(8), 801-803, 1989.

Jensen, K. F., Einset, E. O.,Fotiadis, D. I.,'Flow Phenomena in Chemical Vapor Deposition of Thin Films', Annu. Rev. Fluid Mech., **23**, 197-232, 1991.

Kastelic, M. M., Friedrich, J., Oh, I. -H., Takoudis, C. G., Neudeck, G. W., Proceedings of the Eleventh International Conference on Chemical Vapor Deposition, editors K. E. Spear and G. W. Cullen, 318, 1990.

Kerr, J. A., Moss, S. J., Handbook of Bimolecular and Termolecular Gas Reactions: Volume I, CRC Press, 1981.

Kuech, T. F., Marshall, E., Scilla, G. J., Potemski, R., Ransom, C. M., Hung, M. Y., 'The Effect of Surface Preparation on the Production of Low Interfacial Charge Regrown Interfaces', Journal of Crystal Growth, **77**, 539-545, 1986.

Kuech, T. F., Veuhoff, E., 'Mechanism of Carbon Incorporation in MOCVD GaAs', Journal of Crystal Growth, **68**, 148-156, 1984.

Kuech, T. F., Wang, P. -J., Tischler, M. A., Potemski, R., Scilla, G. J., Cardone, F., 'The Control and Modeling of Doping Profiles and Transients in MOVPE Growth', Journal of Crystal Growth, **93**, 624-630, 1988.

Lee, P.W., Omstead, T. R., McKenna, D. R., Jensen, K. F., 'In Situ Mass Spectroscopy Studies of the Decomposition of Organometallic Arsenic Compounds in the Presence of $Ga(CH_3)_3$ and $Ga(C_2H_5)_3$', Journal of Crystal Growth, **93**, 134-42, 1988.

Leys, M. R., Veenvliet, H., 'A Study of the Growth Mechanism of Epitaxial GaAs Grown by the Technique of Metal Organic Vapour Phase Epitaxy', Journal of Crystal Growth, **55**, 145-153, 1981.

Li, S. H., Larsen, C. A., Chen, C. H., Stringfellow, G. B., Brown, D. W.,'Dimethylarsine: Pyrolysis Mechanisms and Use for OMVPE Growth', Journal of Electronic Materials, **19**, 299-304, 1990.

Li, S. H., Larsen, C. A., Stringfellow, G. B., 'Decomposition Mechanisms of Trimethylarsine', Journal of Crystal Growth, **102**, 117-125, 1990.

Lin, C., Chow, L., Miller, K., 'Vapor Phase Etching of GaAs in the H_2-H_2O Flow System', Journal of the Electrochemical Society, **117**, 407-409, 1970.

Lum, R. M., Klingert, J. K., Kisker, D. W., Abys, S. M., Stevie, F. A., '^{13}C Isotopic Labeling Studies of Growth Mechanisms in the Metalorganic Vapor Phase Epitaxy of GaAs', Journal of Crystal Growth, **93**, 120-126, 1988.

Matsui, T., Sugimoto, H., Ohishi, T., Ogata, H., 'Reactive Ion Etching of III-V Compounds using C_2H_6/H_2', Electronics Letters, **24**, 798-800, 1988.

Munoz-Yague, A., Piqueras, J., Fabre, N., 'Preparation of Carbon-Free GaAs Surfaces: AES and RHEED Analysis', Journal of the Electrochemical Society, **128**, 149-153, 1981.

Nido, M., Komazaki, I., Kobayashi, K., Endo, K., Ueno, M., Kamejima, T., Suzuki, T., 'AlGaAs/GaAs Self-Aligned LD's Fabricated by the Process Containing Vapor Phase Etching and Subsequent MOVPE Regrowth', IEEE Journal of Quantum Electronics, **QE-23**, 720-723, 1987.

Okubora, A., Kasahara, J., Arai, M, Watanabe, N., 'Thermal Etching of GaAs by Hydrogen Under Arsenic Overpressure', Journal of Applied Physics, **60**, 1501-1504, 1986.

Oldham, W. G., Holmstrom, R., 'The Growth and Etching of Si through Windows in SiO_2', Journal of the Electrochemical Society, **114**, 381-388, 1967.

Patnaik, S., 'Modelling of Transport Processes in Chemical Vapor Deposition Reactors', PhD Thesis, Massachusetts Institute of Technology, 1989.

Pearton, S. J., Chakrabarti, U. K., Baiocchi, F. A., 'Electrical and Structural Changes in the Near Surface of Reactively Ion Etched InP', Applied Physics Letters, **55**, 1633-1635, 1989.

Pearton, S. J., Chakrabarti, U. K., Hobson, W. S., Abernathy, C. R., Katz, A., Ren, F., Fullowan, T. R., Perley, A. P., 'Hydrogen Iodide-Based Dry Etching of GaAs, InP, and Related Compounds', Journal of the Electrochemical Society, **139**, 1763-1772, 1992.

Pelosi, C., Attolini, G., Salviati, G., 'Vapour Phase In-Situ Etch of (100) GaAs Substrates', Materials Chemistry and Physics, **9**, 139-146, 1983.

Price, S. J. W., and Richard, J. P., 'The Pyrolysis of Trimethylarsine', Canandian Journal of Chemistry, **48**, 3209-3212, 1970.

Reep, D. H., Ghandi, S. K., 'Morphology of Organometallic CVD Grown GaAs Epitaxial Layers', Journal of Crystal Growth, **61**, 449-457, 1983.

Saito, J., Kondo, K., '*In Situ* Quadrupole Mass Spectroscopy Etching GaAs with a HCl Gas and Hydrogen Mixture', Journal of the Electrochemical Society, **137**, 1305-1306, 1990.

Saito, K., Tahara, H., Kondo, O., Yokubo, T., 'The Thermal Gas-phase Decomposition of Methyl Iodide', Bull. Chem. Soc. Jpn., **53**, 1335-1339, 1980.

Saito, K., Tahara, H., Murakami, I., 'Second-order Rate Constants for the Decomposition of Methyl Iodide in Different Rare Gases', Bull. Chem. Soc. Jpn., **57**, 3023-3024, 1984.

Shimoyama, K., Katoh, M., Noguchi, M., Inoue, Y., Gotoh, H., 'Transverse-Junction Buried Heterostructure (TJ-BH) Laser Diode Grown by MOVPE', Journal of Crystal Growth, **93**, 803-808, 1988.

Silvestri, V. J., Ghez, R., Sedwick, T. O., 'Growth Mechanism for Germanium Deposition near a SiO_2-Ge Boundary', Journal of the Electrochemical Society, **119**, 245-250, 1972.

Sugata, S., Asakawa, K., 'GaAs and AlGaAs Crystallographic Etching with Low-Pressure Chlorine Radicals in an Ultrahigh-Vacuum System", Journal of Vacuum Science and Technology B, **5**, 894-901, 1987.

Sullivan, J. H., 'Rates of Reaction of Hydrogen with Iodine. II', Journal of Chemical Physics, **36**, 1925-1932, 1962.

Tanaka, H., Komeno, J., 'Kinetic Simulations of Gas Phase Reactions in MOVPE Growth', Journal of Crystal Growth, **93**, 115-119, 1988.

van de Ven, J., Schoot, H. G., Giling, L. J., 'Influence of Growth Parameters on the Incorporation of Residual Impurities in GaAs Grown by Metalorganic Chemical Vapor Deposition', Journal of Applied Physics, **60**, 1648-1660, 1986.

Appendix A

Vapor Etching OF GaAs with HI and $(CH_3)_2N_2$

A limited number of GaAs etching experiments were performed with hydrogen iodide (HI) and azomethane ($(CH_3)_2N_2$). Hydrogen iodide is a source of iodine without an organic component whereas azomethane, which is well established to decompose into methyl radicals and N_2, is a source of methyl radicals without iodine. These studies are therefore complementary to the CH3I experiments (considering that CH_3I is a source of iodine and methyl radicals).

The source of HI used was a mixture of 99.99% hydrogen with 97% HI in a 20:1 ratio supplied by Matheson. The etching experiments were performed in the horizontal reactor with a hydrogen carrier gas and the total flow to the reactor was 2100 sccm. Substrates were (100)GaAs +2°(110) half masked with silicon nitride. Feed concentrations of HI were varied between 0.1-1.7%. Substrate temperatures between 500 and 650°C were examined. The activation energy for the reaction was 39 kcal/mol both at 0.1% HI and at 1.3% HI and the concentration dependence was linear, however the reaction order was 0.66. In all cases the surface morphology was severely degraded and faceting was apparent. It was not clear if the morphology degradation was due to an impurity in the HI source and this remains an open question. The etch rates were very close to those observed with similar concentrations of CH_3I however the mechanism of HI etching is not clearly apparent from these data.

Azomethane was synthesized by the following procedure. A solution of potassium acetate and dimethylhydrazine-dihydrochloride was prepared. To this was added (dropwise) 4M copper(II) chloride. The $CuCl_2$ reacts with the dimethylhydrazine ($(CH_3)_2N_2H_2$) to form a solid complex of azomethane with CuCl. This solid was washed and dried under vacuum. On a vacuum line the solid complex was heated, liberating the azomethane gas which was collected in a cold trap and fractionally distilled on the same vacuum line. The azomethane was then collected in a steel cylinder.

The experiments were also performed in the horizontal reactor with azomethane concentrations from 0.06 to 1.0% in H_2. and substrate temperatures from 450-630°C. The raw data is shown in the accompanying table.

In short, the results were inconclusive. In many cases no etching was observed and when etching did occur the rates were low. The possibility of a chlorine or hydrogen chloride impurity in the azomethane means that any etching that was observed cannot be conclusively attributed to methy radicals. However, these results do put an upper bound on etching due to methyl radicals since the azomethane that was in the reactor should have been creating methyl radicals.

Overall the results in this appendix are in agreement with the conclusions reached in the thesis, that iodine atoms are the primary etchant.

RUN ID #	TEMP (C)	TOTAL FLOW (sccm)	AZO FLOW RATE (sccm)	TIME (min)	ETCH DEPTH (Å)	ETCH RATE (Å/MIN)
AZ.001	480	2085.44	5.44	30	2000	66.6666667
AZ.002	500	2085.44	5.44	18		0
AZ.003	520	2085.44	5.44	30	709	23.6333333
AZ.004	630	2085.44	5.44	15		0
AZ.005	580	2085.44	5.44	20	638	31.9
AZ.006	510	2085.44	5.44	30		0
AZ.007	510	2085.44	5.44	30	2100	70
AZ.008	580	2085.44	5.44	30	216	7.2
AZ.009	460	2085.44	5.44	60	1100	18.3333333
AZ.010	530	2085.44	5.44	30		0
AZ.011	505	2101.76	21.76	16	2203.33333	137.708333
AZ.012	505	2096.36	1.36	120	1181.33333	9.84444444
AZ.013	480	2101.76	5.44			
AZ.014	480	2101.76	5.44	60	1551.5	25.8583333
AZ.015	450	2101.76	5.44	60		0
AZ.016	460	2101.76	5.44	60		0
AZ.017	480	2113.6	13.6	60	400	6.66666667
AZ.018	525	2113.6	13.6	30		0
AZ.019	480	2113.6	13.6	60	1584.5	26.4083333
AZ.020	620	2113.6	13.6	30	1727	57.5666667
AZ.021	555	2113.6	13.6	49	3107.66667	63.4217687
AZ.022	555	537.5	3.4	50		
AZ.023	555	537.5	3.4	51	700	13.7254902
AZ.024	450	2113.6	13.6	60	1266.5	21.1083333